POWER REACTOR TECHNOLOGY

A Quarterly Technical Progress Review

Prepared for U. S. ATOMIC ENERGY COMMISSION by GENERAL NUCLEAR ENGINEERING CORP.

September 1960

● VOLUME 3

● NUMBER 4

TECHNICAL PROGRESS REVIEWS

To meet the needs of industry for concise summaries of current atomic developments, the Atomic Energy Commission is publishing this series, Technical Progress Reviews. Issued quarterly, each of the reviews digests and evaluates the latest findings in a specific area of nuclear technology and science.

The four journals published in this series are:

Nuclear Safety, W. B. Cottrell, editor, R. A. Charpie, advisory editor, and associates, Oak Ridge National Laboratory

Power Reactor Technology, Walter H. Zinn and associates, General Nuclear Engineering Corporation

Reactor Core Materials (covering solid material developments), R. W. Dayton, E. M. Simons, and associates, Battelle Memorial Institute

Reactor Fuel Processing, Stephen Lawroski and associates, Chemical Engineering Division, Argonne National Laboratory

Each journal may be purchased ($2.00 per year for subscription and individual issues $0.55) from the Superintendent of Documents, U. S. Government Printing Office, Washington 25, D. C. See back cover for remittance instructions and foreign postage requirements.

Availability of Reports Cited in This Review

Unclassified AEC reports are available for inspection at AEC depository libraries and are sold by the Office of Technical Services, Department of Commerce, Washington 25, D. C. Some of the reports cited are not available owing to their preliminary nature; however, the information contained in them will eventually be made available in formal progress or topical reports.

Unclassified reports issued by other Government agencies or private organizations should be requested from the originator.

Unclassified British and Canadian reports may be inspected at AEC depository libraries. British reports are sold by the British Information Service, 45 Rockefeller Plaza, New York, N. Y.; Canadian reports (AECL series) are sold by the Scientific Document Distribution Office, Atomic Energy of Canada, Ltd., Chalk River, Ontario, Canada.

Classified U. S. and foreign reports identified in this journal as Classified may be purchased by properly cleared Access Permit Holders from the Office of Technical Information Extension, U. S. Atomic Energy Commission, P. O. Box 1001, Oak Ridge, Tenn. Such reports may be inspected at classified AEC depository libraries.

POWER REACTOR TECHNOLOGY

A REVIEW OF RECENT DEVELOPMENTS

Prepared for U. S. ATOMIC ENERGY COMMISSION
by ARGONNE NATIONAL LABORATORY

● SEPT. 1960

● VOLUME 3

● NUMBER 4

foreword

This quarterly review of reactor development has been prepared at the request of the Office of Technical Information of the U. S. Atomic Energy Commission. Its purpose is to assist interested organizations in the task of keeping abreast of new results in reactor technology for civilian application.

The report is a concise discussion of selected phases of research and development for which there have been significant advances or a heightened interest in the past few months. It is not meant to be a comprehensive abstract of all material published during the quarter, nor is it meant to be a treatise on any part of the subject. The intention is to cover the various areas of reactor development from the general viewpoint of the reactor designer rather than from the more detailed points of view of specialists in the individual areas. However, papers which are thought to be of particular significance or particular usefulness in specialized fields will be mentioned in short notes. In the over-all plan of the report, it is intended that various subjects will be treated from time to time and will be brought up to date at that time.

Any interpretation of results which is given represents only the opinion of the editors of the report, who are General Nuclear Engineering Corporation personnel. Readers are urged to consult the original references in order to obtain all the background of the work reported and to obtain the interpretation of the results given by the original authors.

W. H. ZINN
General Nuclear Engineering Corporation

contents

Foreword

1 I ECONOMICS: THE WASTE PROBLEM

1 Magnitude and Time Scale of the Problem
5 Ultimate Disposal of High-Level Wastes
8 Utilization of Wastes
9 Sea Disposal
9 Low-Level Wastes
10 Conclusions
11 References

12 II REACTOR PHYSICS

12 Recent Critical and Exponential Experiments
12 Fission-Product Poisoning
19 References

22 III HEAT TRANSFER

22 The Gas Suspension Coolant Project
24 Geometrical Considerations
25 Water Heat Transfer and Fluid Flow
30 Hot Spots and Hot-Channel Factors
31 Parallel-Channel Flow
32 References

33 IV REACTOR KINETICS AND CONTROL: CONFERENCE ON TRANSFER FUNCTIONS AND REACTOR STABILITY

38 V EFFECT OF RADIATION ON DUCTILE-BRITTLE TRANSITION OF STEEL

38 Unirradiated Brittle Fracture Behavior
44 Test Methods
44 Irradiation Effects on Tensile Properties
46 Effects of Irradiation on the Ductile-Brittle Transition Temperature of Ferritic Steels
52 Application to Reactor Vessels
56 References

58 VI GAS-COOLED REACTORS

59 Fuel Elements for the Experimental Gas-Cooled Reactor
62 Materials for High-Temperature Gas-Cooled Reactors
64 References

66 VII ORGANIC-MODERATED REACTORS: EVALUATION OF IRRADIATED EXPERIMENTAL FUEL ELEMENTS

68 VIII NUCLEAR SUPERHEAT: THE BONUS REACTOR

75 IX THE NEW PRODUCTION REACTOR

79 INDEX, VOLS. 1–3

Issued quarterly by the U. S. Atomic Energy Commission. Use of funds for printing this publication approved by the Director of the Bureau of the Budget on November 1, 1957.

Section I

ECONOMICS: THE WASTE PROBLEM

The disposal of radioactive wastes from nuclear reactors is generally recognized as one of the problems of the nuclear-power industry. That the disposal must be safe goes without saying. How much the operations and investments necessary for safe disposal may contribute to the total cost of nuclear power is a question of economic concern to the industry; whether the problem of disposal may eventually limit the useful amount of nuclear power generated is an equally important question and is of longer range significance. These questions are very complex, and complete answers are not yet possible; but present information indicates that the answers will be favorable.

The latest reviews of the status of the waste problem by the Atomic Energy Commission[1] and by the Joint Congressional Committee on Atomic Energy[2,3] have been reported. This article is an attempt to extract from those reviews a very brief summary of the material which bears on the questions raised above. Current progress on the development of waste-disposal methods is reviewed as a regular feature in the quarterly technical progress review, *Reactor Fuel Processing*, which is available from the Superintendent of Documents, U. S. Government Printing Office, Washington 25, D. C., $0.55 per copy, $2.00 per year.

Waste-disposal problems are not unusual in large-scale industries; however, there are certain unique aspects of the problems faced by the nuclear-power industry. The radioactive wastes generated cannot be converted by any controllable process now known into harmless materials which may be safely released to the general environment. These wastes, although they are extremely toxic, give no evidence of their presence to the general public and could persist undetected for a long time. Further, the harmful effects of exposure of large populations may become apparent only in the succeeding generations. The long-term hazard of such isotopes as Sr^{90} and Cs^{137} demands custodial responsibility that extends far beyond the normal life span of men or corporations. As a result of these factors, special legislative control may be necessary to ensure adequate and continuing safety.

Magnitude and Time Scale of the Problem

The extremely hazardous nature of fission products has been amply documented. It has been generally acknowledged that the capacity of our environment for safe disposal of all wastes by dilution is completely inadequate even for an industry of the size expected within the next 20 to 40 years. Thus the basic problems are (1) to determine how to confine safely the majority of these wastes for a very long period of time with reasonable cost and (2) to determine what quantities of radioactive materials can safely be allowed to "leak" to the environment as low-level wastes of various sorts.

To get an idea of the magnitude of the high-level waste problem, it is convenient to consider a nuclear-power industry producing on the average 100,000 Mw(t) of nuclear power. This would be equivalent, in electrical generation, to slightly less than one-third of the present average generation by utilities in the United States. It thus might be considered to represent an early stage of fully competitive nuclear power in the United States; if increased by a factor of 10, it might represent a situation, some decades later, in which the nuclear generating capacity is determined not by the competition of fossil fuels but by the growth of power demand.

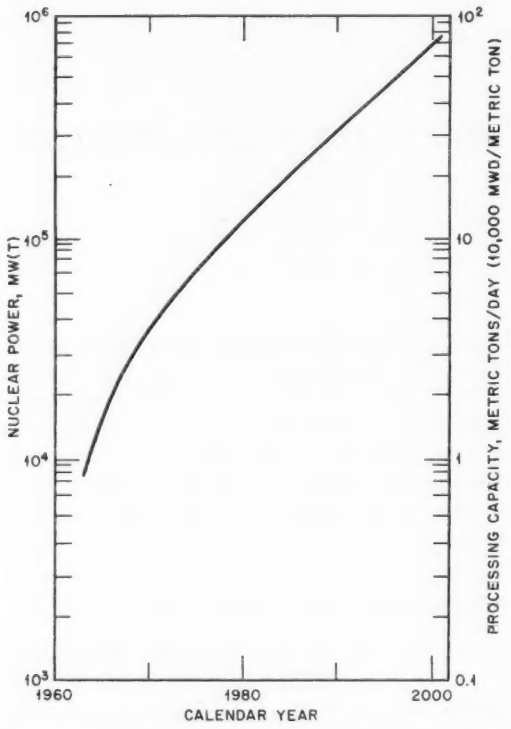

Figure 1 — Predicted power growth and fuel-processing capacity.[4]

Table I-1 ASSUMED DISTRIBUTION[4] OF REACTOR TYPES IN 1980

Reactor type	Fuel	Per cent of nuclear power
Breeders:		
Fast	S.S.-clad	5
Homogeneous	Aqueous	5
Converters:		
Uranium	Zr-clad	40
	S.S.-clad	25
Thorium	Zr-clad	20
	C-clad	5
Total		100

Table I-2 COMPOSITION OF WASTES ANTICIPATED FROM VARIOUS TYPES OF REACTORS[4]

Fuel type	Decladding solution	High-activity waste
Natural or slightly enriched:		
Al-clad U	$NaAlO_2$, 1.2 *M*	HNO_3, 2 *M*
S.S.-clad UO_2	(Fe, Ni, Cr) SO_4, 80 g/liter	HNO_3, 2 *M*
Zr-clad UO_2	Zr^{++}, 0.5*M*; NH_4^+ and 1.5*M* F^-, 3.7*M*; NO_3^-, 0.6*M*	HNO_3, 2 *M*
Highly enriched:		
Al-U alloy		HNO_3, 1.3*M*; $Al(NO_3)_3$, 1.6*M*
Zr-U alloy		HNO_3, 3.2*M*; Zr^{++}, 0.8*M*; NH_4F, 1.8*M*
S.S.-U cermet		S.S., 50 g/liter; $Al(NO_3)_3$, 0.12*M*; HNO_3, 3*M*

Table I-3 VOLUME OF WASTE TO BE STORED FROM POWER-REACTOR FUELS[4]

Fuel type	Waste volume, gal	
	Per kilogram of uranium	Per megawatt-day
Natural or slightly enriched:		
Al-clad U	0.33*	0.033
S.S.-clad UO_2	1.06*	0.106
Zr-clad UO_2	1.46*	0.146
Highly enriched:		
Al-U alloy	125	0.5
Zr-U alloy	300	1.2
S.S.-U cermet	65	0.26

*0.06 gal is high-activity waste; the rest is decladding.

The 100,000-Mw(t) power industry will produce, each day, electricity worth [at 7 mills/kw(e)-hr] about $6 million. If it is assumed that the average fuel exposure is 10,000 Mwd(t) per metric ton of uranium, then the average rate of fuel processing will be 10 metric tons of uranium per day, and the daily output of actual fission products will be slightly more than 100 kg. If it is assumed further that the fuel has been used at an effective specific power of 33 Mw(t) per metric ton, the fuel will have spent an average of 300 days in-reactor; after cooling for a year, the 100 kg of fission products from a single day's operation will be generating heat at a rate of about 40 kw(t) through radioactive disintegrations at a level of about 10^7 curies.

In the form of pure oxides, chlorides, etc., pressed to a density of 3 g/cm^3, the entire yearly production of fission products by the 100,000-Mw(t) industry would amount to about 500 cu ft. The two major long-lived isotopes, Sr^{90} and Cs^{137}, would occupy less than 100 cu ft in this form. Unfortunately, in the raw form, the liquid wastes generated in processing the required 3650 metric tons of fuel are not so

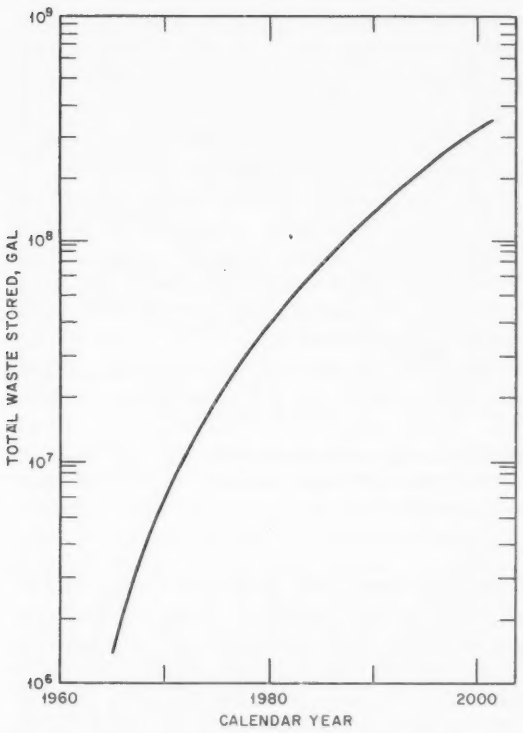

Figure 2—Accumulated volume of high- and intermediate-level wastes (consistent with the power growth curve of Fig. 1).[4]

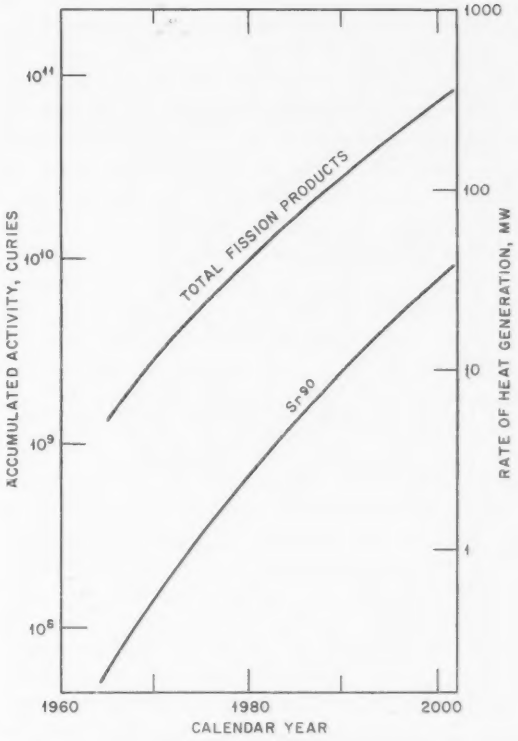

Figure 3—Accumulated radioactivity (consistent with the power growth curve of Fig. 1).[4]

convenient to handle. For example, with current processing practices for zirconium-clad UO_2 fuel, each metric ton of uranium processed yields 1460 gal of liquid waste (1400 gal of decladding solution plus 60 gal of high-activity waste).

It is perhaps more informative to consider the total accumulation of radioactive wastes as a function of time, since it is the long life of the activity that makes the disposal problem difficult. To do this, one must make assumptions regarding (1) the magnitude of the nuclear-power industry as a function of time and (2) the types of reactors used. A forecast of this sort was given by Bruce[4] of Oak Ridge National Laboratory (ORNL) in his statement to the Joint Committee. The material in this section was taken from his statement.

Figure 1 is the curve of nuclear-power growth used for the estimates; it is that estimated by Lane.[5] The 10^5-Mw(t) level will be reached in 1980, and the 10^6-Mw(t) level will be reached sometime after the year 2000. On the same figure is a scale showing the rate at which fuel must be processed if an average exposure of 10,000 Mwd/metric ton is assumed. Table I-1 gives the assumed distribution of reactor types and the assumed fuel types for each. Tables I-2 and I-3 show, respectively, the compositions of the waste solutions and the waste volumes characteristic of several fuel types. It is to be noted that the slightly enriched oxide fuels clad with zirconium or stainless steel, which were assumed for the power reactors, produce considerably less waste volume than the highly enriched fuels which are in intimate mixture with a diluent as an alloy or as a cermet (Table I-3).

Figure 2 presents the accumulated volume of high- and intermediate-level wastes computed on the above assumptions, and Fig. 3 shows the accumulated radioactivity in the wastes. On the assumption that the average energy per disintegration is 0.7 Mev, a scale has been added on the right-hand side of Fig. 3 to give a rough idea of the total thermal power generated in the wastes. Figure 4 shows the thermal-power generation in a waste solution as a function of decay time, on the assumption that 800 gal of waste

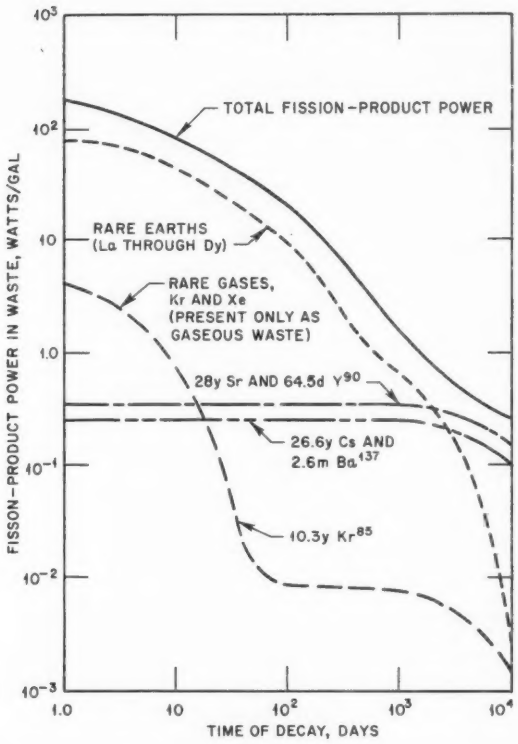

Figure 4 — Fission-product power in waste as a function of decay time (basis: 800 gal of waste per metric ton of uranium, irradiated at 10,000 Mwd/ton exposure and at 33 Mw/ton specific power).[6]

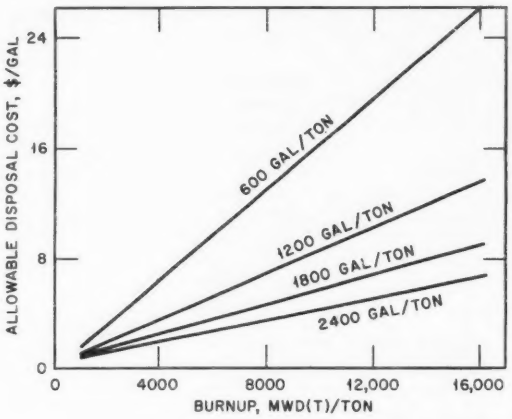

Figure 5 — Allowable waste-disposal cost.[4] (Power cost allocated to waste disposal = 2 per cent = 0.16 mill/kw-hr.)

result from the processing of each metric ton of uranium.

Although the total volume of waste indicated by Fig. 2 is quite large, it does not represent a problem of unfamiliar magnitude. As of 1957, the high-level wastes already in storage in the United States amounted to 72.7 million gallons, and the total tankage capacity at the major processing plants was 103.8 million gallons (170 tanks). (This was quoted by F. L. Culler, Jr., in his statement to the Joint Committee, from Status Report on Handling and Disposal of Radioactive Wastes in the AEC Program, USAEC Report WASH-742.) Thus the United States is already coping with at least twice as much waste as the nuclear-power industry is likely to generate through the year 1980.

To assess the significance of waste-disposal cost in the production of economic nuclear power, Bruce[4] assumed that power is to be produced for 8 mills/kw-hr of electricity and that 2 per cent of this cost, 0.16 mill/kw-hr, may be allocated to waste disposal. Figure 5 illustrates the allowable waste-disposal cost as a function of fuel burnup and of waste volume per ton of fuel. With burnups of 10,000 Mwd/ton and with 1200 to 1300 gal of waste per ton, the industry can, under these rules, afford to spend about $8 per gallon for permanent waste disposal.

In current practice the capital cost of tank storage for neutralized waste from aluminum-clad uranium fuel varies from 40 cents to $1 per gallon. If this cost proves to be typical, the power cost attributable to temporary high-level-waste storage may be about 0.02 mill/kw-hr. Whether the remaining 0.14 mill/kw-hr, which may be devoted to permanent disposal of both the high-level wastes and the low-level wastes, is likely to be adequate remains to be seen.

Although the exact life expectancy of the present tanks is unknown, comparison of an estimated tank life of 20 to 35 years with the 500 to 1000 years required for decay of Sr^{90} and Cs^{137} makes the present tanks appear unattractive as permanent disposal facilities. The temporary nature of tank storage seems to be generally accepted by the majority of experts in this field.

It is apparent, then, that, by the time nuclear power is to become competitive on a large scale, cheaper methods of ultimate disposal must be well enough established to permit the industry to proceed without heavy economic penalties for long-term storage. It is equally apparent that, while more permanent methods of waste disposal are being devised, present AEC methods of

waste management are adequate to protect the public, that reactors can be operated, and that the development of a nuclear-power industry can proceed.

The present lack of an economic solution to the problem of ultimate waste disposal does not in any way imply that the present handling of wastes is inadequate from the standpoint of public safety. Present waste management practices afford excellent containment of high-level waste and tight control, based strictly on accepted maximum permissible concentration (MPC) standards, of the release of low-level wastes, which presently constitute practically all the wastes released to the environment. The average radiation dose delivered to the environment by this release is very low; at present, medical exposure to ionizing radiation constitutes essentially all the man-made radiation exposure (from the statement of K. Z. Morgan, ORNL, to the Joint Congressional Committee).

The problem of ultimate waste disposal is, then, an economic one. The present method of handling the waste problem does not produce a hazard to the general public now, nor will it produce a hazard in the future; but its costs will become burdensome over a period of many years. A cheaper method of ultimate disposal will be needed by the time nuclear power accounts for a substantial fraction of the total power generation, or a few years thereafter, if the contribution of waste disposal to the cost of power is to be low.

Ultimate Disposal of High-Level Wastes

The various methods being studied for ultimate disposal of high-level wastes are summarized in Table I-4. Although the details of each method will not be discussed in this review, comments on some aspects of the general problem are in order.

Heat Generation

The heat generated by high-level wastes does not appear convenient as a practical source of power, but it is sufficient to impose definite limitations on disposal methods. For example, in the case of disposal of wastes to salt domes, if high-level wastes are to be stored without dilution after six years of cooling time, the diameters of the storage cavities would have to be limited to 10 to 20 ft to keep the stored solution below the boiling point (see Fig. 6). Similarly, for methods in which the wastes are trapped in glass, for example, burial of a single isolated glass sphere 15 cm in diameter at a depth of 300 cm would result in a glass surface temperature of 200°C, whereas burial of a continuous row of spheres would raise the surface temperature to 960°C. At temperatures of 900°C, serious volatilization of ruthenium occurs, and volatilization of cesium may occur at even lower temperatures. An interesting sidelight to this problem is that, in cases such as the salt domes, the temperatures are not expected to reach maximum values for approximately 40 years. This makes large-scale verification of calculations a long-term experiment. It appears that the limited heat-dissipation capabilities of natural environments will limit the effective concentration of stored wastes to considerably lower values than one might otherwise be able to achieve. In this regard, even crude decontamination methods for extracting part of the strontium and cesium from the wastes would be of help in reducing the heat generated by the material to be stored.

Transuranic Elements

The recycling of power-reactor fuel will result in the production of substantial quantities of transuranic elements which are second only to Sr^{90} and Cs^{137} with regard to long-term hazard. The approximate quantities of the most important of these elements that would be accumulated in the waste system by 1990 are (for the previously assumed growth curve of nuclear power):

Am^{241} ($T_{1/2}$ = 458 years), 4.8×10^5 curies
Pu^{238} ($T_{1/2}$ = 86.4 years), 3.3×10^5 curies
Pu^{239} and Pu^{240} ($T_{1/2}$ = 24,360 years and 158 years, respectively), 1.2×10^5 curies
Cm^{242} ($T_{1/2}$ = 162.5 days), 1.4×10^6 curies

In recycled or otherwise highly irradiated fuel, Pu^{238} is formed by successive neutron captures by U^{235}, U^{236}, and Np^{237}. Plutonium-239 captures a neutron to produce Pu^{240}. Americium-241 is obtained from neutron capture by Pu^{240} to give Pu^{241} which decays to Am^{241}. Curium-242 arises when Am^{241} captures a neutron to form Am^{242} which then decays to Cm^{242}.

Table I-4 SUMMARY OF METHODS CURRENTLY BEING CONSIDERED FOR ULTIMATE DISPOSAL OF HIGH-LEVEL WASTES

Disposal methods	Some advantages and disadvantages of the methods	Status of studies	Estimated cost of disposal
	Waste in Liquid Form		
Storage of liquid in hollow cavities in natural rock salt formations (also being considered for storage of solids)	Salt formations are solid, nonporous, and do not tend to develop cracks because salt undergoes plastic flow If salt domes are used for solids storage, no water will come in contact with stored materials Formations are homogeneous with limited but predictable heat-transfer characteristics Wastes are probably recoverable in most cases, if desired Maximum cavity size may be seriously limited by heat-dissipation requirements Cavities may tend to migrate due to dissolution of roof by condensation of water thereon	Field tests are now under way in salt mines	For experiments $1.82 per gallon; ultimately 2 to 10 cents per gallon
Pumping liquid wastes down deep wells into porous strata deep in the earth	Volume of wastes which can be stored in a single porous bed is very high Proof of suitability of a given formation is extremely difficult and costly; heat removability is hard to prove Waste recovery would be almost impossible if formation ruptures or is otherwise unsuitable Premature plugging of porous bed can limit capacity	Preliminary studies completed	85 cents per gallon of high-level waste
	Waste Converted to Solid Form		
Adsorption on clay followed by firing to fix activity on solids	Wastes are in a relatively concentrated, noncorrosive, chemically bonded form which is leach resistant and immobile Decontamination factors for Sr^{90} are fairly good Rather extensive handling of wastes is required, and wastes must be heated to ~1700°F during process	Pilot-plant studies are under way	
Absorption by porous ceramic sponges	Porous ceramic sponges can be made to absorb 200 per cent of their weight of Purex wastes Wastes are immobile and become leach resistant after firing Volume occupied by sponge plus wastes is slightly larger than original waste volume	Large-scale laboratory studies are under way	

Table I-4 (Continued)

Disposal methods	Some advantages and disadvantages of the methods	Status of studies	Estimated cost of disposal
	High-temperature firing at 1300°C may volatilize fission products		
Incorporation into glass	Wastes are trapped chemically in an immobile, leach-resistant refractory Glass readily accepts up to 5 wt.% metal ions Volatilization of ruthenium and cesium occurs at processing temperature (~1300°C)	Large-scale laboratory studies are under way; tests involve several thousand curies in samples	About 0.01 mill/kw-hr for storage plus 1.6 to 2.5 cents per liter of waste solution for processing
Fluidized-bed calcination	Volume reduced to $\frac{1}{8}$ that of original liquid wastes Relatively low temperature of 400 to 500°C used volatilizes only ruthenium Water leach will remove strontium and cesium Major dust and off-gas problems exist during processing	Pilot-plant studies have been made; demonstration test facility is under way	58.2 cents per gallon for processing; $1.24 per gallon for storage
Extraction of specific fission products	Extremely high concentration factors can be obtained ($\sim 10^4$) Wastes are put into forms useful as sources, etc. Decontamination factors as high as 10^{10} for Cs^{137} and 3×10^7 for Sr^{90} can be obtained Products are well contained, but costs are high A disadvantage is that the aqueous waste from this process still requires ultimate disposal or at least interim storage	Pilot plant in operation	Costs uncertain owing to dependence on market for products

The quantities of plutonium shown above are based on an assumed loss of 0.1 per cent of plutonium in the fuel during processing. The chemical behavior of americium and curium is similar to that of the rare earths. Any program aimed at chemically extracting hazardous isotopes from wastes prior to discharge must deal with the transuranic elements in addition to the fission products; however, the process chemistry of americium and curium is not well understood at this time.

Solid Fixation

The advantages claimed for solid fixation are as follows:

1. Solids should be retainable in a specific storage location indefinitely with little loss to the surroundings.

2. In the event of floods, earthquakes, or man-made disturbances, solids offer excellent containment.

3. Since water is removed in the process of producing the solids, quite high final concentrations of wastes can be achieved, thus reducing storage volumes.

4. Containment structures for solids can be much simplified since solids are not mobile and are noncorrosive.

5. Solids can safely be allowed to reach higher temperatures in storage than liquids.

From the preceding list it may be noted that many of the advantages claimed for the use of solids do not necessarily require that they be highly leach resistant. Although resistance to leaching by ground water or sea water is highly desirable, it is only essential where the dis-

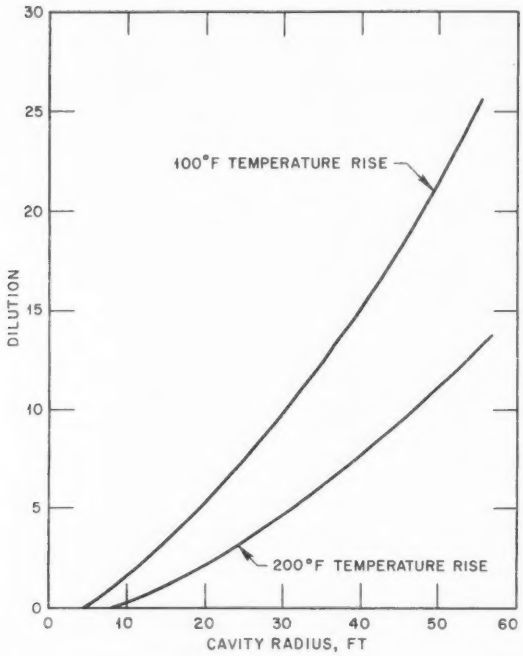

Figure 6 — Dilution requirements of fuel-processing waste stored in salt domes (basis: reactor specific power, 33 Mwd/ton; irradiation level, 10,000 Mwd/ton; waste cooled six years prior to storage; dilution of the initial 800 gal of waste per ton of uranium).[7]

posal method does not provide any protection for the stored solids. Much of the development work at present is still aimed at achieving truly "nonleachable" solids, and preliminary results indicate that this may be a difficult goal to achieve. For example, in tests with nepheline syenite glass, leach rates of only 3×10^{-7} g/cm^2 per day were observed. Even so, the calculated value for the maximum allowable leaching rate for this case was 5×10^{-11} g/cm^2 per day in order to keep the Sr^{90} activity in the water contacting the glass below 8×10^{-10} curie/liter [MPC* for drinking water by International Commission on Radiological Protection (ICRP) standards.] Results of leaching tests for fired clays are shown in Fig. 7.

Incidentally, leachability, as might be expected, is a very uncertain characteristic since minor variations in chemical composition of the leach solutions (the composition of natural ground waters varies widely) can completely alter the leach rate.

*MPC for Sr^{90} is now 1×10^{-9} curie/liter.
Ref. NBS Handbook 69

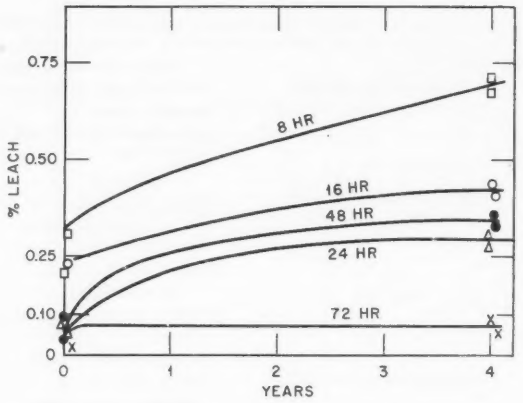

Figure 7 — Mixed fission products leached from clay fired for the times shown on the curves.[8]

Reduction of Waste Volumes

As mentioned earlier, the decladding solutions used in fuel-element processing increase total waste volumes significantly. The substitution of mechanical stripping of cladding for chemical decladding in the case of UO_2 clad with stainless steel or zirconium should materially reduce the volume of intermediate-level wastes produced. Refinements in processing techniques can also assist materially to reduce the volume of wastes to be handled. For example, at the Savannah River Laboratory, the volume of waste generated from processing one unit of uranium has been steadily reduced from 1000 gal in 1955 to 115 gal in 1959.

Transportation and Plant Location

High-level wastes pose a distinct transportation problem, especially if they are in the liquid form rather than fixed in solids. The costs of transporting large quantities of high-level liquids, with adequate control of the hazards involved, are so great that it may be most economical to construct the processing plants only at sites where natural formations are available if methods such as salt-dome or deep-well disposal are ultimately selected.

Utilization of Wastes

Many hopeful opinions have been expressed that eventually enough practical applications would be found for active isotopes to generate a

market demand for fission products. At the present time the prospects of this market demand becoming large enough to significantly reduce waste-disposal requirements appear remote. The decontamination effected by removing, say, 90 per cent of a particular isotope in the course of isotope recovery is not significant when about 99.999999 per cent removal is required to meet MPC values for free discharge. Generally, processes aimed at isotope production cannot economically achieve the very high degrees of decontamination, although some pilot-plant work at ORNL has shown promise in this direction. From the economic point of view, however, the utilization of portions of the waste might provide additional revenue from which part or all of the cost of ultimate disposal might be paid.

Sea Disposal

Although the total dilution capacity of the oceans is tremendous (total volume >300 million cubic miles), disposal of high-level wastes to the oceans is generally not considered practical at this time. The complexity of ocean currents and marine ecology make predictions of the fate of radioactive materials in this environment too uncertain to warrant the release of very high-level wastes. Furthermore, the complete irreversibility of this process makes it impossible to take corrective action once wastes have been released. Reconcentration of specific isotopes by marine organisms which may involve reconcentration factors as high as 10^4 or more also adds uncertainty to predictions of safe levels for disposal.

As a result of the above factors, practice in the United States has been to limit the use of ocean disposal to relatively small amounts of low- and intermediate-level wastes.

For example, for the year 1957, total sea disposal amounted to only 686 55-gal drums of solidified wastes. Since 1946, total sea disposal by AEC has amounted to 45,000 drums containing about 22,000 curies, plus reactor structures from the *Seawolf* prototype reactor at West Milton, N. Y., estimated to contain 33,000 curies of induced activity in stainless steel. Disposal by AEC licensees accounted for about 2600 curies in addition to the above amounts.

British practice has encompassed a considerably greater use of sea disposal. For about five years, carefully monitored experimental discharges of Windscale wastes to the coastal waters off Cumberland have been made at a mean rate of about 3000 curies per month (from H. J. Dunster, The Disposal of Radioactive Liquid Wastes into Coastal Waters, which is included in the record of the Hearings of the Joint Committee on Atomic Energy[2]). The results of this program have convinced the British that discharges up to 20,000 curies per month are safe and have indicated that discharges up to 100,000 curies per month may be safe. These discharge rates require the adoption of relatively high permissible levels of environmental contamination. For example, the permissible level adopted for shore sand is based on the assumption that no one regularly spends more than 100 hr per year on the sands and that a dose of 1.5 rads per year is permissible for the isotope mixtures involved. This policy resulted in adoption of permissible levels of 2.5×10^{-2} μc per gram dry weight for shore samples; for deep and extended layers of contaminated sand, this gives a dose of slightly less than 1.5 rads in 100 hr.

Low-Level Wastes

The volumes of low- and intermediate-level wastes generated generally exceed the volume of high-level wastes by a factor of 600 or more, and the chemical composition of these wastes varies widely. As a result, wastes of this type have usually been disposed of by dilution and by dispersal to the environment. Since it is usually impractical to completely contain low- and intermediate-level wastes, the primary problem becomes one of determining the capacity of the environment to receive these wastes without harmful effects. In most cases to date, it has been necessary to make detailed ecological surveys of each individual location prior to the release of wastes and to follow these studies by extensive monitoring programs. Even with these precautions the possibility of changes in the situation with time must be taken into account. For example, wastes released to rivers may become attached to silt in the bottom of the stream, causing the buildup of considerable activity which may be picked up at any time by flash floods and carried downstream in the concentrated form. Similarly, changes in the ionic composition of wastes discharged to the ground

can cause the release of accumulated materials and prevent readsorption of these materials as they pass on through soil layers. This phenomenon is observed in the case of Sr^{90}, in which calcium ions can cause the release of practically all the strontium trapped by some soils. Despite these problems, disposal to the ground and to various rivers has been successfully practiced on an extensive scale. Hanford, for example, over a period of 12 years, has discharged to the ground more then 3 billion gallons of low-level liquid wastes containing 2.4 million curies of gross beta activity.

Power plants will not always have the benefits of good natural disposal conditions. As the industry grows, the disposal of low-level wastes may become more difficult because of the additive effects of discharges from nearby plants and because plant sites with favorable meteorological, hydrological, and population characteristics may grow scarce. It would appear, however, that with the existing strict release limitations on new plants, few plants will benefit greatly from special site characteristics even in the near future. The present policy of the AEC is that, in normal operation, the effluent streams from the plant must not result in radiation levels (internal and external) at the site boundary or beyond which exceed the maximum permissible levels for continuous exposure. To meet this requirement, nuclear plants even now must be designed to minimize the amount of low-level waste that must be released.

There is still a question as to whether considerations of the general level of contamination of the environment will place a limit on the growth of the nuclear-power industry. It seems unlikely that this will occur if the present criterion of continuous-exposure tolerance on the site boundary is met. Admittedly this tolerance level, which is the level for individuals, is perhaps a factor of 10 higher than the level which will ultimately be adopted as the average for the public at large. There will be a continuous contribution to the contamination of the environment as a whole, whereas the contribution of an individual plant to the contamination of its surroundings occurs only during the 20- to 30-year life of the plant. Nevertheless, the ratio of the populated area of the country to the area devoted to plant sites will be very large (even after the nuclear-power industry becomes large), and general contamination by low-level wastes should not limit the growth of the industry in the predictable future.

Conclusions

The following conclusions, which have significance for the future of the nuclear-power industry, appear to be consistent with our present knowledge of the waste problem.

1. A proven economic method of ultimate disposal for the high-level wastes from fuel processing does not now exist. The present method of handling the problem, by tank storage, does not produce any hazard to the general public and is not unduly expensive over a relatively short period; however, since the wastes retain important activity for hundreds of years, liquid tank storage in its present form can be considered only a temporary expedient.

2. A nuclear-power industry of significant magnitude could operate for some few decades on the basis of tank storage of high-level wastes without requiring excessively large tank capacity. For example, if by 1985 the nuclear-power generation in the United States reaches a level equal to half the present total electric generation, the extra storage capacity filled by the power reactors will probably be comparable to the presently stored waste volume. This will amount to something like 10^8 gal, containing some 2×10^{10} curies of fission products and generating heat at a rate of about 100 Mw.

3. Since the required tankage will increase roughly as the time integral of the nuclear-power generation, tank storage will hardly be attractive for more than a few decades. Ultimate disposal must be achieved at a cost of about $8 per gallon* if the contribution of disposal to power cost is not to exceed an arbitrary level of 0.16 mill/kw-hr.

4. A number of promising methods of ultimate disposal are under investigation and development. There is little doubt that they include feasible methods; the cost estimates are favorable but are as yet inexact.

5. Disposal by dilution in the sea will probably not be used for high-level wastes. The safe capacity of the seas for low- and intermediate-level wastes is large, but its large-scale use is

*This would correspond to a cost in the range 1 to 10 cents per curie for cooling times in the range 2 to 20 years before ultimate disposal.

complicated by the problems of getting the waste out into the general body of the sea water.

6. It is unlikely that the utilization of radioactive wastes will reduce significantly the ultimate requirement for disposal; however, the revenues from such utilization would contribute to the solution of the economic problem of disposal.

7. Low-level wastes presently account for almost all the wastes released to the general environment. Present limits on discharge to the environment from individual plants appear to be adequate for the safety of the general public, even in a large-scale nuclear-power industry. However, if a high density of nuclear plants develops in some areas at some future time, the local problem of low-level waste disposal may become more acute.

References

1. *Major Activities in the Atomic Energy Programs, January–December 1959*, U. S. Government Printing Office, Washington, January 1960.
2. *Industrial Radioactive Waste Disposal, Hearings Before the Special Subcommittee on Radiation of the Joint Committee on Atomic Energy, Congress of the United States (86th Congress)*, Vols. 1 to 5, U. S. Government Printing Office, Washington, 1959.
3. *Industrial Radioactive Waste Disposal, Summary-Analysis of Hearings January 28, 29, and 30; February 2 and 3; and July 29, 1959, Joint Committee on Atomic Energy, Congress of the United States (86th Congress)*, U. S. Government Printing Office, Washington, 1959.
4. Statement of F. R. Bruce, in *Industrial Radioactive Waste Disposal, Hearings Before the Special Subcommittee on Radiation of the Joint Committee on Atomic Energy, Congress of the United States (86th Congress)*, Vol. 3, pp. 2345–2354, U. S. Government Printing Office, Washington, 1959.
5. J. A. Lane, Determining Nuclear Fuel Requirements for Large-Scale Industrial Power, *Nucleonics*, 12(10): 65 (October 1954).
6. J. O. Blomeke, in Status Report on the Disposal of Radioactive Wastes, USAEC Report CF-57-3-114(Rev.), p. 68, Oak Ridge National Laboratory, June 25, 1957.
7. E. F. Gloyna et al., Summary Report, Reactor Fuel Waste Disposal Project, in *Industrial Radioactive Waste Disposal, Hearings Before the Special Subcommittee on Radiation of the Joint Committee on Atomic Energy, Congress of the United States (86th Congress)*, Vol. 3, p. 2246, U. S. Government Printing Office, Washington, 1959.
8. L. P. Hatch, Fixation of Radioactive Wastes in Stable Solids, in *Industrial Radioactive Waste Disposal, Hearings Before the Special Subcommittee on Radiation of the Joint Committee on Atomic Energy, Congress of the United States (86th Congress)*, Vol. 3, p. 1843, U. S. Government Printing Office, Washington, 1959.

Section II

REACTOR PHYSICS

Recent Critical and Exponential Experiments

The initial publication of the Argonne Reactor Physics Constants Center[1] contains summaries of the results of the more significant critical and exponential experiments which had been reported prior to its publication. A considerable number of experiments have been reported since then, both in the papers of the 1958 Geneva Conference and elsewhere. It is not practical to summarize the results here in the detail that would be necessary for usefulness. However, a list of the experiments has been compiled in Tables II-1a to II-1c which should serve to guide the reader to those reports that may be of use to him.

Fission-Product Poisoning

Studies of neutron absorption in reactors by fission products have been summarized, up to 1958, in the publication of the Reactor Physics Constants Center.[1] A rather comprehensive study is also reported in the 1958 Geneva Conference paper of Gordeev and Pupko,[60] and a study by Pattenden[61] appeared in 1959. Recent analyses by Greenhow and Hansen[62] and by Nephew[63] have given particular attention to the effect of the neutron energy spectrum on the poisoning effects of fission products.

Reference 62 considers only the case of the fission products of U^{235}. It avoids the complications of radioactive decay by treating all fission products with half lives less than 50 hr as though they decayed instantaneously and all those with half lives greater than 50 hr as though they were stable. Unless some such simplification is made, the poisoning effect cannot be treated independently of the reactor power schedule.

The neutron energy spectrum is approximated as a Maxwellian distribution plus a $1/E$ component covering the energy range from 4 kT to 10^5 ev. This approximate spectrum may be completely specified by the characteristic temperature T of the Maxwellian distribution and by the ratio (A) of the total epithermal flux (ϕ_{epi}) to the total thermal flux (ϕ_{th}):

$$A = \frac{\int_{4kT}^{10^5 ev} \phi_{epi}\ (E)\, dE}{\int_{0}^{4kT} \phi_{th}\ (E)\, dE}$$

The fission-product absorption cross sections were all assumed to vary as $1/v$ in the thermal region; the cross-section values were those of USAEC Report BNL-325(2nd Ed.). In those cases for which no epithermal data were available, the $1/v$ variation was assumed to hold up to the upper energy limit considered, 10^5 ev. In most cases, however, the epithermal cross sections were either taken from the data of Westcott[64] or computed by (1) using the statistical analysis of Greebler et al.[65] for the energy range from 10^2 to 10^5 ev and (2) assuming $1/v$ dependence, or integrating over the known resonances, for the energy range from 4 kT to 10^2 ev.

The computed average cross section per fission fragment is listed, for U^{235}, as a function of percentage burnup of the U^{235}, in Table II-2. The effects of all fission products except Xe^{135} are included; in addition, the effect of U^{236} is included as though it were a fission product of yield 18.8 per cent. The average cross section per fission fragment decreases with continuing exposure to neutron flux, since the fission products having the higher absorption cross sections absorb, relatively, the most neutrons and, on the aver-

Table II-1a RECENT REPORTS OF CRITICAL AND EXPONENTIAL EXPERIMENTS: HEAVY-WATER-MODERATED LATTICES

Type of assembly	Type of fuel element	Reference	Quantity measured
		Savannah River Laboratory (U. S.)	
Critical and exponential	U metal plates; U rod clusters; U tubes; UO_2 rod clusters	2–5	Material buckling (D_2O and gas coolants); fast-to-slow fission ratio; coolant removal from fuel tube; temperature coefficient; light-water poisoning; control-rod studies; void coefficient; flux distribution; effect of bayonet tubes; worth of safety system
		Saclay Center for Nuclear Studies (France)	
Critical	U metal plates; U rods and rod clusters; UO_2 rod clusters	6	Material buckling; anisotropy; temperature coefficient; reactivity variation as a function of the geometric buckling; fine flux distribution; coolant removal
		AB Atomenergi (Sweden)	
Exponential	UO_2 rod clusters; U rods and rod clusters	7–9	Buckling; disadvantage factors; effective resonance integral; diffusion length in D_2O; temperature coefficient; control-rod effectiveness
		Chalk River (Canada)	
Critical	U rods and rod clusters; UO_2 rod clusters	10	Buckling; fine-flux distribution; fast-fission ratio; effective resonance integral; initial conversion ratio
		Dutch-Norwegian Establishment for Nuclear Energy Research (Norway)	
Exponential	UO_2 rod clusters	11	Temperature coefficient; buckling
		Hanford Atomic Products Operation (U. S.)	
Critical	UO_2 rod clusters; UO_2 and Pu-Al alloy rod combinations	12–17	k_∞; thermal utilization; flux-traverse data; resonance escape probability; fast-fission factor; initial conversion ratio; metal temperature coefficient of k_∞
		Argonne National Laboratory (U. S.)	
Exponential and critical	ThO_2-UO_2 rods and rod clusters	18	Buckling; reflector savings; resonance escape probability; neutron age τ; disadvantage factor; void coefficient of reactivity; worth of cross and blade control elements

Table II-1b RECENT REPORTS OF CRITICAL AND EXPONENTIAL EXPERIMENTS: LIGHT-WATER-MODERATED LATTICES

Type of assembly	Type of fuel element	Reference	Quantity measured
		Brookhaven National Laboratory (U. S.)	
Exponential	U rods	19	Material buckling; reflector savings; thermal utilization; ratio of the fission rate in U^{238} to that in U^{235}; ratio of epicadmium to subcadmium fission rates in U^{235} and capture in U^{238}; effective neutron temperature in the moderator; temperature coefficient; buckling coefficient; migration area; buckling for plutonium lattice

(Table continues)

Table II-1b (Continued)

Type of assembly	Type of fuel element	Reference	Quantity measured
		Hanford Atomic Products Operation (U. S.)	
Critical and exponential	U rods	20–25	Poisoned moderator; critical masses; reflector savings (extrapolation lengths); material buckling; criticality measurements; buckling for fuel elements in random arrays
		Knolls Atomic Power Laboratory (U. S.)	
Critical	U rods	26, 27	Temperature coefficient
		Bettis Atomic Power Laboratory (U. S.)	
Critical	U rods	28, 29	Fission rates for U^{235}, Pu^{239}, and Pu^{241}; thermal utilization; resonance escape probability; fast-fission ratio; interaction effect for resonance neutrons due to neighboring rods (U and UO_2 rods)
		Westinghouse Reactor Evaluation Center (U. S.)	
Critical	UO_2 fuel rods (stainless-steel-clad)	19	Critical size; buckling; reflector savings; migration area; disadvantage factor; temperature coefficient; void coefficient; control-rod worths and interactions; flux distribution with partially inserted control rods, through water gaps and stainless-steel regions
Critical	UO_2 rods	30, 31	Loose-lattice experiments; critical core sizes; reflector savings
Critical	UO_2 rods	32	Thermal-flux peaking in moderator adjacent to fuel region
		Harwell (U. K.)	
Exponential	U rods	33	Buckling; neutron fine structure; intensity of the epithermal group; neutron temperature; fast-fission factor; conversion factor
		Battelle Memorial Institute (U. S.)	
Critical (GCRE)	Highly enriched U fuel	34–36	Critical mass; flux power distribution; thermal utilization; temperature coefficient; worth of control and safety-shutdown blades; reactivity effect of changes in axial reflector material; reactivity effect and power perturbation caused by fast safety-control-blade guides; effect of changes in fuel-element material composition; effect of changes in fuel-element spacing designed to produce uniform radial power-generation rates; detailed intracell flux distribution
		Oak Ridge National Laboratory (U. S.)	
Critical	Enriched U metal slabs; enriched U metal slugs	37	Reactivity effects of large voids in the reflector; multiplication measurements of critical parameters
		Idaho Operations Office – Phillips Petroleum Co. (U. S.)	
Critical	Fully enriched UO_2 plates	38	Hot critical and cold initial critical studies; cold, clean critical loading; temperature coefficient; pressure coefficient; control-rod worth

Table II-1b (Continued)

Type of assembly	Type of fuel element	Reference	Quantity measured
		Babcock & Wilcox Co. (U. S.)	
Critical	UO_2 fuel pins	19	Reactivity versus water height; buckling; temperature coefficient; cadmium ratio; disadvantage factor; control-blade worth; integral water height; k_{eff}
Critical	Th metal rods and plates; ThO_2 rods	39	Effective resonance integral

Table II-1c RECENT REPORTS OF CRITICAL AND EXPONENTIAL EXPERIMENTS: GRAPHITE-MODERATED LATTICES

Type of assembly	Type of fuel element	Reference	Quantity measured
		Hanford Atomic Products Operation (U. S.)	
Exponential	U rods; tube-in-tube; U rod clusters	40–44	Material buckling; thermal utilization; k_∞ for rod and rod clusters
		Atomics International (U. S.)	
Exponential	Multirod U fuel clusters; multirod Th-U fuel clusters	45–47	Buckling; intracell flux distribution; thermal utilization; resonance escape probability; diffusion length for AGOT graphite
		Calder Hall (U. K.)	
Critical	U rods	48	Axial and radial flux distribution; buckling; extrapolation length; control-rod calibration; temperature coefficient
		Harwell (U. K.)	
Exponential	U rods	33	Buckling; neutron fine structure; intensity of the epithermal group; neutron temperature; fast-fission factor; conversion factor
		Commissariat à l'Énergie Atomique (France)	
Critical*	Pu homogeneous	49	Critical mass; control-rod calibrations; temperature coefficient; axial and radial thermal- and resonance-neutron-flux distribution
Critical†	U cartridges; U-Th lattice	50	Buckling; thermal utilization; resonance escape probability; diffusion length in graphite; flux distribution, gross and fine; anisotropic effect of the channels on diffusion in the graphite; anisotropy of lattices; reflector economy; variation of Laplacian with the uranium diameter
		Brookhaven National Laboratory (U. S.)	
Exponential (graphite-bismuth)		51	Thermal-diffusion length in graphite; transport mean free path in graphite, bismuth, and two mixtures of graphite and bismuth; age to indium resonance in graphite and in one of the two mixed systems

(Table continues)

Table II-1c (Continued)

Type of assembly	Type of fuel element	Reference	Quantity measured
		Oak Ridge National Laboratory (U. S.)	
Critical	Aqueous solution of UO_2F_2 fully enriched in U^{235}	52–54	η for U^{233} and Pu^{239}; poisoning effect of copper lattices; radial flux measurements; buckling; critical and kinetic data
		Hanford Atomic Products Operation (U. S.)	
Critical	H_2O-UO_3 homogeneous mixture	17, 55–57	k_∞
		Atomics International (U. S.)	
Exponential	U rods with liquid diphenyl moderator	58	Transport mean free path; diffusion length and slowing down length for moderator; buckling and thermal-flux distribution within lattice cell for lattices
		Los Alamos Scientific Laboratory (U. S.)	
Critical	UO_3–H_3PO_4 solution	59	Critical mass

*"Proserpine," a homogeneous critical experiment with plutonium.
†Department of Reactor Studies, Marcoule, France.

Table II-2 AVERAGE THERMAL AND EPITHERMAL ABSORPTION CROSS SECTIONS[62] PER FISSION FRAGMENT FOR THE FISSION PRODUCTS OF U^{235}

($\sigma_{eff} = \sigma_{th} + A\sigma_{epi}$)

Fractional burnup of U^{235}	σ_{th}, barns	σ_{epi}, barns	$\sigma_{epi,1/v}$,* barns
0.1	59.0	14.2	4.82
0.2	37.7	11.7	3.08
0.3	29.7	10.6	2.43
0.4	25.5	9.84	2.08
0.5	22.7	9.24	1.86
0.6	20.6	8.70	1.69
0.7	18.9	8.24	1.55
0.8	17.3	7.76	1.42

*This column gives the epithermal cross section that would be consistent with the listed thermal cross section if the cross sections of all fission products varied as $1/v$.

age, are transmuted to isotopes having lower cross sections. The neutron exposure level is conveniently expressed in terms of the fractional burnup of the U^{235}.

Table II-2 lists also, for comparison, the quantity $\sigma_{epi,1/v}$. This is the epithermal cross section that would be consistent with the thermal cross section if the cross sections of all fission products varied as $1/v$.

The reference states that for $A = 0$ (i.e., for purely thermal absorption) the average cross sections lie within a few per cent of those previously computed by Deutsch.[66]

The treatment in reference 63 is somewhat different and covers the fission products of U^{233} and Pu^{239} as well as those of U^{235}. The analysis covers only the low-cross-section fission products (those having absorption cross sections less than about 500 barns). The remaining high-cross-section products are listed in Table II-3.

Table II-3 HIGH-CROSS-SECTION FISSION PRODUCTS[63]

Fission product	Half life	σ_0, barns	y* for U^{235}, %	$y\sigma_0$, barns per fission
Xe^{135}	9.2 hr	2.72×10^6	6.3	1.714×10^5
Sm^{149}	Stable	40,800	1.13	461.04
Sm^{151}	80 years	10,000	0.45	45.00
Gd^{155}	Stable	61,000	0.03	18.30
Gd^{157}	Stable	240,000	0.0078	18.72
Eu^{155}	1.9 years	14,000	0.03	4.20
Cd^{113}	Stable	20,000	0.01	2.00

*y = yield.

In all but one case, the analysis neglects the absorption cross sections of nuclides formed by neutron absorption in the members of the pri-

mary fission-product chains. The single exception to this "first order" treatment is the mass chain 151.

As in reference 62, the simplification is made (with one exception) that nuclides with short half lives decay instantaneously and that nuclides with long half lives are stable. The exception is Pm^{147}, which is an important contributor to the gross fission-product absorption and which has a half life of 2.65 years. In this case the radioactive decay rate is added to the rate of destruction of the nuclide by neutron absorption on the assumption of a neutron-flux level corresponding to a specific power of 2000 kw per kilogram of fissionable isotope. Variations from this specific power by ±1000 kw per kilogram have only minor effects.

In computing the concentrations of the various nuclides as functions of exposure, the neutron spectrum is assumed to consist of a Maxwellian distribution at a temperature of 1000°K plus a $1/E$ component above 5 kT. The thermal absorption cross sections of the various nuclides are taken from USAEC Report BNL-325(2nd Ed.); the resonance parameters in the range 5 kT to 10^2 ev are taken from the same compilation plus other sources. Above 10^2 ev the entire aggregate of the low-cross-section fission products is treated as a unit, and the estimate of Gordeev and Pupko,[60] of 23 barns per fission, for the resonance integral above 10^2 ev, is adopted.

The results of the study for U^{233}, U^{235}, and Pu^{239} fission products are presented by deriving, for each fissionable isotope, a set of four pseudoelements, with specified thermal cross sections, resonance parameters, and yields, which will approximate the absorption effects of the true fission products.

Table II-4 YIELDS, THERMAL CROSS SECTIONS, AND ENERGY-DISTRIBUTED EXCESS RESONANCE INTEGRALS OF THE PSEUDOELEMENTS REPRESENTING THE FISSION-PRODUCT AGGREGATES OF U^{235} (FROM REFERENCE 63)

Pseudoelement No. 1 (γ = 11.24%; $g\sigma_0$ = 216.81 barns; I_T = 71.0 barns)		Pseudoelement No. 2 (γ = 21.0%; $g\sigma_0$ = 31.52 barns; I_T = 283.1 barns)				Pseudoelement No. 3 (γ = 5.82%; $g\sigma_0$ = 140.94 barns; I_T = 905.54 barns)	
E_0, ev	I_{res}, barns	E_0, ev	I_{res}, barns	E_0, ev	I_{res}, barns	E_0, ev	I_{res}, barns
56	7.206	4.37	22.790	40.9	4.714	1.257	504.261
66.2	0.039	5.62	31.238	43.1	23.010	14.1	346.220
71.8	3.559	5.90	91.729	45.0	28.781	46.5	0.378
72.4	0.472	9.80	11.571	46.3	0.195	68.0	0.052
73.5	5.071	15.2	6.571	47.8	4.643	95.0	0.464
85.5	1.246	20.5	0.081	66.3	0.014	100.0	0
95.6	0.027	22.6	7.848	78.5	0.105		851.375
100	0	24.1	5.00	83.1	0.771		
	17.620	31.4	0.395	91.0	0.752		
		37.8	0.538	94.8	1.157		
				100	1.427		
					243.330		

Pseudoelement No. 4
(γ = 2.95%; $g\sigma_0$ = 129.15 barns; I_T = 2449.83 barns)

E_0, ev	I_{res}, barns	E_0, ev	I_{res}, barns	E_0, ev	I_{res}, barns	E_0, ev	I_{res}, barns
1.04	8.373	6.25	1.865	16.3	0.034	40.8	0.067
1.46	10.813	6.64	55.017	16.8	0.543	41.4	31.08
1.76	2.068	7.00	139.457	18.1	1.085	43.2	6.339
2.46	21.865	7.60	0.305	18.8	1.119	47.2	21.593
3.29	9.525	8.1	710.169	20.0	14.508	50.3	16.610
3.86	0.170	8.87	4.847	20.1	2.644	56.7	0.102
3.94	7.424	9.10	0.136	21.1	0.136	72.4	0.170
4.81	0.271	11.7	2.712	24.1	0.509	89.0	0.067
5.20	13.254	13.3	0.102	30.9	0.203	100	0
5.43	1254.949	15.6	13.186	33.4	11.763		2365.080

The characteristics of the four pseudoelements representing the U^{235} fission products are given in Table II-4. Listed for each pseudoelement is: the yield (y); the product of the 2200 m/sec cross section (σ_0) and the factor (g) which, in the Westcott notation,[64] takes account of the departure from $1/v$ behavior in the thermal region; the total excess resonance integral (excess over the $1/v$ integral) from $5\,kT$ to 10^6 ev (I_T); and the excess resonance integrals (I_{res}) for individual resonances, along with the individual resonance energies (E_0). The total excess resonance integral is larger than the sum of the individual integrals because of the contribution of the resonances above 10^2 ev. The reference also contains a table of effective thermal cross sections for the pseudoelements for neutron temperatures ranging from 69 to 2704° F.

Table II-5 shows the results of an application of the pseudoelements to compute the effective cross sections and resonance integrals of the U^{235} fission products for various degrees of fuel burnup and for several different ratios of thermal-to-epithermal flux. For comparison, the computations have also been made by summing directly over the fission products. In the table, P is the percentage of fissions due to the epithermal neutron flux, and F specifies the degree of burnup of the U^{235}.

$$F = \int \hat{\sigma}_f \, \phi(t) \, dt$$

where $\hat{\sigma}$ is the effective cross section over the entire neutron energy spectrum.

Table II-5 VARIATION OF THE U^{235} FISSION-PRODUCT AGGREGATE ABSORPTION CROSS SECTION WITH FRACTIONAL BURNUP AND FLUX SPECTRUM AT A NEUTRON TEMPERATURE OF 1000°K AND A REACTOR SPECIFIC POWER OF 2000 KW/KG (FROM REFERENCE 63)

(U^{236} Is Not Included in the Aggregate)

P	Calculational method*	$F = 0$	$F = 0.5$	$F = 1.0$	$F = 1.5$	$F = 2.0$
		Thermal Cross Section, Barns per Fission				
0	A	43.00	39.23	36.02	33.27	30.90
	B	43.00	39.83	37.00	34.48	32.24
0.1	A	43.00	37.86	33.68	30.33	27.58
	B	43.00	38.26	34.32	31.02	28.22
0.2	A	43.00	36.64	31.95	28.33	25.45
	B	43.00	36.92	32.32	28.68	25.73
0.3	A	43.00	35.60	30.59	26.86	23.95
	B	43.00	35.77	30.74	26.96	23.94
0.4	A	43.00	34.72	29.49	25.73	22.81
	B	43.00	34.77	29.47	25.59	22.56
		Excess Resonance Integral Below 100 Ev, Barns per Fission				
0	A	172.40	161.11	151.41	142.65	134.82
	B	172.40	164.21	156.63	149.63	143.13
0.1	A	172.40	145.38	125.70	110.95	99.54
	B	172.40	146.76	127.55	112.76	101.13
0.2	A	172.40	131.64	107.24	91.07	79.54
	B	172.40	132.86	108.32	91.85	80.07
0.3	A	172.40	121.62	95.03	78.79	67.74
	B	172.40	121.59	94.76	78.55	67.13
0.4	A	172.40	112.71	85.27	69.47	59.02
	B	172.40	112.28	84.68	68.71	58.14

*Method A: Summing over the individual fission products.
Method B: Summing over the four pseudoelements.

Although, for a given mixture of nuclides, the thermal cross section and the excess resonance integral are both independent of P, the rate of destruction of the fission products by neutron absorption per unit of fuel burnup does depend on P; hence the variations with P in Table II-5.

The reference also provides, for each pseudoelement, a set of 32-group cross sections, which can be used to extend their usefulness to any multigroup calculation scheme that might be desired.

At the June 1960 meeting of the American Nuclear Society, other studies of fission-product poisoning were reported. Reference 67 is a description of a method of estimating the capture cross sections for those cases in which no measurements are available, and reference 68 is a description of the application of the method to the calculation of fission-product poisoning in a high-temperature graphite reactor. The results show that resonance capture makes an important contribution (at least 35 per cent) to the total fission-product poisoning and indicate that effective capture cross sections of 50 barns or less per fission, which have often been assumed in the past, are too low.

Reference 69 is a report on an investigation of the error which results when the radioactive decay of fission products is neglected or is treated only approximately in calculations of fission-product poisoning. A sample of UO_2 was irradiated to a burnup of 6300 Mwd/ton and was measured repeatedly in a reactivity facility over a period extending from 4 to 7200 hr after irradiation. The results indicated that the total poisoning effect of all fission products other than Xe^{135} and Sm^{149} decreases by about 13 ± 6 per cent over a period of a year. The results support the assumption that the gross effect of fission products may be approximated by an accumulation of

"stable" products dependent only upon the time-integrated neutron flux, plus an accumulation of a few transient isotopes.

References

1. Argonne National Laboratory, Reactor Physics Constants, USAEC Report ANL-5800, July 1, 1958.
2. G. Dessauer, Physics of Natural U–D_2O Lattices, A/CONF.15/P/590, Second United Nations International Conference on the Peaceful Uses of Atomic Energy, Geneva, 1958.
3. N. P. Baumann, Process Development Pile Measurements of Lattice Parameters of Natural Uranium in Heavy Water, USAEC Report DP-407, Savannah River Laboratory, July 1959.
4. D. S. St. John, Moderator Temperature Coefficients in Heavy Water Reactors, USAEC Report DP-452, Savannah River Laboratory, December 1959.
5. L. M. Arnett, comp., Heavy Water Components Test Reactor, Papers Presented to the American Nuclear Society on June 17, 1959, USAEC Report DP-413, Savannah River Laboratory, October 1959.
6. Y. Girard et al., Natural Uranium–Heavy Water Lattices, A/CONF.15/P/336, Second United Nations International Conference on the Peaceful Uses of Atomic Energy, Geneva, 1958.
7. B. Pershagen et al., Calculation of Lattice Parameters for Uranium Rod Clusters in Heavy Water and Correlation with Experiments, A/CONF.15/P/151, Second United Nations International Conference on the Peaceful Uses of Atomic Energy, Geneva, 1958.
8. R. Persson et al., Exponential Experiments on Heavy Water Natural Uranium Metal and Oxide Lattices, A/CONF.15/P/160, Second United Nations International Conference on the Peaceful Uses of Atomic Energy, Geneva, 1958.
9. C. E. Wikdahl and F. Akerhielm, Measurements of Disadvantage Factors in a Small Mock-Up, A/CONF.15/P/162, Second United Nations International Conference on the Peaceful Uses of Atomic Energy, Geneva, 1958.
10. D. W. Hone et al., Natural Uranium Heavy-Water Lattices, Experiment and Theory, A/CONF.15/P/212, Second United Nations International Conference on the Peaceful Uses of Atomic Energy, Geneva, 1958.
11. E. Anderson and O. Aspelund, Exponential Experiments with Uranium Oxide Clusters in Heavy Water, A/CONF.15/P/575, Second United Nations International Conference on the Peaceful Uses of Atomic Energy, Geneva, 1958.
12. F. C. Engesser and J. R. Lilley, Plutonium Spike Enrichment, in Nuclear Physics Research Quarterly Report for January, February, and March 1958, USAEC Report HW-55879, p. 16, Hanford Atomic Products Operation, Apr. 29, 1958.
13. J. R. Lilley and F. C. Engesser, k_∞ Measurements for a Three Piece, Annular UO_2 Fuel Element in an Eight-Inch Triangular D_2O Lattice, in Nuclear Physics Research Quarterly Report for January, February, and March 1958, USAEC Report HW-55879, p. 24, Hanford Atomic Products Operation, Apr. 29, 1958.
14. T. J. Oakes, Determination of Lattice Parameters for a 19-Rod UO_2 Cluster, in Nuclear Physics Research Quarterly Report for January, February, and March 1958, USAEC Report HW-55879, p. 26, Hanford Atomic Products Operation, Apr. 29, 1958.
15. J. R. Lilley and F. C. Engesser, Measurements of k_∞ for a UO_2-D_2O Lattice, in Nuclear Physics Research Quarterly Report for October, November, and December 1958, USAEC Report HW-59126, p. 16, Hanford Atomic Products Operation, Jan. 20, 1959.
16. F. C. Engesser, The Metal Temperature Coefficient for 19-Rod Clusters of Uranium Oxide with Air Coolant, in Nuclear Physics Research Quarterly Report for April, May, and June 1958, USAEC Report HW-56919, p. 46, Hanford Atomic Products Operation, July 21, 1958.
17. R. E. Heineman, Experience in the Use of the Physical Constants Testing Reactor, A/CONF.15/P/1929, Second United Nations International Conference on the Peaceful Uses of Atomic Energy, Geneva, 1958.
18. W. C. Redman and J. A. Thie, Properties of Exponential and Critical Systems of Thoria, Urania, and Heavy Water and Their Application to Reactor Design, A/CONF.15/P/600, Second United Nations International Conference on the Peaceful Uses of Atomic Energy, Geneva, 1958.
19. H. Kouts et al., Physics of Slightly Enriched, Normal Water Lattices (Theory and Experiment), A/CONF.15/P/1841, Second United Nations International Conference on the Peaceful Uses of Atomic Energy, Geneva, 1958.
20. R. C. Lloyd, Buckling Measurements for Fuel Elements in a Random Array, in Nuclear Physics Research Quarterly Report for January, February, and March 1958, USAEC Report HW-55879, p. 12, Hanford Atomic Products Operation, Apr. 29, 1958.
21. R. C. Lloyd and R. B. Smith, Criticality Measurements on Heterogeneous 3.1 Per Cent Enriched Uranium–Water Systems, p. 10; N. Ketzlach, Buckling Calculations for 3.0 Per Cent Enriched Uranium Dioxide Rod–Water Lattices, p. 18; N. Ketzlach, Buckling Calculations for 5.0 Per Cent Enriched Uranium Rod–Water Lattices, p. 24; in Nuclear Physics Research Quarterly Report for July, August, and September 1958, USAEC Report HW-57861, Hanford Atomic Products Operation, Oct. 20, 1958.
22. R. C. Lloyd et al., Criticality Measurements of Heterogeneous 3.1 Per Cent Enriched Uranium–Water Systems, in Nuclear Physics Research

Quarterly Report for October, November, and December 1958, USAEC Report HW-59126, p. 52, Hanford Atomic Products Operation, Jan. 20, 1959.

23. R. C. Lloyd, Exponential Experiments with Poisoned Moderator, p. 61; R. C. Lloyd et al., Criticality Measurements of Heterogeneous 3.1 Per Cent Enriched Uranium–H_2O Systems, p. 59; in Nuclear Physics Research Quarterly Report for July, August, and September 1959, USAEC Report HW-62727, Hanford Atomic Products Operation, Oct. 20, 1959.
24. R. C. Lloyd et al., Criticality Parameters for Lattices with 1.6 Per Cent Enriched Uranium Rods in Light Water, p. 22; R. C. Lloyd, Buckling Measurements for Fuel Elements in a Random Array Versus a Uniform Array, p. 20; in Nuclear Physics Research Quarterly Report for April, May, and June 1958, USAEC Report HW-56919, Hanford Atomic Products Operation, July 21, 1958.
25. R. C. Lloyd et al., Criticality Measurements of Heterogeneous 3.1 Per Cent Enriched Uranium–Water Systems, in Nuclear Physics Research Quarterly Report for April, May, and June 1959, USAEC Report HW-61181, p. 52, Hanford Atomic Products Operation, July 20, 1959.
26. G. D. Hickman and J. A. Bistline, Investigation of Temperature Coefficients Obtained from the Pressurized Test Reactor, in Reactor Technology Report No. 11, Physics, USAEC Report KAPL-2000-8, p. B.8, Knolls Atomic Power Laboratory, December 1959.
27. G. D. Hickman and J. A. Bistline, Investigation of Temperature Coefficients Obtained from Pressure Test Reactor, USAEC Report KAPL-M-GDH-1, Knolls Atomic Power Laboratory, July 23, 1959.
28. D. Klein, Plutonium Fission Rates, in Technical Progress Report, Reactor Physics and Mathematics for the Period September 1, 1959 to December 1, 1959, USAEC Report WAPD-MRJ-8, Westinghouse Electric Corp., Bettis Atomic Power Laboratory, 1959.
29. Westinghouse Electric Corp., Bettis Atomic Power Laboratory, Technical Progress Report, Reactor Physics and Mathematics for the Period December 1, 1959 to March 1, 1960, USAEC Report WAPD-MRJ-9, 1960.
30. Ira H. Coen, Quarterly Progress Report for the Period October 1 to December 31, 1959, USAEC Report WCAP-1408, Westinghouse Electric Corp., Atomic Power Dept., Jan. 30, 1960.
31. Ira H. Coen, Quarterly Progress Report for the Period June 1 to September 30, 1959, USAEC Report WCAP-1404, Westinghouse Electric Corp., Atomic Power Dept., Oct. 30, 1959.
32. Robert A. Dannels and Walter J. Eich, Neutron Flux Peaking and Power Shapes: A Comparison of Theory and Experiment, USAEC Report YAEC-151, Westinghouse Electric Corp., Atomic Power Dept., October 1959.
33. C. G. Campbell and I. S. Grant, Critical and Subcritical Experiments with a Two-Group Correlation of Results, A/CONF.15/P/40, Second United Nations International Conference on the Peaceful Uses of Atomic Energy, Geneva, 1958.
34. David A. Dingee et al., Further Studies with the GCRE Critical Assembly, USAEC Report BMI-1306, Battelle Memorial Institute, Dec. 29, 1958.
35. David A. Dingee et al., GCRE Critical-Assembly Studies, USAEC Report BMI-1288, Battelle Memorial Institute, Sept. 10, 1958.
36. Richard A. Egen et al., ML-1-1A Core Studies with the GCRE Critical Assembly, USAEC Report BMI-1396, Battelle Memorial Institute, Nov. 27, 1959.
37. A. B. Reynolds et al., Reactivity Effects of Large Voids in the Reflector of the Pool Critical Assembly, p. 3; J. K. Fox and L. W. Gilley, Critical Parameters of Slightly Enriched Annular Cylindrical Uranium Metal Slugs, p. 71; in Neutron Physics Division Annual Progress Report for Period Ending September 1, 1959, USAEC Report ORNL-2842, Oak Ridge National Laboratory, Nov. 16, 1959.
38. F. Schroeder et al., Phillips Petroleum Co., Mar. 18, 1960. (Unpublished)
39. I. E. Dayton and W. G. Pettus, The Effective Resonance Integral of Thorium and Thorium Oxide, *Nuclear Sci. and Eng.*, 3(3): 286–295 (March 1958).
40. E. Z. Block and C. R. Richey, Bucklings of Natural Uranium–Graphite Lattices, in Nuclear Physics Research Quarterly Report for October, November, and December 1957, USAEC Report HW-54591, p. 37, Hanford Atomic Products Operation, Mar. 5, 1958.
41. E. Z. Block, Buckling Measurements on Seven-Rod Clusters of Natural Uranium Rods in Graphite, in Nuclear Physics Research Quarterly Report for April, May, and June 1958, USAEC Report HW-56919, p. 56, Hanford Atomic Products Operation, July 21, 1958.
42. G. W. R. Endres and E. Z. Block, Material Bucklings of Natural Uranium Cluster Fuel Elements in Graphite Lattices, in Nuclear Physics Research Quarterly Report for October, November, and December 1958, USAEC Report HW-59126, p. 21, Hanford Atomic Products Operation, Jan. 20, 1959.
43. E. Z. Block and R. I. Smith, Measurement of k_∞ and f for a Natural Uranium Cluster Fuel Element in a Graphite Lattice, in Nuclear Physics Research Quarterly Report for April, May, and June 1959, USAEC Report HW-61181, p. 42, Hanford Atomic Products Operation, July 20, 1959.
44. G. W. R. Endres and D. E. Wood, Material Bucklings of Graphite Uranium Lattices, p. 35; R. I. Smith, k_∞ and f for 1.92-Inch-Diameter Natural Uranium Fuel Elements, p. 48; in Nuclear Physics Research Quarterly Report for July, August, and September 1959, USAEC Report HW-62727, Hanford Atomic Products Operation, Oct. 20, 1959.
45. W. W. Brown et al., Exponential Experiments with Graphite Lattices Containing Multirod Slightly

Enriched Uranium Fuel Clusters, USAEC Report NAA-SR-3096, Atomics International, Jan. 15, 1959.

46. C. H. Skeen et al., Exponential Experiment with a Thorium-Uranium Fuel in Graphite, USAEC Report NAA-SR-4238, Atomics International, Mar. 1, 1960.
47. R. A. Laubenstein, Exponential Experiments on Graphite Lattices Which Contain Multirod Fuel Elements, A/CONF.15/P/594, Second United Nations International Conference on the Peaceful Uses of Atomic Energy, Geneva, 1958.
48. F. M. Leslie, Reactor Physics Measurements During the Commissioning of the Calder Reactors, A/CONF.15/P/315, Second United Nations International Conference on the Peaceful Uses of Atomic Energy, Geneva, 1958.
49. J. Bertrand, "Proserpine," A Homogeneous Critical Experiment with Plutonium, A/CONF.15/P/1203, Second United Nations International Conference on the Peaceful Uses of Atomic Energy, Geneva, 1958.
50. P. Bacher et al., Natural Uranium Graphite Lattices, A/CONF.15/P/1191, Second United Nations International Conference on the Peaceful Uses of Atomic Energy, Geneva, 1958.
51. J. M. Hendrie et al., Slowing Down and Diffusion Lengths of Neutrons in Graphite-Bismuth Systems, A/CONF.15/P/601, Second United Nations International Conference on the Peaceful Uses of Atomic Energy, Geneva, 1958.
52. R. Gwin and D. W. Magnuson, Radial Flux Measurements in a Cylindrical Annular Critical Assembly of $U^{235}O_2$ F_2-H_2O, p. 69; J. K. Fox and L. W. Gilley, The Poisoning Effect of Copper Lattices in Aqueous Solutions of Enriched Uranyl Oxyfluoride, p. 73; in Neutron Physics Division Annual Progress Report for Period Ending September 1, 1959, USAEC Report ORNL-2842, Oak Ridge National Laboratory, Nov. 16, 1959.
53. Oak Ridge National Laboratory, Neutron Physics Division Annual Progress Report for Period Ending September 1, 1958, USAEC Report ORNL-2609, Oct. 28, 1958.
54. R. Gwin et al., Experimental and Theoretical Studies of Unreflected Aqueous U^{235} Critical Assemblies, A/CONF.15/P/593, Second United Nations International Conference on the Peaceful Uses of Atomic Energy, Geneva, 1958.
55. R. A. Bennett and E. Z. Block, Reflector Savings of One Per Cent Enriched Uranyl Nitrate, in Nuclear Physics Research Quarterly Report for October, November, and December 1957, USAEC Report HW-54591, p. 43, Hanford Atomic Products Operation, Mar. 5, 1958.
56. J. A. Berberet and V. I. Neeley, The Measurement of k_∞ of Three Per Cent Enriched UO_3 Hydrogen Moderated Systems, in Nuclear Physics Research Quarterly Report for April, May, and June 1958, USAEC Report HW-56919, p. 25, Hanford Atomic Products Operation, July 21, 1958.
57. V. I. Neeley, Measurements of k_∞ for Three Per Cent UO_3 – Hydrogen Moderated Homogeneous Systems, in Nuclear Physics Research Quarterly Report for July, August, and September 1959, USAEC Report HW-62727, p. 56, Hanford Atomic Products Operation, Oct. 20, 1959.
58. W. W. Brown, Exponential Experiments with Organic Moderated Uranium Lattices, A/CONF.15/P/595, Second United Nations International Conference on the Peaceful Uses of Atomic Energy, Geneva, 1958.
59. J. C. Allred et al., Critical Measurements in UO_3-H_3PO_4 Solutions, *Nuclear Sci. and Eng.*, 4(3): 498 (September 1953).
60. I. V. Gordeev and V. Ya. Pupko, Absorption Cross Section of U^{235} Fission Fragments, A/CONF.15/P/2223, Second United Nations International Conference on the Peaceful Uses of Atomic Energy, Geneva, 1958.
61. N. J. Pattenden, Fission Product Poisoning Data, USAEC Report ORNL-2778, Oak Ridge National Laboratory, Oct. 14, 1959.
62. C. R. Greenhow and E. C. Hansen, Reactor Spectra Effects on Fission Fragment Cross Sections, USAEC Report KAPL-2057, Knolls Atomic Power Laboratory, Dec. 1, 1959.
63. E. A. Nephew, Thermal and Resonance Absorption Cross Sections of the U^{233}, U^{235}, and Pu^{239} Fission Products, USAEC Report ORNL-2869, Oak Ridge National Laboratory, Mar. 1, 1960.
64. C. H. Westcott, Effective Cross Section Values for Well-Moderated Thermal Reactor Spectra, Canadian Report CRRP-787 (AECL-670), Aug. 1, 1958.
65. P. Greebler et al., Statistical Evaluation of Fission-Product Absorption Cross Sections at Intermediate and High Energies, *Nuclear Sci. and Eng.*, 2(3): 334–351 (May 1957).
66. R. W. Deutsch, Fission-Product Buildup in Enriched Thermal Reactors, *Nucleonics*, 14(9): 89 (September 1956).
67. J. D. Garrison and B. W. Roos, Estimation of Fission Product Capture Cross Sections, *Trans. Am. Nuclear Soc.*, 3(1): 299–300 (June 1960).
68. J. D. Garrison et al., Poisoning by Stable Fission Products in High Temperature Graphite Reactors, *Trans. Am. Nuclear Soc.*, 3(1): 300–301 (June 1960).
69. J. C. Connor and S. B. Gunst, The Dependence of "Stable" Fission-Product Poisoning upon the Time-Integrated Exposure, *Trans. Am. Nuclear Soc.*, 3(1): 301–302 (June 1960).

Section III

HEAT TRANSFER

The Gas Suspension Coolant Project

The low heat-transfer and -transport capabilities of gases have been generally recognized as disadvantages in their use as reactor coolants; most gas-cooled power-reactor designs use high coolant pressures to improve these characteristics. Reference 1 is a report of experimental and analytical work completed by the Babcock & Wilcox Co. on the effects of adding solid material to the coolant gas phase in an attempt to obtain improved thermal properties of the gas-solid mixture. The Gas Suspension Coolant Project was initiated to obtain high-temperature heat-transfer data and to corroborate and extend existing low-temperature data.

The basic tool used in the investigations was the heat-transfer test loop. The loop consisted of the following: electrical heating and cooling sections; a solids feeder and separator assembly; heavy- and light-phase pumps; and instrumentation. After passing through the heating and cooling sections of the test loop, the gas-solids suspension was introduced into a separator assembly wherein the two phases were separated. The gas phase, containing a small amount of solids, was then compressed and recirculated, and the solid phase was pumped separately and then introduced back into the gas before the heating section. The design parameters for the test loop are given in Table III-1. The resistance-heated section of the loop was fabricated of $^3/_4$- and 1-in. type 304 stainless-steel tubing. Several "turbulence promoters" were incorporated in the smaller diameter test heater; these took the form of spiral ribbon with varying pitch. Holes were punched in the edge of the strip and were expanded to provide for a tight fit of the promoter within the tube. Four coolers followed the heater in the flow path. These were countercurrent, concentric tube exchangers, with the tube side containing the suspension and the shell side containing demineralized water. Instrumentation was provided to measure the necessary temperatures, densities, pressures, and flow rates.

In general, operation of the test loop appeared to be quite satisfactory. After operation of a modified loop for about 30 hr for the purpose of testing the pumps, instrumentation, etc., the heating section was added and the loop was operated for about 100 additional hours at wall temperatures up to 1255°F. The density of the fluid at the pump outlet varied from 1.0 to 11.0 lb/cu ft at a system pressure of 140 psig. The wall temperature of 1255°F corresponded to a

Table III-1 TEST PARAMETERS FOR HEAT-TRANSFER TEST SYSTEM[1]

Suspension:	
Density, lb/cu ft	0 to 8
Solids	Graphite with or without additions of dispersing materials
Gases	Nitrogen and/or helium
Velocities in test section, ft/sec	Up to 100
Velocities in loop piping, ft/sec	Up to 40
Pressure, psig	0 to 100
Temperature, °F	300 to 1000
Maximum heat flux, Btu/(hr)(sq ft):	
Heating	300,000
Cooling	200,000
Additive materials, if any	Bentonite or other materials defined experimentally
Circular test flow channel ID sizes, in.:	
Cooling	$^1/_2$ and 1
Heating	$^3/_8$, $^5/_8$, and $^3/_4$
Turbulence-promoter pitch length, tube diameters	6, 12, and 18

fluid temperature of 1100° F. After the 130 hr of testing, a metallurgical examination of the type 348 stainless-steel elbow following the heater exit showed that the material "was apparently not affected by the loop operating conditions." During the course of system operations, fluid flow was interrupted frequently. The reference states that "at no time was the slightest difficulty encountered in reestablishing flow of the gas suspension."

The heat-transfer data given in reference 1 are presented in graphical and tabular form for various heater-cooler and turbulence promoter combinations and for the two gases used. No dimensionless equation fitting all the data was found, but for several of the runs the data correlated as follows:

$$h = aV^b \left(W_s / W_g\right)^c$$

where h = film coefficient, Btu/(hr)(sq ft)(° F)
V = suspension velocity, ft/sec
W_s/W_g = solids loading, lb solid/lb gas
a,b,c = empirical constants

Part *a* of Fig. 8 is a comparison of the velocity and the heat-transfer coefficient (with and without solids loading), and part *b* of Fig. 8 shows the effect of the various turbulence promoters on h. Table III-2 shows the 10 correlations developed to represent the nitrogen-graphite suspension data. Attempts to correlate the helium data were not successful. Reference 2 gives additional data taken during the "Task II" phase of the investigation. These data involve tests with pure gas in a circular channel, tests with gas suspension in a circular channel, and tests with gas suspension in an annular channel. The first area of investigation was for "calibration" purposes; it is stated that the apparatus produced results in close agreement with those obtained by other workers using similar equipment. The annular-flow heating-element instrumentation failed completely because of inadequate thermocouple installation, and no temperature data were obtained. The gas suspension (nitrogen-graphite) data taken without turbulence promoters fall about a factor of 2 below the pure-gas runs without turbulence promoters, which were correlated by the conventional Dittus-Boelter relation ($Nu/Pr^{0.4}$ versus Re). No explanation was given for this behavior, but evidently the turbulence promoters perform

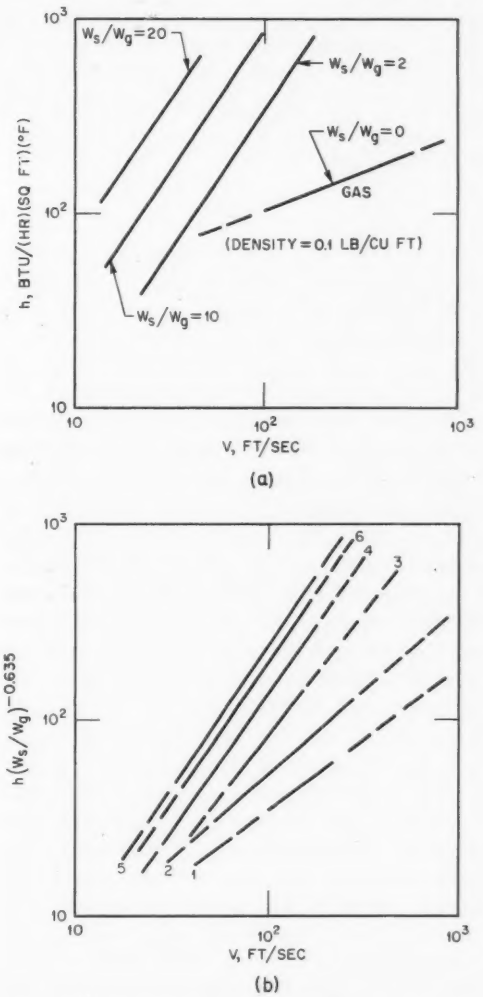

Figure 8 — (*a*) The effect of velocity on heat-transfer coefficient. (*b*) The effect of turbulence on heat-transfer coefficient.[1] 1, no turbulence promoter. 2, turbulence promoter, pitch length 15 to 17 in. (cooler). 3, turbulence promoter, pitch length 12 in. (cooler). 4, turbulence promoter, pitch length 6 in. (heater and cooler). 5, turbulence promoter, pitch length 4 in. (heater). 6, turbulence promoter, pitch length 3 in. (heater).

an essential function in achieving the benefits of the gas suspension.

The friction factor for the flow of nitrogen-graphite mixtures in a 0.532-in.-ID tube containing a 4-in.-pitch turbulence promoter was found to correlate within 50 per cent by

$$f = 72\ \mathrm{Re}_g^{-0.715}$$

Table III-2 CORRELATION FUNCTIONS FOR NITROGEN-GRAPHITE SUSPENSION[2]

Function	Tube ID, in.	Promoter pitch, in.	Density, lb/cu ft	h
Heater	0.532	3	0.1	$15\,V^{0.4}$ (fog)
Heater	0.532	3	1–8	$0.25\,V^{1.45}(W_s/W_g)^{0.635}$
Heater	0.532	4	1–8	$0.315\,V^{1.45}(W_s/W_g)^{0.635}$
Heater	0.532	6	1–8	$0.23\,V^{1.40}(W_s/W_g)^{0.635}$
Cooler 1	0.620	None	1–8	$1.5\,V^{0.72}(W_s/W_g)^{0.635}$
Cooler 2	0.620	6	1–8	$0.237\,V^{1.45}(W_s/W_g)^{0.635}$
Cooler 3	0.620	6	1–8	$0.82\,V^{1.08}(W_s/W_g)^{0.635}$
Cooler 2	0.620	12	1–8	$0.34\,V^{1.26}(W_s/W_g)^{0.635}$
Cooler 3	0.620	15–17	1–8	$1.2\,V^{0.86}(W_s/W_g)^{0.635}$
Heater	0.834	6.25	2–6	$2.5\,V^{1.57}(W_s/W_g)^{0.635}$

Data for the other nitrogen-graphite tests did not establish a correlation between f and the gas Reynolds number, Re_g.

Reference 1 concludes with a discussion of the change in design characteristics and performance of a gas-cooled power reactor when a gas suspension is substituted for the conventional pure-gas coolant. The study is based on the Kaiser-ACF[3] partially enriched gas-cooled design study. (This concept was reviewed in the June 1959 issue of *Power Reactor Technology*, Vol. 2, No. 3, and the December 1958 issue, Vol. 2, No. 1.) However, the fuel element postulated for the gas suspension version of the reactor is quite unconventional in design. It is of the re-entrant, or thimble, type. It contains an assembly of seven uranium carbide annuli in a graphite column. The graphite column is canned in a low-absorption metal (e.g., zirconium) which is cooled by the initial pass of the coolant. In the return pass, the coolant flows inside the uranium carbide annuli, which are jacketed inside with a high-temperature metal and which contain twisted ribbons to promote turbulence. The results of the study are summarized in Table III-3.

Table III-3 CALCULATED THERMAL PERFORMANCE OF A REACTOR COOLED BY PURE CO_2 AND BY A GAS SUSPENSION COOLANT

Parameter	CO_2 coolant	Gas suspension coolant (nitrogen + graphite)
Total thermal power, Mw	600	800
Mass flow rate, lb/hr	14.4×10^6	15.25×10^6
Coolant temp., °F:		
Inlet	473	473
Exit	1000	1000
Maximum cladding surface temp., °F	1300	1070
Active fuel length per rod, ft	25.75	25
Fuel rods per element	7	
Fuel rod OD, in.	0.745	
Flow channels per element		7
Flow channel ID, in.		0.745
Total no. of elements	980	980
Core height, ft	25.75	25
Inlet pressure, psia	400	165
Pressure drop, psi:		
Core	30	68
Primary loop	40	110
Pumping power, % of gross electrical power	11.1	10
Net power increase, %		34.5
Ratio of weight of graphite to weight of nitrogen		15
Average velocity of coolant, ft/sec:		
At inlet	*	29
At exit	*	75
Film heat-transfer coefficient, Btu/(hr)(sq ft)(°F):		
At inlet	*	213
At exit	*	828

*These values were not calculated owing to lack of information or were not available.

Geometrical Considerations

The June 1960 issue of *Power Reactor Technology*, Vol. 3, No. 3, contained a discussion of the Deissler-Taylor analytical treatment of turbulent-flow heat transfer in certain noncircular passages, namely, triangular and square ducts. Reference 4 is the report of an experimental investigation of pressure drop and heat transfer in a duct with triangular cross section. The case studied consisted of a duct having a cross section the shape of an isosceles triangle

with 5.0-in. sides and a 1.0-in. base. The hydraulic diameter of the duct was 0.904 in., with an apex angle of 11.46°. Heat was electrically generated in the stainless-steel walls of the duct. Appropriate instrumentation was provided for the accurate measurement of pressure and temperature.

The pressure drop in the laminar-flow regime was found to be in good agreement with calculated friction factors of a circular-sector duct with the same opening angle. Above a Reynolds number of 1000, the experimental friction factors gradually departed from the laminar solution. This is explained to be the result of (1) the onset of turbulence near the base of the triangle and (2) the gradual filling of more and more of the duct as the Reynolds number is increased. As the flow became fully turbulent, however, the experimental data fell about 20 per cent below the Blasius solution for a circular tube. The authors[4] recognize that this is contrary to other experimental data on noncircular ducts, wherein frictional pressure drops were calculated on the basis of the hydraulic diameter, but they state that the apex angle of 11.46° is smaller than the angles previously studied. A calculation of the velocity field by the method of Deissler and Taylor was accomplished, and the resulting analytical friction factor was found to be in "very good" agreement with the experimental data. It thus appears that the use of the hydraulic diameter in calculating noncircular-duct pressure drops is open to question when surfaces intersecting at small angles are involved.

The heat-transfer experiments were limited to the turbulent regime, since free convection flows were noted at low Reynolds numbers. As Reynolds number increased, the thermal entrance length increased also; and, at values above about 15,000, the wall temperatures were still a function of duct length, although a distance equivalent to 116 diameters had been traversed. This can be contrasted to the case for turbulent flow in circular pipes, in which the thermal entrance length is generally not greater than 20 diameters. The average Nusselt numbers for turbulent flow in the triangular duct were found to be about one-half as large as the Nusselt numbers for turbulent pipe flow when both were based on the hydraulic diameter. A plot of the local heat-transfer coefficient around the periphery of the duct was presented; the values ranged from a minimum of about 10 per cent of the average, at the small apex angle, to a maximum of about 2.2 times the average, near the base.

Water Heat Transfer and Fluid Flow

Swirl Flow

The effects of swirl flow of water are given in reference 5, which is an outgrowth of an earlier study of boiling burnout with water in vortex flow through test sections.[6] The basic piece of apparatus, the heat-transfer loop, accommodated test sections consisting of pipes containing twisted tapes. The construction of these test sections was accomplished by making the tape diameter slightly smaller than the tubing inside diameter and by drawing the tube down onto the twisted tape. Both copper and aluminum tubes were fabricated containing 15-mil Inconel twisted tapes. The ranges of parameters studied for the nonburnout runs are given in Table III-4.

Table III-4 TEST PARAMETERS FOR NONBURNOUT RUNS

Tube ID, in.:	
Copper	0.136, 0.189, 0.249
Aluminum	0.249
Tape twist ratio, y, internal diameters/180° twist	2.3 to 12.0
Heated length/internal diameter, L_h/D_i	45 to 70
Heat flux based on internal surface area, ϕ, Btu/(hr)(sq ft):	
Nonboiling runs	0.8×10^6 to 8.0×10^6
Boiling runs	2.3×10^6 to 9.3×10^6
Test-section pressure, psia	30 to 220
Axial Reynolds number,* $(Re)_a$	5000 to 427,000

*The axial $(Re)_a$ contains the superficial axial coolant velocity, and the rotational $(Re)_r$ contains the resultant coolant velocity at the inner tube wall.

After an analytical discussion of nonboiling forced-convection heat-transfer coefficients, the authors[5] present a recommended correlation for average twisted-tape vortex-flow heat-transfer coefficients, as follows:

$$\left(\frac{h_{vm}}{C_{P_b} G_a}\right)\left(\frac{y^{0.09}}{2.18}\right) = \frac{0.023\left[1 + (D_i/L_h)^{0.7}\right]}{(\mathrm{Pr})_b^{2/3}\,(\mathrm{Re})_b^{0.2}} \qquad (1)$$

The symbols have their conventional meanings with the subscript a representing axial flow and b signifying that properties are based on bulk stream temperatures. The correlation repre-

sents 47 data points with an average deviation of 10.1 per cent. The ratio of the experimental mean vortex-flow coefficient, h_{vm} to the equivalent mean axial-flow coefficient, h_{am} evaluated at equal bulk coolant temperature and weight flow rate, is correlated by the following equation:

$$\frac{h_{vm}}{h_{am}} = 2.18y^{-0.090} \quad (2)$$

Since the tape twist ratio, y, was on the order of unity in the experiments, it can be seen from Eq. 2 that the swirl flow resulted in film coefficients about twice those for axial flow.

A few local boiling coefficients were calculated and correlated by Eq. 3 with an average deviation of 14.8 per cent.

$$\Delta t_{sat} = \frac{y^{0.81}\phi^{1.35}}{0.34} \quad (3)$$

Burnout heat flux data for the vortex-flow experiments were tabulated; Table III-5 shows the ranges of parameters studied. The burnout heat flux was defined as that heat flux existing when physical burnout occurred. The physical destruction of the tube always occurred, in the vortex tests, at the downstream end near the exit of the test section. Comparison of the straight-flow burnout data was made with the Gunther and the Bernath correlations, and the agreement was considered "fairly good." The following equation is the recommended swirl-flow burnout correlation and represents the data, with a −0, +20.2 per cent average deviation for 38 of the 40 data points.

$$(\phi_{BO})_{v_{min}} = \frac{130{,}000(\rho_b V_a)^{0.645}(D_i)^{0.24}[1 + (\pi^2/4y^2)]^{0.323}}{(L_h)^{0.44}} \quad (4)$$

The subscript v_{min} on ϕ_{BO} signifies that the vortex flow burnout correlation represents the minimum values observed (−0 per cent deviation) for ϕ_{BO}.

It can be noted that Eq. 4 does not contain any terms to account for pressure and degree of subcooling. The experimental data demonstrated that coolant pressure and subcooling were not significant variables; data to substantiate this fact are shown in Table III-6. (Although several mechanisms are postulated to explain the conclusion that coolant pressure and subcooling

Table III-5 TEST PARAMETERS FOR BURNOUT RUNS

Variable	Swirl flow (40 tests)	Straight flow (24 tests)
D_i, in.	0.136–0.402	0.125–0.305
y, diameters/180° twist	2.08–12.03	
L_h/D_i	6.6–88.2	6.55–88.4
Tube material	Al, Cu, A-nickel	Al, A-nickel
V_{a2}, ft/sec	14.7–156.0*	23.6–174.0
t_{b1}, °F	48–138	48–75
t_{b2}, °F	91–350	74–174
ΔP (over-all), psi	3.0–432	8.6–545
$(\Delta t_{sub})_2$, at wall	17 wt.% quality: 260°F subcooling	1.1 wt.% quality: 222°F subcooling
ϕ_{BO}, Btu/(hr)(sq ft)	2.77×10^6–37.35×10^6	2.23×10^6–17.25×10^6

*Corresponds to a range of exit resultant velocity of 16.6–195.3 ft/sec.

Table III-6 EFFECT OF PRESSURE AND EXIT SUBCOOLING ON SWIRL-FLOW BURNOUT HEAT FLUX[5]

Test No.	D_i, in.	L_h/D_i	y	V_{a2}, ft/sec	P_{2_i}, psia	$(\Delta t_{sub})_{2_i}$, °F	ϕ_{BO},* 10^6 Btu/(hr)(sq ft)
19	0.249	48.4	2.30	35.4	16	4	5.35
20	0.249	48.2	2.30	34.0	545	255	5.14
21	0.189	63.5	7.70	67.4	35	48	6.90
22	0.189	63.5	7.70	67.4	470	248	6.82
24	0.136	88.2	2.46	69.4†	15	17 wt.% quality	10.82
23	0.136	88.0	2.46	74.4	495	116	9.41
32	0.189	60.5	2.49	71.2†	29	1.9 wt.% quality	11.00
31	0.189	60.1	2.49	73.6	445	195	10.92
35	0.249	69.7	12.03	27.8	47	7	3.64
36	0.249	69.7	12.03	25.8	245	75	4.26

*Average difference for the five pairs of tests is 7.6 per cent.
†Based on exit flow of liquid only.

were not significant variables, no one mechanism appeared to be completely satisfactory.)

A total of 149 pressure-drop determinations were made in the course of the experimentation on twisted-tape tubes. The pressure drop across a twisted-tape vortex tube is given in Eq. 5.

$$\Delta P = 0.00089 \frac{V_a^2}{2g_c} \frac{L_a}{D_i} \frac{\rho_b}{144} \times D_i^{-1.2} y^{-0.6} \left(\frac{\mu_i}{\mu_b}\right)^{0.18} \quad (5)$$

The reference cautions against extrapolation of Eq. 5 and states that swirl flow f is quite sensitive to roughness.

Of interest is the ratio of heat transfer to friction in comparing swirl flow and axial flow. Figure 9 shows such a comparison. The left

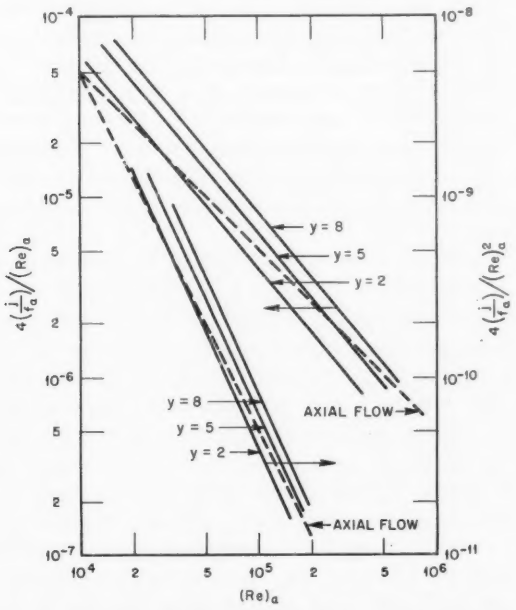

Figure 9 — Heat-transfer coefficient per unit pressure drop and per unit frictional pumping power for 1/4-in.-ID tubes.[5] In the ordinate labels, j is the Colburn heat-transfer factor, f_a is the axial friction factor (dimensionless), and $(\mathrm{Re})_a$ is the axial Reynolds number (dimensionless).

ordinate is proportional to the relative heat-transfer coefficient per unit frictional pressure drop for the same fluid flowing at the same bulk temperature through tubes of equal dimensions, and the right ordinate represents the relative heat-transfer coefficient per unit frictional pumping power.

The reference also includes a discussion of six other swirl-flow heat-transfer studies and outlines the results.

Departure from Nucleate Boiling

Reference 7 is a report of a general dimensional analysis of departure from nucleate boiling (DNB)* in vertical channels. One of the reasons for such an analysis is to develop tools for organizing and for comparing the results of a large number of experiments. The report begins with a statement of the Navier-Stokes equation, of the continuity equation, and of the energy equation and appropriate boundary conditions. The dimensionless groups occurring in these equations and boundary conditions are then collated. A key point in the dimensional analysis is the definition of DNB, and a new term, X_S (the static quality), is introduced and defined as the fraction of time the gas phase occupies a given point within a channel.

$$X_S = t_g \rho_g / (t_g \rho_g + t_f \rho_f)$$

where X_S is the static quality, t is the time a point is occupied by vapor (g) or liquid (f), and ρ is the density. X_{DNB} is then defined as the static quality associated with DNB and can be visualized as a vapor-liquid structure existing at the DNB point. This structure is determined by the flow equations and boundary values, and X_{DNB} is determined when all dimensionless groups are fixed. The following equation is the result:

$$\frac{\phi_{\mathrm{DNB}}}{h_{f_g} \rho_g V_i} = f\left(\frac{L}{S} \frac{V_i S \rho_f}{\mu_f} \frac{V_i S \rho_g}{\mu_g} \frac{C\mu_f}{k} \times \frac{\sigma}{\rho_f V_i^2 S} \frac{k(T_s - T_i)}{h_{f_g} \rho_g S V_i} \frac{\rho_f}{\rho_g} \beta\right) \quad (6)$$

The symbols used in this discussion of DNB are given[7] as follows:

C = specific heat at constant pressure for the liquid
L = boiling length
S = channel spacing

*DNB is a term used in the Naval Reactors Program and can be thought of, similarly to burnout heat flux, as being an upper limit on design.

T = temperature
V = velocity
h = enthalpy
h_{fg} = enthalpy change from liquid to vapor
k = liquid thermal conductivity
f = liquid
g = vapor
i = inlet
s = saturation
β = contact angle measured through the liquid
ρ = density
μ = viscosity
ϕ = heat flux
σ = surface tension

If the system is restricted to a constant pressure, the fluid properties are not necessary and Eq. 6 takes the form

$$\phi_{DNB} = f\,(VLSh) \tag{7}$$

The author's conclusions are as follows:[7]

1. For a single fluid at one pressure flowing in wide channels, DNB is a function of four independent variables. These variables could be h, G, L/S, and S.

2. When the above four variables are used to correlate DNB, any apparent inlet subcooling effect is caused by an inadequate assumption of the form of the functional relation between these variables.

3 The mechanism of DNB in forced convection is still not understood.

4. L/S affects DNB through the distribution of phases at the DNB point. Simply specifying velocities and qualities is not sufficient; a specification of the phase distribution is also needed.

5. Further improvements in DNB correlations will probably result from better assumptions for the functional relations and the use of larger numbers of undetermined constants. There is no reason to expect that a function of one variable alone times a function of another variable alone, etc., will suffice in correlating the data.

It is planned to use these various dimensionless groups in producing DNB correlations that would be applicable over a comparatively wide range of water conditions and pressures. It is not expected that a simplified relation between these groups will be found. Perhaps a graphical representation will be necessary to produce the optimum correlation. (This type of representation is now used in many other fields of heat transfer and hydraulics.)

Steam Slip

The problems of steam slip in forced convection of boiling water are analyzed in reference 8. The basic equation, a momentum balance, is written for both phases, and it results in an analytical expression (Eq. 8) for steam slip as a function of the system variables:

$$\frac{d}{dx}\left[\frac{(1-x)^2}{1-\alpha}+\frac{x^2}{\alpha}\frac{\rho_L}{\rho_G}-\frac{1}{2}\frac{(1-x)^2}{(1-\alpha)^2}\right]=-\frac{\alpha G h_{fg} f_0}{2DC}$$

$$\times\left[\frac{\left(\frac{dP}{dy}\right)_{GTP}-\left(\frac{dP}{dy}\right)_{LTP}+(\rho_L-\rho_G)\sin\theta}{\left(\frac{dP}{dy}\right)_0}\right] \tag{8}$$

where x = steam quality
α = void fraction
ρ = density, lb/cu ft
G = mass velocity, lb/(hr)(sq ft)
h_{fg} = heat of vaporization, Btu/lb
f_0 = single-phase friction factor
D = pipe diameter or equivalent hydraulic diameter, ft
C = heat generation per unit volume of coolant, Btu/(hr)(cu ft)
θ = angle of inclination of test section

The dP/dy terms are frictional pressure drops. The subscripts GTP and LTP represent the two-phase, gas and liquid frictional pressure drops, respectively; the subscript zero represents the pressure drop for the initial flow of 100 per cent water. If the pressure-drop ratios could be expressed in terms of the equation variables, Eq. 8 would yield a functional relation between α and x. Unfortunately these ratios cannot be measured experimentally, and the recourse is to obtain them from a study of a model. The author[8] chooses the "momentum exchange model." The basis of this model is that x, α, and ρ_L/ρ_G are sufficiently slowly varying that the left side of Eq. 8 can be equated to zero. This states that momentum is exchanged between water and steam every time x, α, or ρ_L/ρ_G varies, and the exchange tends to maintain the equality of frictional and head losses of the two phases. One would expect this to be particularly true in the case of flow in unheated channels where pressure drops are small enough not to affect steam density or water flashing appreciably. Comparison of the model to test data from various sources indicated good agreement for

test data wherein no heat was added and/or changes in steam quality were small.

Under reactor conditions of practical interest, however, steam quality changes rapidly within the heated channel, and the pressure drops of steam and water are not equal. This can be represented by equating the brackets on the right side of Eq. 8 to a parameter β. The right side of the equation thus becomes:

$$-\frac{\alpha G h_{fg} f_0}{2DC}\beta = -\frac{\alpha}{2}K\beta$$

Although the term β has not been determined in functional form, the reference suggests definitive experiments to determine it.

Finally, the author[8] compares the calculated ratio of two-phase frictional pressure drop to single-phase (water) pressure drop, using the simplified case for $\beta = 0$, to the experimental data of Moen and Larson at 1000 psia. The comparison is "satisfactory." Comparison of the calculated results to date of Sher at 14.7 psia were somewhat less satisfactory, since the predicted frictional plus head losses fell from 30 per cent below to 50 per cent above the experimental measurements.

Corrosion of Aluminum

A somewhat unusual experiment is reported in reference 9, wherein preliminary results on the effect of heat flux on the corrosion of aluminum by water are recorded. The equipment consisted of an 1100 aluminum test piece placed in an electrically heated heat-transfer loop and cooled by demineralized water. The loop was fabricated of type 347 stainless steel and contained a pressurizer, ion columns, coolers, and necessary process instrumentation.

The test specimen consisted of an aluminum bar into which had been bored a rectangular channel that was 0.050 in. wide by 0.500 in. on a side. The specimen had a heated length of 6.5 in. Since it was anticipated that film coefficients would be low near the corners, the exterior of the bar was milled so that the heat flux was reduced at the extremities of the flow channel. After the channel was machined, the bar was annealed for 1 hr at 650°F, and the flow channel was brought to final dimensions by drawing a sizing die through the test piece. After the exterior of the bar was machined, the specimen was degreased in acetone and then assembled into the test loop. After assembly, 12 thermocouples were spot-welded to the outer surface of the specimen so that temperatures could be recorded during the test. A summary of the test conditions is given in Table III-7.

Table III-7 SUMMARY OF TEST CONDITIONS[9]

Flow rate, gal/min:	
Main loop stream	80
Test-specimen cooling channel	2.95 (33 ft/sec)
Letdown and feed	0.26
Ion-exchange column	0.13
Pressures:	
Specimen inlet, psia	370–420*
Pressure drop through specimen, psi	25
Temperatures, °F:	
Loop	155
Specimen inlet cooling water	155–157
Specimen outlet cooling water	191–193
Average cooling water Δt	37
Heat generation:†	
Specimen total	55,000 Btu/hr (16 kw) [190×10^6 Btu/(hr)(cu ft) or 2.0 kw/cm^3]
In 0.10-in.-thick center section	44,000 Btu/hr
In 0.025-in.-thick edges	11,000 Btu/hr
Heat flux:	
Flow-channel surface under 0.100-in.-thick section	1.62×10^6 Btu/(hr)(sq ft)
Flow-channel surface at edges (0.025-in.-thick section)	0.50×10^6 Btu/(hr)(sq ft)

*The pressure remained constant during the run. An uncertainty in the accuracy of the pressure gauge is the reason for the range.

†Total heat generated in the specimen, as calculated (1) from measurements of current flow and voltage drop and (2) from a heat balance of the cooling water (flow rate and temperature use), usually agreed to within ±5 per cent.

The heat-transfer loop was operated for a period of 240 hr (10 days), and temperatures were continuously recorded. The temperature-time curves for the various thermocouples are given in the reference.[9] Although the inlet and outlet water temperatures did not fluctuate significantly, the wall temperatures steadily increased with time; the maximum increase occurred at the coolant outlet and amounted to 189°F. At the end of the test, the temperature of the aluminum specimen was about 380°F near the inlet and about 560°F near the outlet. (Since the temperature near the outlet at the start of

the test was about 370°F, the increase was thus about 189°F.)

At the termination of the test, the specimen was carefully "opened" and the flow channel was examined. Under microscopic examination, it was apparent that all surfaces had been roughened and that they contained some tightly adherent oxide film. The region of the specimen near the outlet suffered the heaviest corrosion damage, with the thickness of the film increasing from inlet to outlet. In addition, intergranular attack to a depth of about 0.005 in. was observed near the test-specimen outlet. Since about 2 mils of general attack could be expected during the 10-day test, the total penetration of the aluminum was estimated to be 7 mils.

The intergranular attack was not expected during this test since previous isothermal tests, in which 1100 aluminum was exposed to water flowing from 20 to 65 ft/sec at a temperature of 500°F, indicated no intergranular attack. No satisfactory explanation has thus far been given as to why this phenomenon occurred; the maximum temperature that the water could have reached in the newer test was calculated to be 504°F, and this temperature would have occurred if the water had penetrated the film to the film-aluminum interface. The corrosion-product thermal-conductivity values were calculated from the known heat-flux and temperature gradients, but a large spread was found owing to uncertainties in measuring the thickness of the oxide films. In general, the calculated values of k were distributed around 1 Btu/(hr)(ft)(°F).

In conclusion, the authors[9] recognize that one test is not sufficient data but do state that the corrosion of 1100 aluminum is "severe" under the conditions studied and recommend that aluminum-corrosion inhibitors be studied in future experiments.

Hot Spots and Hot-Channel Factors

Reference 10 presents information on how hot-channel factors are used in the design of the Army Gas-Cooled Reactor Experiment I (GCRE-I). The hot-channel factors are shown in Table III-8. The reference presents four possible methods of combining hot-channel factors; these are summarized in Table III-9. The second and third columns are the bulk and film hot-channel factors computed by the calculational methods illustrated. The last column, the hot-spot wall temperatures, results from application of the hot-channel factors to the nominal bulk and film temperatures. The reference states that the product method probably overestimates the hot-spot temperature since many of the factors will not obtain simultaneously; whereas the statistical method probably underestimates the hot-spot temperature since some of the factors definitely will superimpose. The choice preferred is the weighted-product method with a resulting hot-spot temperature of 1839°F. It can be noted, however, that the statistical method shown in Table III-9 is not equivalent to the statistical method described in reference 11.

Table III-8 GCRE HOT-CHANNEL FACTORS[10]

Cause of deviation from nominal conditions	Film factor	Bulk factor	Fuel factor
Fuel considerations:			
Enrichment variation	1.002	1.002	1.002
Density variation	1.015	1.015	1.015
Pellet diameter variation	1.011	1.011	1.011
Central-plug ID variation	1.015	1.015	1.015
Pellet stack-length variation		1.011	
Reasonable combined effect	1.02	1.027	1.02
Neutron-flux considerations:			
Intracell flux depression	1.05		1.05
Control-rod flux averaging	1.01	1.01	1.01
Uncertainty in flux calculation or measurement	1.03	1.10	1.03
Flow distribution due to control-rod insert	1.008	1.01	
Flux depression across a pin	1.091		
Combined effect	1.20	1.12	1.092
Metal-fabrication considerations:			
Surface roughness variation		1.016	
Cladding OD variation	1.008	1.030	
Liner ID variation	1.006	1.030	
Orifice tolerances	1.033	1.005	
Spacer tolerances	?	?	
Pin spacing variation	1.021		
Reasonable combined effect	1.055	1.040	
Heat-transfer considerations:			
Uncertainty in film correlation	1.10		
Local velocity effects (including intracell thermal conductivity)	1.05		
Insulation conductance uncertainty	1.008	1.008	1.008
Fuel conductivity uncertainty			1.200
Gap conductance uncertainty			1.030
Combined effect	1.162	1.008	1.245
Fluid-flow considerations:			
Uncertainty in pressure loss calculations	1.02	1.025	
Combined effect	1.02	1.025	
Reactor operations considerations:			
Deviation from design power	1.150	1.150	1.150
Reasonable combined effect	1.080	1.080	1.080
Over-all combined effect	1.660	1.340	1.500

Table III-9 APPROACHES TO CALCULATING HOT-SPOT TEMPERATURES[10]

Calculation method	$F_{\Delta t}$	F_θ	T_s (max.), °F
Product:			
$\prod_1^n F_i$	1.83	1.53	1960
Weighted product:			
$\prod_1^m F_i\left[1+\frac{1}{2}\left(\prod_{m+1}^n F_i-1\right)\right]$	1.66	1.34	1839
Weighted statistical:			
$\prod_1^m F_i\left[1+\sqrt{\sum_{m+1}^n (f-1)_i^2}\right]$	1.57	1.30	1792
Statistical:			
$1+\sqrt{\sum (f-1)^2}$	1.21	1.18	1612
Ideal	1.00	1.00	1478

Reference 10 also contains considerable information on the pressure-drop and heat-transfer characteristics of a 19-pin bundle type fuel element. Data are reported for 15 different models tested with three pin diameters, two spiders, and five spacer shapes. A seven-pin bundle was also tested as an alternate to the 19-pin design.

Several publications have been recently issued containing typical flow distribution data necessary for the computation of hot-channel factors for that effect.[12,13] In reference 13, for example, air flow measurements were made for flow through a quarter-scale flow model of a gas-cooled reactor. After in-place calibration of the mockup fuel-element flow orifices and manometer systems, successive runs were made, and flow measurement data were reproduced within ±0.2 per cent.

In many reactors, provisions are made for measurement of coolant temperatures and various surface temperatures during operation. Reference 14 is an account of experiments designed to measure the true surface temperature of a mockup OMRE fuel element by means of a thermocouple welded to the surface of the element. The thermocouple tested was welded to the element's surface, and the lead wires were brought "outside" in quartz insulating sleeves. The back of the plate was insulated, and a reference temperature was obtained by a thermocouple extending through the insulation and welded to the back of the plate. Coolant was pumped over the test surface, and the element was heated electrically. Data were obtained for coolant temperatures of 500 and 600° F, for coolant velocities of 12 and 15 ft/sec, and for heat fluxes of about 70,000 to 170,000 Btu/(hr)(sq ft).

Six test and six reference thermocouples were installed; the reference thermocouples were displaced 1 in. in an axial direction downstream of the test thermocouples to minimize the thermal interaction of the two.

The results of the experiment are shown in Table III-10. The author[14] recommends that the temperatures observed during OMRE operations be corrected to include the percentage errors tabulated in Table III-10. The magnitude of error associated with the temperature measurements was determined; the maximum probable error in the actual OMRE surface temperatures after applying the correction factors is 2 to 3 per cent.

Parallel-Channel Flow

A new method for determining the stability of two-phase flow in parallel heated channels is the subject of reference 15. Using perturbation theory, a stability criterion equation (Eq. 9) is developed:

$$S(\lambda) = 0 = \sum_{i=1}^{n} \frac{b}{\mu_i \lambda - \frac{\partial \Delta P_i}{\partial G_i}} \qquad (9)$$

where P_i is the frictional pressure drop in the ith channel, G_i is the flow in the ith channel, and

Table III-10 EXPERIMENTALLY DETERMINED SURFACE-TEMPERATURE MEASUREMENT ERROR*[14]

Coolant temp. (T_c), °F	True surface temp. (T_s), °F	Indicated surface temp. (T_θ), °F	$T_s - T_c$, °F	$T_s - T_\theta$, °F	Error,† %
607	693	667	86	26	30
500	689	658	89	31	35

*Data shown are for representative test thermocouple specimens.
†Average of thermocouple specimens.

μ_i, λ, and b are constants.* The roots of Eq. 9 are of importance since, if the real parts of all roots are negative, the flows are stable and, if any real part is positive, the flows are unstable. It is shown that, if all the terms $\partial \Delta P_i / \partial G_i$ are positive, flows will be stable and, if two or more of the partial derivatives are negative, flows will be unstable. If, however, only one of the partial derivatives is negative, the flows may or may not be stable depending upon design conditions.

Hydrodynamic instability of flow in heated, parallel channels has been the subject of some experimentation described in reference 16. Flow tests were run in parallel, uniformly heated channels having dimensions of 0.097 by 1.0 by 27 in. in length. The data show that the channel exit quality at which stable flow oscillations begin depends primarily on inlet temperature and pressure. A summary of these fluid conditions is presented in Table III-11. In some of the runs, DNB occurred before flow oscillations began. The DNB values of heat flux calculated from data taken on the parallel-channel apparatus agreed with those that had been previously calculated with single-flow-channel apparatus.

Table III-11 MEASURED EXIT STEAM QUALITY AT BEGINNING OF FLOW OSCILLATIONS

Pressure, psia	Inlet subcooling, °F	Exit quality at oscillations
600	36	0.32
800	5	0.56
800	55	0.29
1200	9	0.71
1200	61	0.46
1600	145	0.34

*The defining equations for b and λ are the expressions for the random variations in flow and pressure drop, and μ_i is an integration constant.

References

1. Babcock & Wilcox Co., Aug. 15, 1959. (Unpublished)
2. Babcock & Wilcox Co., Gas Suspension Task II, Final Report, USAEC Report BAW-1181, November 1959.
3. Kaiser Engineers Div. of Henry J. Kaiser Co. and Nuclear Products-Erco Div. of ACF Industries, Inc., Gas-Cooled Power Reactor, Feasibility Study, Optimum Partially Enriched Uranium Nuclear Power Plant, USAEC Report IDO-2024 (Rev. 1), March 1958.
4. E. R. G. Eckert and T. F. Irvine, Jr., Pressure Drop and Heat Transfer in a Duct with Triangular Cross Section, *J. Heat Transfer*, 82(2): 125–138 (May 1960).
5. W. R. Gambill et al., Heat Transfer, Burnout, and Pressure Drop for Water in Swirl Flow Through Tubes with Internal Twisted Tapes, USAEC Report ORNL-2911, Oak Ridge National Laboratory, Apr. 11, 1960.
6. W. R. Gambill and N. D. Greene, Boiling Burnout with Water in Vortex Flow, *Chem. Eng. Progr.*, 54: 68–76 (October 1958).
7. P. Griffith, A Dimensional Analysis of the Departure from Nucleate Boiling Heat Flux in Forced Convection, USAEC Report WAPD-TM-210, Westinghouse Electric Corp., Bettis Atomic Power Laboratory, December 1959.
8. S. Levy, Steam Slip: Theoretical Prediction from Momentum Model, *J. Heat Transfer*, 82(2): 113–124 (May 1960).
9. J. C. Griess et al., Effect of Heat Flux on the Corrosion of Aluminum by Water. Part I. Experimental Equipment and Preliminary Test Results, USAEC Report ORNL-2939, Oak Ridge National Laboratory, May 13, 1960.
10. Aerojet-General Nucleonics, Army Gas-Cooled Reactor Systems Program Semiannual Progress Report for July 1 Through December 31, 1959, USAEC Report IDO-28549, Feb. 15, 1960.
11. C. F. Bonilla, *Nuclear Engineering*, p. 445, McGraw-Hill Book Company, Inc., New York, 1957.
12. J. Wilson and R. Styles, Pathfinder Atomic Power Plant Coolant Distribution Tests, USAEC Report ACNP-5920, Allis-Chalmers Mfg. Co., Nov. 15, 1959.
13. Lawrence J. Flanigan et al., Model Studies of Flow and Mixing in the Partially Enriched Gas-Cooled Power Reactor, USAEC Report BMI-1397, Battelle Memorial Institute, Nov. 30, 1959.
14. S. Sudar, OMRE Fuel Plate Surface Temperature Measurement, USAEC Report NAA-SR-4047, Atomics International, May 1, 1960.
15. J. H. Bick, A New Method for Determining the Stability of Two-Phase Flow in Parallel Heated Channels with Applications to Nuclear Reactors, USAEC Report NAA-SR-4927, Atomics International, May 1, 1960.
16. Westinghouse Electric Corp., Bettis Atomic Power Laboratory, Reactor Engineering Technical Progress Report for the Period January 1, 1960, to April 1, 1960, USAEC Report WAPD-MRQ-2. (Classified)

Section IV

REACTOR KINETICS AND CONTROL: CONFERENCE ON TRANSFER FUNCTIONS AND REACTOR STABILITY

On May 2 and 3, 1960, a conference was held at the Argonne National Laboratory (ANL) on transfer-function measurements and reactor stability analyses. Proceedings of the conference will be published by ANL in the near future. An appreciable fraction of the papers and discussions at the conference concerned experimental techniques for the measurement of reactor transfer functions, including methods of circumventing the effects of reactor noise as well as methods of utilizing the noise as the exciting function for the reactor. These papers demonstrated that transfer-function methods are rapidly becoming precise and generally applicable techniques, and they contained a considerable amount of useful information for experimenters. The papers of more general interest to the reactor designer, however, were those which dealt with the theoretical aspects of reactor dynamics and stability and those which presented the results of measurements on operating power reactors. These will be summarized briefly here.

A Describing Function for Handling Nonlinearity

The nonlinearity of the kinetic behavior of the neutron chain reaction was discussed, as well as means of accounting for its effects in reactor stability analyses. Two references (1 and 2) which deal with these questions were cited. The latter[2] describes a method of handling the nonlinear response by a describing function, analogous to the transfer function of a linear system. Thus, if one applies a sinusoidal oscillating reactivity $\rho = \mu \sin \omega t$ to the reactor and observes the time-dependent variation in the neutron density n, the describing function is a function that specifies the amplitude and phase relations between $\rho(t)$ and $n(t)$.

The approximate describing function derived by Smets[2] may be pictured as follows. The reactivity oscillation ρ may be considered to be applied to a transfer function Z, which is the usual linearized transfer function, to yield an output x:

$$x(s) = \rho(s)\, Z(s) = \rho(s)\left[\frac{1}{s\left(l + \sum_i \frac{B_i}{s + \lambda_i}\right)}\right]$$

where l is the effective neutron lifetime and B_i and λ_i are, respectively, the fractional yield and the decay constant of the ith delayed-neutron emitter.

From this relation, $x(t)$ could be found in the usual way; the signal $x(t)$ is then considered to be applied to a nonlinear amplifier whose gain is a function of the magnitude of x and whose output gives the variation of neutron density $n(t)/n_0$. The magnitude K of the fundamental of $n(t)/n_0$, which depends on the magnitude of x or on $\mu|Z|$, is given by:[2]

$$K(\mu|Z|) = \mu|Z| + \left[\frac{(\mu|Z|)^3}{3!}\frac{3}{4}\right] + \left[\frac{(\mu|Z|)^5}{5!}\frac{3\times 5}{4\times 6}\right] + \cdots$$

$$\doteq \mu|Z|\,[1 + 0.10\,(\mu|Z|)^2]$$

In this approach, the introduction of higher harmonics by the nonlinearity of the system is neglected: the phase of the output is determined entirely by the linearized function Z. In many reactor cases this neglect can be justified because the gain of the reactor system falls off sufficiently rapidly with frequency to make the effects of higher harmonics insignificant.

Space-Dependent Effects

Certain space-dependent effects were treated by E. R. Cohen and R. N. Cordy, and measurements on the Kinetic Experiment on Water Boilers (KEWB) reactor were presented which demonstrated the spatial effects. Ordinarily, in

transfer-function theory the reactor is treated, at least so far as the kinetic behavior of the neutron chain reaction is concerned, as a lumped component, although it is well known that sufficiently rapid oscillation of the reactivity can excite higher modes of the neutron distribution in space. These effects are usually negligible in reactor stability theory since the neutron lifetime is usually very short compared to any reactivity feedback effects, and, for all practical purposes, the reactor power oscillates according to the fundamental mode distribution. If, however, a reactor is surrounded by a reflector in which the neutron lifetime is much longer than that in the core, these spatial effects may not be negligible, or, at least, they may be susceptible to demonstration by transfer-function measurements. The effect of the reflector in determining the effective neutron lifetime is well known. Usually the reflector neutrons are lumped in with the core neutrons, and an effective lifetime is determined by averaging the lifetimes of reflector and core neutrons according to a suitable importance function. It was shown by Cohen that, when a frequency analysis is made, the neutrons that have their lifetimes lengthened because of spending part of their lifetime in the reflector can be distinguished as a separate group of neutrons; these neutrons affect the transfer function as though they constituted an additional group of delayed neutrons from a very short half-life precursor. To demonstrate the effect of the reflector neutrons, the KEWB reactor transfer function was measured at frequencies up to 260 cycles/sec. The effect of these neutrons in the transfer function was clearly demonstrated.

SPERT Experiments

In the field of boiling-water reactors, R. W. Wright described experiments by Ramo-Wooldridge Corporation on an electrically heated mockup of one of the Special Power Excursion Reactor Test No. 1-A (SPERT-I-A) coolant channels. The SPERT-I-A reactor, operating at atmospheric pressure, had been found to oscillate at a power density level of about 13 kw/liter when the reactivity compensated by steam amounted to 1.5 per cent. In the laboratory experiments a single 2-ft-long coolant channel with a $\frac{1}{8}$- by 1-in. cross section was mocked up and electrically heated from a power source that could be oscillated to yield a transfer function for the steam void content. The power density of 13 kw/liter was simulated when the power input to the channel was about 500 watts. The void content was measured by gamma-ray transmission over an area of about 2 cm^2 of the channel elevation.

With the channel boiling under a power input of 500 watts, the natural-circulation flow rate was about 28 cm^3/sec, corresponding to a velocity of 45 cm/sec in the channel. This velocity is near the peak of the curve of the natural-circulation flow velocity as a function of power input. The transit time around the circulation loop was about 75 sec, of which about 1 sec was spent in the heated channel.

The time variation of the steam void content was found to be very noisy. At a mean void fraction of about 30 per cent, the actual measured fraction over the 2-cm^2 area of observation varied from zero to 70 per cent, with response times as short as 10 msec. The noise was found to decrease farther up the channel where the average void fraction was higher. As would be expected, the natural-circulation flow rate was much less noisy than the void fraction. The noise of the boiling, of course, obscured the coherent response of the void fraction to the power oscillation, and it was necessary to employ special techniques to extract that response from the noise.

The void-fraction response was found to be proportional to the amplitude of the power oscillation over a wide range of amplitudes. The phase lag increased with frequency, reaching 180° at approximately 1 cycle/sec. The phase lag increased approximately linearly with frequency above 2 cycles/sec and exceeded 360°, indicating a time lag in the system. At 1 cycle/sec the phase shift was observed to be nearly constant at about 180° throughout the boiling length of the channel. It was stated that most of the phase response of the void fraction came from the one-sixth of the channel length centered at about a position of 40 per cent mean void fraction. Also, the results were said to suggest that the amplitude of the void-fraction response to power modulation may be simply a shifting of the constant-power average-void-fraction curve, $\alpha(y)$, up and down the channel as the point of initial boiling oscillates in response to the modulated power input to the water traversing the nonboiling length of the channel.

Although the theoretical work for the application of the results to the SPERT reactor was in-

complete, it appeared that the oscillating tendency was predicted with reasonable agreement as to the frequency of oscillation and power density level at which the oscillation would begin. It was concluded that the SPERT oscillation was not a purely hydrodynamic oscillation, but involved significant coupling to the neutron chain reaction. It was, however, possible to observe purely hydrodynamic oscillations both in flow and in void fraction in the experimental channel at constant power, but at a power level of about 700 watts. In a different experimental channel, which was made smoother in order to provide fewer nucleating sites, hydrodynamic instability was observed at a somewhat lower power level.

EBWR Measurements

ANL measurements of the transfer function of the Experimental Boiling Water Reactor (EBWR), and the analyses of these measurements to yield the reactivity feedback function, were discussed. This work was previously reviewed in the December 1959 issue of *Power Reactor Technology*, Vol. 3, No. 1.

Self-Sustained Power Oscillation

There was an informal discussion of the behavior of boiling-water reactors near the stability limit. A characteristic mode of operation has been observed in a number of boiling reactors that have been operated at power levels just below the level at which instability occurs. In this power range the reactors, when operated with all reactor and plant controls fixed, displayed a self-sustained power oscillation, which typically has a frequency of 1 cycle/sec or less and which is amplitude-modulated at a frequency of about one-tenth of the oscillation frequency. Sustained oscillations of this type have been observed over long periods of time—of the order of hours. In commenting on this phenomenon, Z. Akcasu cited findings of Rice relative to the passage of noise by a band-pass filter. If a narrow band-pass filter is excited by a white noise, the output displays oscillations which have a frequency equal to the frequency of the filter and which are amplitude-modulated at a modulation frequency that is given by the band width. Akcasu commented that, when the reactor power approaches the instability level, the reactor resonance peak becomes very narrow, and the reactor can behave as a narrow band-pass filter which is excited by the noise of the boiling. Consequently, it may be reasonable to expect sustained modulated oscillations of reactor power, which are characteristic of the region near the instability level. Akcasu stated that a model, which has not yet been tested by experiment, has been developed for this behavior. On this model the reactor behaves as a resonance circuit of variable damping. Above a certain power level, it can be shown mathematically that an instability occurs in the mean square power level, although the power itself may satisfy the classical criteria of stability.

Spatial Power Oscillation

The spatial oscillation of xenon content in large reactors, as well as the resulting spatial oscillation of power, was discussed. E. S. Beckjord discussed methods of treating the oscillations theoretically by considering the reactor to be composed of a number of coupled space regions. Beckjord emphasized both the fact that the behavior of the reactor operator must be taken into account in determining the course of these oscillations and the importance of in-pile instrumentation for guiding the operator. He stated that, although the Dresden reactor is provided with such instrumentation, there is no evidence of spatial instability in the reactor.

P. F. Lacy discussed methods of calculating spatial oscillations of power and described the behavior of the Shippingport reactor in this respect. Lacy stated that, during a long steady power run from the 600th to the 1700th hour of operation, spontaneous spatial oscillations, which were controlled by the control rods, had been observed. As the run progressed, the oscillation tendency decreased, presumably because the effective power density in the high-power region of the core decreased as the control rods were withdrawn to compensate for fuel burnup. In a succeeding run from the 1700th to the 2000th hour, a similar tendency was observed. During this run the operating temperature was decreased from 525°F (the level for the preceding run) to 500°F, thus yielding some additional reactivity because of the lower temperature defect.

Fast-Reactor Dynamics and Stability

Several papers were given on the dynamics and stability of fast-neutron reactors. A. R. Baker summarized the oscillation experiments that have been done on British fast reactors.

Since, up to the present time, these have been done at low power, the work is of most interest from the standpoint of technique. Baker also discussed the results of Doppler coefficient measurements in the Zero Energy Uranium System (ZEUS). He stated that the experimental results for U^{235} are consistent with zero Doppler effect. For natural uranium a small negative coefficient was observed, corresponding to increased capture in U^{238} with increasing temperature, which is given by:

$$d\sigma_c/dT = 0.0006 \pm 0.0002 \text{ mb}/^\circ\text{C}$$

Baker stated that the estimated Doppler coefficient for the whole reactor was zero within experimental error, with an estimated uncertainty of $10 \times 10^{-7}/^\circ\text{C}$.

The power coefficient of reactivity of the Dounreay fast reactor is expected to result from five effects, which are listed below in order of decreasing promptness:

1. Axial expansion of fuel elements
2. Bowing of fuel elements in a temperature gradient
3. Expulsion of coolant from the core due to coolant expansion
4. Radial movement of fuel elements due to expansion of the lower support plate
5. Blanket effects similar to those listed for the preceding core

In order to minimize fuel-element bowing, a central core structure called the "tube-nest" has been introduced into the reactor design. Each fuel-element channel in the tube-nest is somewhat farther from the core axis than the corresponding holes in the upper and lower support plates. The fuel elements are thus given an initial outward bowing, and no inward bowing should be possible.

Analytical studies of the dynamics of the Experimental Breeder Reactor No. 2 (EBR-II) and the Enrico Fermi fast reactor were described by D. Okrent of ANL and F. Storrer of Atomic Power Development Associates (APDA). The analyses indicate that the reactors will be very stable.

Recent work on the stability of EBR-I was described by R. R. Smith. The spontaneous oscillations and the positive component of the power coefficient of reactivity observed for this reactor with the Mark II core were briefly discussed in the December 1957 issue of *Power Reactor Technology*, Vol. 1, No. 1; the initial results with the Mark III core, which was specially designed to eliminate the possibility of fuel-element bowing, are described in reference 3. The more recent results have shown that, with this rigid core, the reactor is very stable, and there is no evidence of a positive power or temperature coefficient of reactivity.

In order to identify more conclusively the source of the Mark II core behavior, certain experiments were undertaken with the Mark III core to decrease its rigidity. In particular, the spacer ribs, by means of which the fuel elements could be made to maintain solid contact with their surrounding subassembly cans over very nearly the entire length, were partially removed from some of the elements. This modification resulted in a fuel assembly in which the rods were rigidly held at the two ends but were free to bow over the remainder of their length. It appears to be difficult to obtain entirely conclusive results from these modifications, but they do apparently introduce some fuel-element bowing that can be detected in the transfer function of the reactor. The effect appears as a small positive power coefficient of reactivity, with a time constant of about 1.9 sec. With all the ribs removed (except near the ends of the elements), the reactor apparently would still be considerably more stable than the reactor with the Mark II core. By extrapolation of the transfer-function measurements, it was estimated that, if the spacer ribs were removed from all the fuel rods, the reactor would reach the instability point at a power level of about 10 Mw (which is, of course, far above the operating limit of the reactor) and at a frequency of about 0.14 cycle/sec.

F. Storrer reported analyses that he had made on the experiments with the Mark II EBR-I core. Storrer extrapolated the measured amplitude response of the transfer function to zero frequency and compared the power coefficient of reactivity consistent with this extrapolation to the observed steady-state power coefficient of reactivity for the Mark II core. The extrapolated zero-frequency coefficient was considerably smaller than the steady-state coefficient. This leads to the conclusion that there must be a negative component of the power coefficient of reactivity having a time constant which is long, relative to the period of oscillation used for the lowest frequency measurements on the Mark II core.

References

1. H. B. Smets, Reactor Dynamics at Low Power, A/CONF.15/P/107, Second United Nations International Conference on the Peaceful Uses of Atomic Energy, Geneva, 1958.
2. H. B. Smets, The Describing Function of Nuclear Reactors, *IRE Trans. on Nuclear Sci.*, NS-6(4): 8–12 (December 1959).
3. F. W. Thalgott et al., Stability Studies on EBR-I, A/CONF.15/P/1845, Second United Nations International Conference on the Peaceful Uses of Atomic Energy, Geneva, 1958.

Section V

EFFECT OF RADIATION ON DUCTILE-BRITTLE TRANSITION OF STEEL

It has been recognized since the beginning of reactor development that the effects of radiation must be taken into account in the design of reactor structures and in the design of those other structures (particularly the pressure vessel) which are close enough to the reactor to receive important irradiation. The preservation of the integrity of the pressure vessel is, of course, especially important since the consequences of a failure could be very serious. In those vessels which contain high pressures, and therefore have thick walls, it has usually been found necessary to provide an internal thermal shield to avoid excessively high thermal stresses in the vessel walls from the heat produced by radiation absorption. The thermal shield, of course, also provides incidentally a substantial degree of shielding against other possibly harmful effects of radiation. It is not immediately apparent, however, that a shield which protects adequately against thermal effects will in all cases provide automatically the desired shielding against fast neutrons.

In general, the effects of fast-neutron irradiation on steel[1] are typical of those for most metallic structural materials. In ferritic steels, irradiation increases the yield strength and the ultimate strength, decreases the elongation and the reduction in area, increases the hardness, raises the ductile-brittle transition temperature, and lowers the energy to fracture in notched impact specimens. Of these, the effects on the ductile-brittle properties are among the most obscure, and there has recently been concern as to whether these effects might in some cases limit the useful pressure-vessel life.

Unirradiated Brittle Fracture Behavior

The importance of avoiding brittle behavior is, of course, well recognized in conventional design practice. The factors determining the incidence of brittle failure are, however, complex, and many of them are not susceptible to precise specification. A few cases in which the realm of brittle behavior has inadvertently been entered have resulted in rather spectacular failures. An example[2] is the failure of the hull of a T-2 tanker in 1943. This ship, while lying quietly at her dock, suddenly broke in two. The brittle fracture occurred with no apparent cause; it extended across the deck, down both sides, and across the bilges, but it did not cross the bottom shell plating. The computed deck stress at the time was only 9900 psi.

Ship incidents of this kind have inspired extensive investigations which have yielded much information on the brittle behavior of materials. Reference 2 contains a detailed review of this information. A number of sections from reference 2 are quoted below as background material for the discussions of radiation effects and the treatment of ductile-brittle effects in reactor vessel design. These extracts have been selected purely to illuminate the reactor problem. Obviously, selected quotations out of context can convey distorted information; the reader is urged to consult the reference for the original information.

Notch Effects

Under what conditions can brittle fracture occur? The general principles indicate that any loading condition involving a low ratio of maximum shear stress to maximum normal stress tends to promote brittle behavior in steel. Certain design practices introduce unfavorable stress systems into structures and hence should be avoided or modified whenever possible. Even with satisfactory designs, however, structural discontinuities in the form of notches may be introduced inadvertently during construction. These discontinuities provide the conditions necessary to introduce low shear and high tensile stresses. Examples of such discontinuities are

incompletely penetrated weld joints, weld cracks, base metal or underbead cracks, and accidental notches.

. . . . . .

It is evident that a sharp deep notch not only acts as a stress raiser but greatly alters the state of stress locally. Uniaxial tensile loading of a specimen containing a notch may thus create a local state of triaxial tension with a consequent dangerous lowering of the maximum shear stress to maximum tensile stress ratio. The sharper and deeper the notch, and the thicker the plate, the lower the ratio.

The exact ratio of shear to normal stress that can be tolerated without inducing brittle behavior varies for each steel and even for each condition of heat-treatment or cold work for a given steel.

Furthermore, there is no simple or straightforward means for controlling this stress ratio, so that it is impossible to obtain a quantitative measurement of the sensitivity of a steel to brittle behavior in terms of the principal stresses. This is unfortunate because indirect means must be employed for evaluating the relative brittleness of steels. The only satisfactory way of doing this at present is by means of notch-toughness tests conducted at several temperatures. These tests indicate the temperature (or temperature range) over which changes in behavior take place. The results of these tests cannot be interpreted directly in terms of design requirements. This, however, may not be a permanent shortcoming because contemporary investigations indicate that there is a correlation between notch-toughness test results and service performance in at least one field of application.

All sharp deep notches in thick plates are potential brittle fracture nuclei. How sharp and how deep any notch must be in any thickness of plate to initiate a fracture depends upon many factors. Of these, temperature is of paramount importance. With a given geometry and for a specific strain rate, there is always a temperature above which brittle fractures will not occur in mild steel. This temperature is in reality a temperature range, but for convenience it is defined and described as a "transition temperature."

There are several criteria currently in use to define a transition temperature. It has been found experimentally that, when a given type of specimen, whether it be a standard unnotched tensile specimen or a Charpy bar, is tested over a wide enough temperature range, there is a change in behavior at some temperature; with certain specimens the change is abrupt; with others it occurs gradually over a wide temperature range. . . . for example, unnotched tensile specimens made from hot-rolled 0.2 per cent carbon steel remain ductile almost down to liquid air temperature, but as this temperature is approached, the ductility drops rapidly to almost zero. The mode of fracture changes from

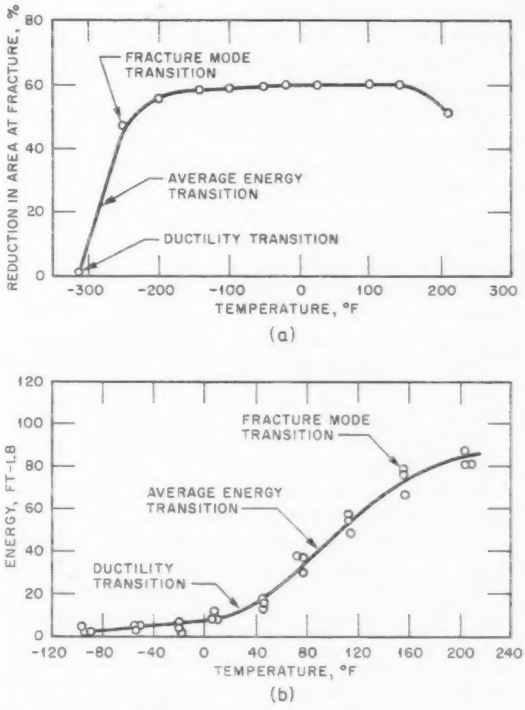

Figure 10 — Data for a hot-rolled 0.2 per cent carbon steel showing the transition from ductile to brittle behavior as the testing temperature is lowered. (*a*) Data for unnotched 0.505-in.-diameter tensile specimens. (*b*) Data for V-notched Charpy specimens.[2]

shear to cleavage; there is a corresponding change in the appearance from the gray silky surface characteristic of shear to the coarse crystalline type associated with cleavage. Obviously, then, the transition temperature can be defined in terms of the fracture mode as judged from the fracture appearance.[*] This is called the fracture-appearance criterion, commonly abbreviated to "fracture criterion."

Another criterion for the transition temperature is based on the lack of ductility, for example, when the ductility drops to some specified low value. This is called the ductility-transition temperature.[*] For a given type of test specimen, a lower temperature is usually obtained for the ductility transition than is found for the fracture-appearance transition.

Another commonly used measure of transition temperature is the temperature corresponding to the energy halfway between the maximum and minimum values.[†] The multiplicity of criteria presently in use makes correlation of published data dif-

*As indicated in Fig. 10.

†See part *b* of Fig. 10.

ficult. The complications are discussed more fully in Chapter V;[*] for the present it is sufficient to consider the transition temperature as a dividing line between relatively ductile and relatively brittle behavior. Figure [10,† part *b*] shows the three transition temperatures for the same steel as determined with V-notched Charpy specimens.

Since the transition temperature for a given mild steel may range from liquid air temperature for unnotched ½-in.-diameter cylindrical tensile specimens to above room temperature for sharply notched bars, how can engineers use transition temperature data for design purposes? Only recently has satisfactory progress along this line been made. Tests on many plates taken from structures that failed in service have indicated that a correlation between notched bar data and service failures is possible. However, the problem still remains relatively complex. It seems that various types of notched specimens can be used to supply useful information. For example, when the energy absorbed by a V-notch Charpy specimen is below a critical value at the operating temperature, brittle fractures may initiate at nominal stresses below those normally considered safe. Whether or not a crack, once started, will propagate depends upon many factors such as the toughness of the steel, the average stress in the structure, the amount of stored energy, and the details of the structural design. In general, the conditions are such that a crack can continue to grow more easily than it can start. This, of course, leads to the spectacular catastrophic type of failure found too often in large structures.

It is important to realize at the outset that no single magic number can be used in procurement specifications to automatically preclude brittle behavior. The engineer must be cognizant of the effects on transition temperature of chemical composition, heat-treatment, type of welding electrode, preheat, postheat, notches, design, energy available in the system, and many other factors before he can hope to cope with the problem.

. . . . . .

Effects of Composition of Steel

SUMMARY [‡]

Data illustrating the influence of chemical composition are too incomplete to permit a reliable quantitative estimate of the effect of the individual elements. However, enough tests have been made on laboratory heats of steel to define the approximate effects of the elements present in carbon structural steel. Carbon was found to raise the 50% fibrous fracture transition temperature for the tear test by about 33°F for each 0.1% increase in the carbon content and the 20 ft-lb keyhole Charpy transition by about the same amount. The 15 ft-lb transition temperature for V-notch Charpy specimens was raised about 25°F for each increase of 0.1% carbon; the 10 ft-lb transition was raised about 20°F. Carbon has a marked effect on maximum energy for fracture; the higher the carbon content, the lower the maximum energy.

Manganese lowers the transition temperature of steel at a much slower rate than carbon raises it. The 50% fibrous fracture tear test transition temperature is lowered only about 4°F for each 0.1% increase in manganese content. The 15 ft-lb keyhole Charpy transition, however, was lowered about 10°F for each 0.1% increase.

Silicon apparently acts in a complex manner, and its effect is still somewhat uncertain. Up to about 0.3% it appears to be slightly beneficial, but larger amounts raise the transition temperature.

Phosphorus increases the transition temperature even more rapidly than equal amounts of additional carbon. Consequently, it is important to restrict the phosphorus to the lowest practicable amount.

Sulphur seems to have little, if any, direct effect on low-temperature brittleness, but it does create nonmetallic inclusions, which reduce ductility and which influence brittle behavior in a minor manner.

Nitrogen is apparently effective in raising the transition temperature, but the effect varies markedly with the criterion selected and with the composition of the steel. Some investigators report large effects; others, none. The effect of nitrogen seems to depend largely upon the deoxidation practice employed during melting and casting. The embrittling effect of nitrogen was found to be largely overcome by aluminum in steels fully deoxidized with silicon and aluminum, particularly when the steels were normalized; aluminum additions to incompletely deoxidized steels were ineffective in reducing the effectiveness of nitrogen, probably because the aluminum was completely converted to oxide—leaving none to react with the nitrogen.

Oxygen appears to have an embrittling effect on mild steel, as has been reported, and may cause grain boundary cracking. The effect of oxygen on the properties of commercial steel is not understood; the presence of oxides, however, is known to lower the notch ductility, even when the fracture is 100% shear.

Aluminum, as mentioned above, is effective in neutralizing the deleterious effect of nitrogen in fully deoxidized steels. Aluminum is beneficial in normalized steels at least in amounts up to 2 pounds per ton. In hot-rolled steels the effect of aluminum is generally beneficial, but its effectiveness varies with the type of steel and particularly with the silicon content.

---

*In reference 2.

†The figure number has been changed to be compatible with other illustrations in this Review.

‡Quoted from reference 2, pp. 183–185.

Table V-1 APPROXIMATE CHANGES IN TRANSITION TEMPERATURE PRODUCED BY VARIOUS ELEMENTS[2]

(Change in Transition Temperature, °F)

Varied	Tear test	20 ft-lb Charpy keyhole	10 ft-lb Charpy keyhole	Average-energy Charpy V-notch	15 ft-lb Charpy V-notch	10 ft-lb Charpy V-notch
0.1% C	+33	+35	+20	+50	+25	+20
0.1% Mn	−4	−7	−7	−10	−10	−10
0.1% Si (0.2% max.)	−30	−30				
0.1% Si (0.3% min.)	+15	+15		+13	+13	+13
0.01% P	+5	+3		+15	+13	+11
0.01% N (low Mn)	+50	+25		+40		0
0.01% N (high Mn)	+20	+3		+70		+40
1.0% Ni				−10	−35	
0.1% Al	−30	−30				
S (0.06% max.)	0	0			0	
Change from 50 to 100 ferrite grains/sq in. at 100 ×	−80	−50				

Nickel is generally recognized as being effective in lowering the transition temperature. However, it is not as potent in this respect as manganese.

The ferrite grain size generally has a marked effect on transition temperature, but the magnitude of the effect varies with the manufacturing and heat-treating practice. The smaller the ferrite grain size, the lower the transition temperature in a given test. The ferrite grain size depends upon the final rolling temperature and the rate of cooling from above the transformation temperature. Hot-rolling practice thus has a predominant influence in establishing the grain size. Low finishing temperatures and fast cooling favor the formation of small ferrite crystals. Thinner plates normally cool faster than thicker ones, hence have a more favorable grain structure.

Cold work, particularly when combined with aging, raises the transition temperature. The average-energy transition temperature for keyhole Charpy specimens is raised about 25°F for steels prestrained 5% and aged.

The effects of various elements on the tear test and Charpy transition temperatures are summarized in Table [V-1*].

. . . . . .

*The table number has been changed to be compatible with other tables in this Review.

Effects of Welding

SUMMARY [*]

Defective welding has been largely responsible for most of the recent structural failures in service. Almost without exception the origins of cleavage cracks in welded ships have been at weld defects. Very rarely have cracks been observed to start in sound welds in any type of engineering structure.

The transition temperatures of weld metal vary over a wide range of temperature depending upon the welding conditions, the type of electrode used, and the design of the specimen employed for the test. Fast cooling leads to poor notch ductility. Consequently, small fast stringer beads or fillet welds should be avoided. Preheating retards cooling and hence generally lowers the ductility transition temperature. Postheating to 1100 to 1200°F generally produces a substantial improvement in the notch ductility of weld metal or in weldments made without preheat. Deposits made with low hydrogen (E6015 or E6016) electrode or by the submerged arc process generally have lower ductility transition temperatures than E6010 deposits made without preheat. Preheat and postheat treatments have little effect upon the (already good) notch toughness of E6016 deposits. The rather poor notched bar properties of E6010 weld metal are due in large part to microcracks that form at temperatures below 212°F

*Quoted from reference 2, pp. 215–216.

in rapidly cooled weld metal. Preheating even to 200°F retards the cooling sufficiently to prevent microcracks from forming.

The fracture-appearance transition temperature has been shown to be relatively insensitive to variations in the welding condition. This criterion reflects the propensity of the base plate to fail by cleavage but does not indicate whether or not the fracture was preceded by extensive plastic flow. The amount that a metal can flow before forming a crack that will propagate through the base plate is best indicated by the ductility transition temperature. The criterion seems to be satisfactory for evaluating the performance of weldments, whereas the fracture transition is not.

The performance of a weldment is best indicated by specimens that contain the entire weld zone as well as a portion of the base plate. Furthermore, the specimens should be notched so that the notch extends across the weld, the heat-affected zone, and the base plate. Specimens having notches parallel to the direction of the weld reflect only the properties of the particular zone of the weldment containing the notch. Such tests, however, are particularly useful for disclosing which zone has the highest ductility transition temperature.

. . . . . .

Effects of Residual Stresses

SUMMARY [*]

The conflicting evidence concerning the effect of residual stresses has led to a great deal of confusion, and it is impossible at the present time to reach unambiguous conclusions concerning the possible effects of residual stresses on the brittle behavior of engineering structures; laboratory test results and theoretical analyses indicate that such stresses are of minor importance to the life of large structures. However, operating field engineers are familiar with an uncomfortably large number of failures that are apparently unexplainable on any other basis. Since it is recognized by all that large residual stresses do exist and a truly critical laboratory test has not yet been devised to determine their effects on the occurrence of brittle failures, it would appear to be advisable at this time to take every possible precaution to minimize such stresses wherever possible.

Designs and fabrication techniques should be refined to minimize residual stresses, and one of the available methods of relieving residual stresses should be used in critical assemblies. Abrupt changes in section should be eliminated, and weld defects should be avoided. Preheating and postheating are very beneficial. There is an impressive amount of evidence to indicate that service life probably is affected by residual stresses in structures made of materials that can fail in a brittle manner. Medium carbon structural steels fall in this class only when the temperature is well below the ductility transition temperature. The use of normalized steels (preferably fully deoxidized) welded with low hydrogen electrodes should provide an adequate safeguard against failures due to residual stresses.

It has been established that cleavage cracks can propagate spontaneously in structures subjected to stresses above about 10,000 psi, provided, of course, that the temperature is below the ductility transition of the steel. The conditions necessary for the spontaneous initiation of cracks in structures subjected to low nominal stresses are still obscure. Perhaps several factors can operate to help start cracks—the sudden fracturing of an incompletely penetrated weld being one and the presence of triaxial tensile stresses due to welding being another.

. . . . . .

Types of Test Specimens

There are 30 or 40 types of notched specimens in current use.[*] With the diversity of specimen designs, testing procedures, and interpretations that presently exist, it is difficult to make any meaningful comparisons of the results obtained in different investigations. Probably a single standard test and a uniform interpretation of the test data will never be adopted because of the variations in service conditions, fabrication procedures, and designs from one application to another. When a particular type of test, however, is used to evaluate behavior in a specific service, an effort should be made to avoid nonstandard specimen designs and testing procedures. Such changes may preclude accurate comparison or correlation of the test results with other data. It is to the advantage of all concerned to use, whenever possible, generally accepted specimen designs and testing procedures rather than modifications thereof and also to employ standard methods of interpreting the test data. Two of the most commonly used and most discriminating tests are the V-notch Charpy (for an individual material) and the slow notchbend (Kinzel or Lehigh) test (for a weld-plate combination). It is specifically recommended that V-notch Charpy tests always be made in addition to any other desired tests for purposes of comparison.

The literature on the brittle behavior of steel is extensive and contains vast amounts of data based on different types of tests and on different methods of evaluation. Despite the many papers presented

*Quoted from reference 2, pp. 230–231.

*Quoted from reference 2, pp. 306–309.

on the subject, few contain critical analyses or summaries useful for clarifying and correlating the results. Hence, it is important to dwell at some length on this subject.

Notch bar tests are conducted at various temperatures to determine the temperature range over which an appreciable change takes place in some measured value, such as energy absorption, ductility, or fracture appearance. This change frequently occurs rather abruptly; for example, the energy absorbed to failure may drop abruptly from a high value to a much lower one within a narrow temperature range. The width of the transition range varies with the test conditions, the specimen geometry, and the chemical composition of the steel. In certain cases it is only a few degrees; in others it is several hundred. With any particular test specimen the transition range can be determined from any one of several different measurements having to do with energy absorption, ductility, or the appearance of the fracture. These measurements, however, will not all necessarily give the same transition range even in a single type of test. This is an important fact that is not universally recognized.

Transitions from "ductile" to "brittle" behavior based upon fracture appearance always yield higher values of transition temperature range than do those based on ductility measurements at the notch. This is a consequence of the observed physical behavior of the specimens and of the manner in which the fracture appearance and ductility transitions have been defined. The fracture-appearance criterion is, as the name implies, based upon the appearance of the fracture surface. The temperature at which the surface is 50 per cent granular and 50 per cent fibrous is defined as the "fracture-appearance (or fracture) transition temperature." Below this temperature the energy to failure may be appreciably below the maximum, but the ductility at the base of the notch is usually higher (e.g., 5 to 30 per cent). The "ductility transition" is almost always at a lower temperature because this criterion is based on an arbitrarily selected low value of notch ductility (e.g., one per cent lateral contraction at the notch apex). With V-notch Charpy specimens this corresponds to the 10 to 15 ft-lb energy level for semi-killed structural carbon steels.

Either transition can be measured by any of several variables; for example, the fracture-appearance transition can be determined by fracture appearance or by energy absorption, and the ductility transition can be determined by ductility or energy measurements. The fracture transition cannot, however, be determined by notch ductility measurements, and the ductility transition cannot readily be established by observing the nature of the fracture surface.

Variations in specimen geometry affect the ductility and the fracture-appearance transition temperatures quite differently. The evidence shows that the ductility transition temperature varies markedly with notch geometry and with specimen shape, whereas the fracture-appearance transition temperature is relatively insensitive to changes in specimen geometry, particularly in specimens more than $\frac{1}{2}$ in. thick. As the notch is made sharper and deeper, the strains are more localized; the strain rates are higher for a given loading rate; and the degree of triaxial tension becomes greater. These factors favor higher ductility transition temperatures. The fracture-appearance transition depends upon how the crack, once formed, progresses rather than upon the amount of plastic flow that precedes the initiation of the crack. Once the first crack forms, the fracture characteristics no longer depend upon the geometry of the original notch. Rounded notches, of course, permit more local ductility than sharp ones before a crack forms and are thus associated with low ductility transition temperatures. Specimens with different sizes and shapes of notches often show widely different ductility transitions and yet show about the same fracture-appearance transition temperature.

Ductility transition temperatures are sensitive to variations in notch geometry, rate of loading, and conditions of welding; fracture-appearance transitions are considerably less sensitive to such variations. Since "transition temperature" is so dependent upon the criterion selected and upon the test method used, it is obvious that no exact correlation between results from widely varying tests is possible unless great care is taken to obtain comparable data, such as data based upon ductility at the notch apex. Any correlation based upon fracture appearance will not, in general, hold for the ductility transitions in the same series of tests. There may, indeed, even be reversals in the order of rating. There are two reasons for this: (1) the fracture-appearance transitions are near the top of the energy-temperature curves, whereas the ductility transitions are near the bottom; and (2) the slope of the steeply rising portion of the curve varies with the type of test and with the type of steel.

Some reasonably good correlations between ductility transitions have been established. For example, the 10 ft-lb V-notch Charpy transition temperature (for a number of steels of the same general class) was found to be related to the ductility transition for keyhole Charpy specimens (as defined by the temperature at the middle of the scatter zone). Another correlation of value was found between the 10 ft-lb V-notch Charpy temperature and the temperature at the 20,000 in.-lb level for internally notched 12-in.-wide plates.

The only available direct correlation between service failures and notched bar tests is with the V-notch specimen. It was found that the 7 or 8 ft-lb transition temperature for V-notch Charpy specimens made from plates in which fracture initiated in

service corresponded approximately to the temperature of the service failure. Fracture-appearance transitions do not appear to correlate with the temperatures at which cracks initiate in service. They do, however, seem to correlate with the temperatures at which cracks are arrested.

Test Methods

Because of the extensive use of Charpy and Izod type tests for determining the susceptibility of steels to notch-brittle behavior, a brief review of these tests is presented.

The Charpy and Izod type tests are known as impact tests because of the use of impact or pendulum machines for applying the energy required to rupture the specimen. The energy values obtained are comparative only for the particular specimens and cannot be used for engineering-design calculations. Similarly the notch-brittle behavior obtained applies only to the particular specimen size, notch geometry, and test conditions and cannot be directly applied to other sizes of specimens and other conditions.

The test specimen used in the standard Charpy V-notch type of test is illustrated in part *a* of Fig. 11; this specimen is impact-tested as a simple beam, as shown in part *b* of Fig. 11.*

The standard Izod test specimen is shown in part *a* of Fig. 12; this specimen is impact-tested as a cantilever beam, as shown in part *b* of Fig. 12.

Detailed data on these tests are given in reference 3.

It should be noted that Charpy or Izod tests do not directly predict the ductile-brittle behavior of thick sections of steels used in pressure vessels. They do, however, form a basis for acceptance tests for choosing between steels when they can be correlated with established service behavior of the steels.

Irradiation Effects on Tensile Properties

Although the most significant information on the brittle behavior of steel is obtained from

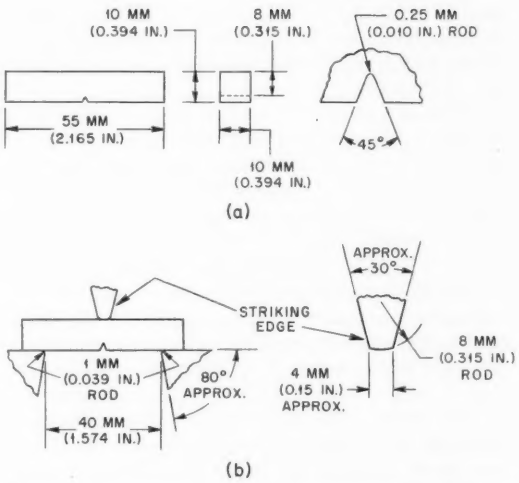

Figure 11—Charpy V-notch impact test.[3] (*a*) Simple beam impact test specimen. Permissible variations of the values shown are as follows: adjacent sides, 90° ± 10′; cross-section dimensions, ±0.025 mm (0.001 in.); length of specimen, +0 −2.5 mm (0.100 in.); angle of notch, ±1°; radius of notch, ±0.025 mm (0.001 in.); dimensions to bottom of notch specimen, 8 ± 0.025 mm (0.315 ± 0.001 in.). (*b*) Simple beam test. The angle between specimen support members and the plane of the anvil surface is 90° ± 10′; all dimensional tolerances are ±0.002 in.

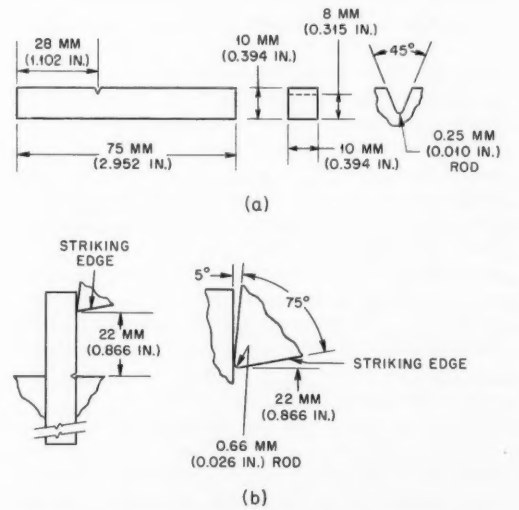

Figure 12—Izod impact test.[3] (*a*) Cantilever beam impact test specimen. Permissible variations of the values shown are as follows: cross-section dimensions, ±0.025 mm (0.001 in.); length of specimen, +0 −2.5 mm (0.100 in.); angle of notch, ±1°; radius of notch, ±0.025 mm (0.001 in.); dimension to bottom of notch, 8 ± 0.025 mm (0.13 ± 0.001 in.). (*b*) Cantilever beam test. All dimensional tolerances are ±0.002 in.

*Figures 11 and 12 are reprinted here by permission from *ASTM Standards, Part 3, Metals Test Methods (Except Chemical Analysis)*, American Society for Testing Materials.[3]

Table V-2 TENSILE PROPERTIES OF IRRADIATED STEELS[4,9]

Line	Alloy	Fast-neutron dose, $10^{18}/cm^2$	Irradiation temp., °F	Yield strength, 10^3 psi	Tensile strength, 10^3 psi	Uniform elongation, %
1	A-106	0		40	76	18
2	(fine	20	580	81	102	8
3	grain,	20	680	55	87	11
4	0.24% C) .	20	760	48	82	12
5		80	580	79	106*	6
6		80	780	47	79	11
7		100	175	97	102	4
8	A-106	0		46	80	14
9	(coarse	20	580	93	115	8
10	grain,	20	680	67	98	9
11	0.24% C)	20	760	43	84	14
12		70	580	87	103*	3
13		70	780	64	94	11
14		100	175	116	121	2
15	A-212	0		40	75	25
16	(0.2% C)	20	175	92	98	6
17		20	560	76	102	9
18		20	680	61	90	12
19		20	760	56	84	14
20		60	700	82	105*	6
21		60	780	59	81	13
22		100	175	109	116	4
23	A-301	0		41	66	23
24	(0.1% C,	5	150	55	69	23
25	1% Cr,	5	575	47	71	26
26	0.5% Mo)	0		44†	68	21
27		5	150	57†	71	23
28		5	575	52†	73	23
29		15	740	53	78	18
30		45	740	63	86	12
31		45	700	91	103	
32	E7016	0		59	73	16
33	weld	5	175	69	78	11
34	metal	5	600	61	77	17
35		20	175	108	108	0
36		60	700	83	94	12
37		60	740	77†	85	12
38		60	780	69	77	15
39		100	175	115	115	0
40	8.5% Ni,	0		92	119	22
41	0.1% C	17	175	138	148	11
42		100	175	183	184	2
43	Carilloy	0	0	120	129	8
44	T-1	17	175	170	171	0.5
45		100	175	186	187	0.3

*Broke without necking; work-hardening rate was greater than for an unirradiated specimen.
†Testing rate = 2.0 per minute; for all others, 0.05 per minute.

data on the ductile-brittle transition temperature, the effects of irradiation on the tensile properties of steels are appreciable and give a clear indication of radiation damage. Some of the general effects of irradiation[1] on the tensile properties of steel were reviewed briefly in previous issues of *Power Reactor Technology* (Vol. 1, No. 1, December 1957, and Vol. 2, No. 4, September 1959). Further data were presented at the Second United Nations International Conference on the Peaceful Uses of Atomic Energy.[4-8] Table V-2 presents data on the tensile properties of irradiated steels. These results may be summarized as follows:

1. The yield stress may increase by a factor of 2 or 3 at high doses (10^{20} nvt). The yield-stress increase is strongly dependent upon irradiation temperature; the higher the irradiation temperature, the smaller the yield-stress increase.

2. The tensile strength is increased less than the yield strength. In some cases irradiation at higher temperatures has resulted in a larger increase in tensile strength than irradiation at a lower temperature.

3. The elongation is reduced. In particular, the uniform elongation is sharply reduced at high doses. In many cases necking begins at or soon after yielding.

4. The reduction in area shows little effect except at high doses. All but a few specimens showed reductions in area of at least 25 or 30 per cent at the highest doses. In all but a few cases the uncorrected true-fracture stress (at room temperature) is not greatly changed.

Tensile data obtained by ORNL[9] on irradiated high-purity iron and an alloy of high-purity iron with 0.14 per cent carbon indicate that the shapes of the stress-strain curves are often remarkably altered by irradiation. Similar data for ASTM A-212 grade B steel and ASTM E7016 weld metal were presented in reference 4. Figure 13 is a typical plot of stress versus elongation for high-purity iron, and Fig. 14 (reference 10) presents preliminary data from step-annealing of ASTM A-212 grade B carbon-silicon steel hardness specimens irradiated to 1×10^{18} nvt (energy greater than 1 Mev) at 140° F and 5×10^{18} nvt at 140 and 575° F. Data for unirradiated specimens of the same steel with a 5 per cent cold work are also shown in Fig. 14.

Because it is difficult to correlate the effects of irradiation on the tensile properties of steel with the possible brittle behavior of the material, investigations of the impact strength of steels are being conducted.

Effects of Irradiation on the Ductile-Brittle Transition Temperature of Ferritic Steels

Irradiation of ferritic steels by fast neutrons produces two effects on their impact strength: (1) the ductile impact energy absorbed is reduced, by a factor of approximately 3 in the worst cases, and (2) the ductile-brittle impact transition temperature is increased, by approximately 400° F in the worst cases. Typical data obtained are shown in Fig. 15 and Tables V-3 and V-4. The first effect does not appear to be as important as the second since the ductile impact energy absorption remains at a value considered as adequate (greater than 15 ft-lb on the Charpy V-notch impact test). The second effect is important because the service failure evidence mentioned earlier indicates that, if the operating temperature of the material falls below the ductile-brittle impact transition temperature of the material, brittle failure of the material is likely. For this reason a considerable amount of irradiation and testing of impact

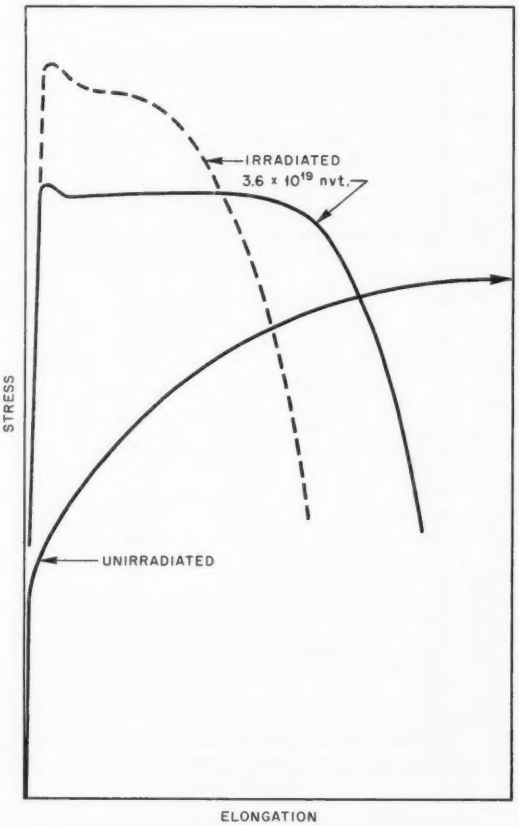

Figure 13 — Effect of irradiation on stress-strain curves of high-purity iron (typical of both fine- and coarse-grained material. The change of uniform (and total) elongation with strain rate is large. The uniform elongation tends to be reduced more at lower doses in the fine-grained material).[9] – – –, strain rate is 2.0 per minute. ——, strain rate is 0.05 per minute.

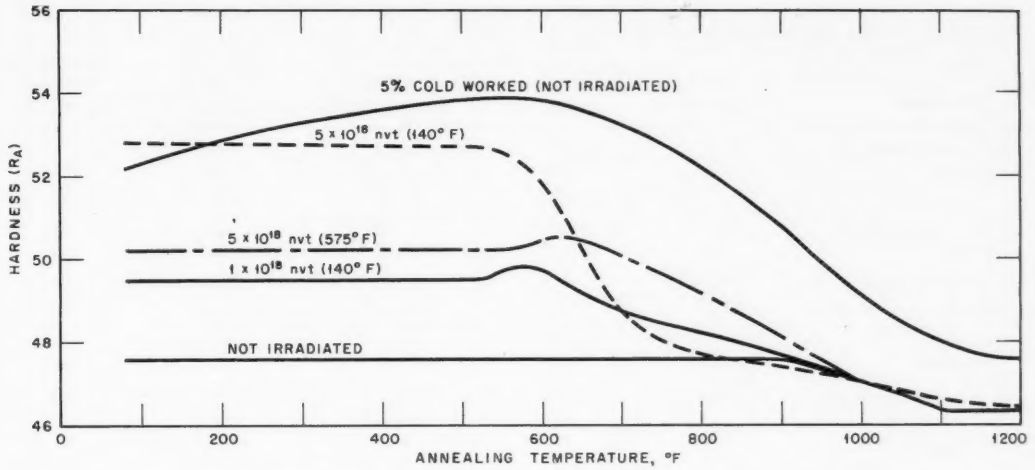

Figure 14 — Postirradiation annealing of irradiated ASTM A-212 grade B carbon-silicon steel.[10]

Table V-3 CHARPY V-NOTCH IMPACT TRANSITION TEMPERATURES OF SEVERAL IRRADIATED STEELS[9]

Material	15-ft-lb transition temp., °F			
	Irradiation*			
	None	1×10^{18} neutrons/cm^2 at 175°F	5×10^{18} neutrons/cm^2 at 175°F	5×10^{18} neutrons/cm^2 at 575°F
ASTM A-212 grade B, hot-rolled ¾-in. plate	−85	−30	25	−40
ASTM A-212 grade B, normalized ¾-in. plate	−65	−20	55	−30
ASTM A-212 grade B, normalized 6-in. plate, ¼ thickness	−30		70	35
ASTM A-285 grade A, hot-rolled ¾-in. plate	40	105	200	125
ASTM A-285 grade A, normalized ¾-in. plate	10	60	150	115
ASTM A-301 grade B, furnace-cooled from 1675°F, ¾-in. plate	15	70	170	110

*Flux values are integrated neutron flux >1 Mev.

specimens has been done in an effort to understand the factors which influence the rise in the ductile-brittle impact transition temperature.

Both types of specimens, subsize Izod and standard-size Charpy V, have been used in testing. The subsize Izod specimens used are approximately one-half the size of the full-size Izod and standard Charpy V. They are 0.2 in. square with a 0.005-in.-radius V-notch, 0.050 in. deep. Standard-size Charpy V specimens measure 0.394 in. square, 2.165 in. long, with a 0.010-in.-radius V-notch that is 0.079 in. deep (see parts *a* and *b* of Fig. 12).

Qualitatively, the subsize Izod specimens give the same results; quantitatively, they do not. The transition temperatures of the two types are substantially different both before and after irradiation. Wilson and Sisman[10] found that the initial transition temperature of the subsize Izod specimens was 50°F lower than that of the Charpy V, and Trudeau[8,11] found the difference to be 80 to 108°F. After irradiation, Wilson and Sisman[10] found that the transition-temperature rise in the subsize Izod specimens as compared to Charpy V specimens was slightly greater at 2×10^{18} nvt and about 100°F less at 10^{20} nvt.

Table V-4 NOTCH IMPACT (SUBSIZE IZOD) PROPERTIES OF STEELS AND WELDS[4]

Steel	Heat-treatment*	Irradiation temp., °F	Dose, fast neutrons/cm^2	Increase in transition temp., °F	Decrease in "ductile" energy, %
ASTM A-212 grade B	N	175	5×10^{18}	45	0
(No. 18)		575	5×10^{18}	15	0
		175	5×10^{19}	100	35
ASTM A-212 grade B	HR	175	5×10^{18}	45	20
(No. 43)		175	5×10^{19}	275	50
ASTM A-212 grade B	N and SR	175	5×10^{19}	220	30
(No. 65)	HAZ	175	8×10^{19}	350	60
E7016	SR	175	2×10^{19}	210	40
weld metal	Q and T	175	8×10^{19}	360	55
High-strength quenched	Q and T	175	5×10^{18}	175	20
and tempered		575	5×10^{18}	100	0
(Carilloy T-1)		175	7×10^{19}	450	50
8½%	S	175	5×10^{18}	100	20
nickel		175	7×10^{19}	500	60
ASTM A-106	N	175	5×10^{19}	85	0
(fine grain)		175	8×10^{19}	250	30
ASTM A-106	N	175	5×10^{19}	30	
(coarse grain)		175	8×10^{19}	300	55

*N = normalized.
SR = stress relieved.
Q and T = quenched and tempered.
S = special heat-treatment.
HAZ = heat-affected zone near weld.

Table V-5 IMPACT TEST STEELS[10]

Item No.	Description	Chemical composition, %					
		C	Mn	P	S	Si	Others
1	ASTM A-212 grade B C-Si steel, ½-in. plate; normalized	0.24	0.81	0.020	0.040	0.248	
2	ASTM A-302B Mn-Mo steel, 8½-in. plate	0.19	1.36	0.020	0.025	0.26	0.48 Mo
3	ASTM A-285 grade A C-steel, ¾-in. plate	0.11	0.32	0.018	0.020		
4	ASTM A-301 grade B Cr-Mo steel, ¾-in. plate	0.11	0.36	0.020	0.026	0.22	0.98 Cr; 0.47 Mo
5	ASTM A-200 grade T-22 Croloy 2¼-in. alloy steel pipe, ½-in. wall by 6-in. OD	0.10	0.45	0.018	0.019	0.031	2.18 Cr; 1.00 Mo
6	High-strength quenched and tempered steel (Carriloy T-1)[12]	0.2 max.	Also contains Mn, Cu, Ni, Cr, Mo, V, and B; actual percentages not known				
7	Swedish 2112 C-Si steel, 3¾-in. plate	0.16	1.29	0.012	0.031	0.32	0.08 Cr; 0.08 Ni; 0.14 Cu
8	High-purity Fe-C alloy, ¾ by 3¾-in. bar	0.180	0.002	<0.003	0.003	0.03	0.0039 O; 0.0003 H; 0.0001 N; other metals ≦0.01
9	High-purity[8] Fe	0.004		0.001	0.003	0.009	<0.002
10	Fe-C alloy[9]	0.138		0.002	0.006	0.02	<0.002
11	ASTM A-106[13]	0.24	0.3–1.0	0.040 max.	0.050 max.	0.12 min.	
12	ASTM A-201[13]	0.2–0.35 max.	0.80 max.	0.035 max.	0.040	0.15–0.30	
13	Ducol W-30[14]	0.155	1.24	0.015	0.038	0.18	0.49 Cr; 0.09 Ni; 0.15 Cu; 0.28 Mo; 0.02 V

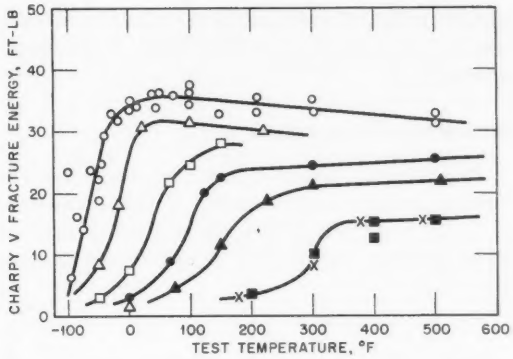

Figure 15—Charpy V impact strength of irradiated ASTM A-212 grade B carbon-silicon steel (hot-rolled condition).[10] ○, unirradiated. △, 1×10^{18} nvt(>1 Mev) at 175°F. □, 5×10^{18} nvt(>1 Mev) at 175°F. ●, 7×10^{18} nvt(>1 Mev) at 175°F. ▲, 1.2×10^{19} nvt(>1 Mev) at 175°F. ■, 5.6×10^{19} nvt(>1 Mev) at 270°F. ×, 1×10^{20} nvt(>1 Mev) at 330°F.

As indicated by these comparisons, the Charpy V specimens give a more sensitive measurement of impact strength. In addition, most impact testing of unirradiated materials is done using the standard-size Charpy V-notch specimens. In future investigations, ORNL plans to use Charpy V specimens.

In the investigations carried out by various organizations, many materials were tested, and an effort was made to determine the various factors that influence the change in transition temperature. Some of the factors investigated are (1) grain size; (2) impurities; (3) composition; (4) postirradiation annealing; (5) welding; (6) irradiation temperature; and (7) integrated flux. The various steels used in the tests along with their typical composition are shown in Table V-5.

Grain Size

The influence of grain size has received only a small amount of investigation. Wilson[4] irradiated fine- and coarse-grained specimens of A-106 steel to the same integrated fluxes and found that the fine-grained specimens showed 16 per cent less rise of transition temperature after 10^{20} nvt than the coarse-grained specimens (Table V-6). However, ORNL[9] has reported data on high-purity iron, wherein the transition-temperature rise for the fine-grained (0.02 to 0.06 mm) specimens was found to be 150 per cent greater than for the coarse-grained (0.1 to 1.0 mm) specimens. It would appear that more study is required to clarify the effect of grain size.

Table V-6 SHIFT IN SUBSIZE IZOD 2 FT-LB IMPACT TRANSITION TEMPERATURE FOR COARSE- AND FINE-GRAINED A-106 STEEL[4]

Irradiation	Grain size	Subsize Izod impact transition temp., °F		
		Initial	Final	Rise
5×10^{18} nvt at 600°F	Coarse grain	+15	+50	40
	Fine grain	−75	−50	25
5×10^{18} nvt at <200°F	Coarse grain	+15	+55	40
	Fine grain	−75	+10	85
~10^{20} nvt at <200°F	Coarse grain	+15	300	285
	Fine grain	−75	165	240

Impurities

The influence of impurities has been investigated by ORNL[9,10] and by the British.[14] It was found that high-purity iron and high-quality mild steels exhibited less radiation-induced transition-temperature rise than the commercial steels containing their normal amounts of sulfur, phosphorus, etc. (see Tables V-1 and V-5). The rise in transition temperature for high-purity iron and iron alloy specimens (items 8 to 10 in Table V-5), as compared to commercial steels, was 40 per cent less for the subsize Izod specimens and 60 per cent less using Charpy specimens.

Composition

Trudeau[8] at Chalk River has also investigated the effect of composition on the transition-temperature rise. Iron was alloyed with each of the following elements: 3.25 per cent nickel, 1.5 per cent manganese, 0.5 per cent molybdenum, and 1.0 per cent chromium. The chromium and molybdenum alloys showed the least rise, being no more than 20 per cent greater than the unalloyed iron. The nickel and manganese alloys showed the greatest rise, but because of their low initial transition temperature, their final transition temperature was of about the same magnitude as that of the other materials. The

net effect of composition was therefore negligible for the alloys tested. Trudeau[11] in examining T-1 steel found this material did not behave as well as other quenched and tempered steels. This poor behavior may be attributable to the boron content of T-1 steel and the greater damage it may undergo because of the (n,α) reaction with B^{10}.

Postirradiation Annealing

Postirradiation annealing has been investigated as a means of reversing the rise in transition temperature. Trudeau[8] found that annealing A-201 mild steel subsize Izod specimens (irradiated to 6.2×10^{19} nvt at <200°F) for 6 hr at 500°F raised the 2 ft-lb transition temperature 18°F. However, annealing at 635°F for 6 hr produced a 50 per cent recovery. Berggren[15] investigated annealing of A-212B base-metal and weld-metal specimens which had been irradiated at 575°F. He found that annealing effects became significant at 560°F and above. Golik[16] irradiated A-302B and A-212B specimens to 1.4×10^{18} nvt and noted increases in the Charpy V transition temperatures of 55 and 60°F, respectively. Annealing for 50 hr at 750 and 850°F gave some recovery. However, annealing at these temperatures resulted in temper embrittlement. Balai[17] at ANL also investigated the effects of postirradiation annealing in A-212B steel irradiated in the Materials Testing Reactor (MTR) to 1×10^{20}, 4×10^{20}, and 7×10^{20} nvt (flux >1 Mev). Base-metal, weld-metal, and heat-affected zone materials lost all resistance to impact at temperatures to at least 250°F; saturation of damage, as measured by the increase in nil ductility temperature (NDT), occurred below the lowest exposure. Annealing in an inert atmosphere at 700 to 1150°F for 1 to 3 hr was increasingly effective in restoring impact properties to preirradiation levels.

Welding

Wilson[4] irradiated subsize Izod specimens of type E7016 weld metal joining A-212B plate and specimens taken from the heat-affected zone. The weldment had been stress-relieved at 1200°F. The rise in transition temperature for the weld metal and transition-zone metal was substantially greater than for the parent metal. However, the heat of welding had lowered the initial transition temperatures of the weld metal and transition-zone metal below that of the parent metal. Consequently the irradiated transition temperatures of all three were comparable.

Irradiation Temperature

The effect of irradiation temperature has received considerable attention. ORNL[9] irradiated A-212B subsize Izod specimens at temperatures ranging from 175 to 600°F and fluxes ranging

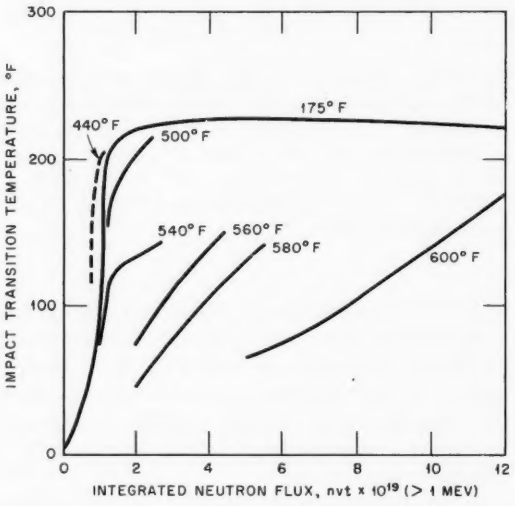

Figure 16—Estimated impact transition temperatures of irradiated ASTM A-212B high-tensile-strength carbon-silicon steel; subsize Izod test, 4-in. plate, hot-rolled.[9] The figures on the plot indicate the irradiation temperature.

from 2.0×10^{19} to 12×10^{19} nvt. The results are shown in Fig. 16, and the following facts are indicated:

1. Irradiation temperatures of 500°F and below have little effect on the rise of the transition temperature.
2. At irradiation temperatures of 500 to 600°F, there is substantial reduction in the rate of transition-temperature rise; however, it would appear that there is no reduction in the ultimate rise.

Integrated Flux

ORNL[10] has irradiated standard Charpy V specimens from a number of different commercial ferritic steels and of differently heat-treated specimens of the same steel. These include the steels listed as items 1 to 7,

Table V-5. The irradiation temperatures ranged from 120 to 330°F, and the fast-neutron doses were up to 1×10^{20} nvt (>1 Mev). A plot of the 10 ft-lb Charpy V transition temperature versus the integrated flux for all the steels tested is shown in Fig. 17. Two conclusions are apparent

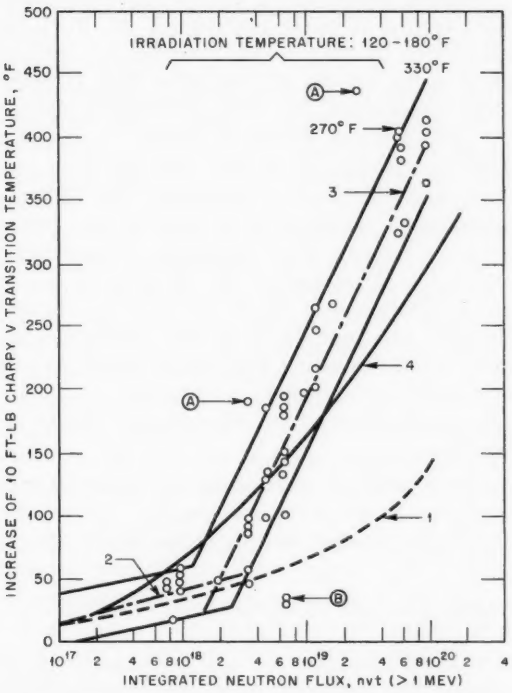

Figure 17 — Effect of fast-neutron irradiation on Charpy V impact transition temperatures of several steels.[10] Ⓐ, Carriloy T-1. Ⓑ, High-purity iron. Other points are for the materials listed in Table V-5. Curves 1 to 4 are the plots of Eqs. 1 to 4 shown in the text. Data points are from reference 10.

from the data on the effect of integrated flux on the rise of the Charpy transition temperature:

1. A number of commercial ferritic steels with different heat-treatments experience approximately the same transition-temperature rise for a given integrated flux.

2. For these ferritic steels, the transition temperature increases approximately linearly with the logarithm of the integrated flux once the exposure exceeds 1×10^{18} to 2×10^{18} nvt.

It will be noted that two of the steels fall outside the general limits of these conclusions. Carilloy T-1 shows significantly higher increases, and the high-purity iron shows significantly lower increases in Charpy V transition temperature. As was discussed previously, the high-purity iron specimens consistently show lower transition-temperature rises. In the case of Carilloy T-1, there appear to be two explanations. ORNL[10] indicated that the specimen used was from an early heat of the Carilloy and that the properties and composition of the specimen were not well known. A second explanation may lie in the fact that Carilloy T-1 contains boron as an additive. Because of the B^{10} neutron-capture cross section, it would appear that a greater radiation damage may occur in this steel and thus may cause the higher rise in the transition temperature.

Prediction of Transition Temperature Rise

Cottrell[18] has proposed that the rise in transition temperature of slow-bend notched specimens can be predicted by the semiempirical equation

$$\Delta TT = 31.5\ \phi^{1/3} \qquad (1)$$

where ΔTT is the rise in ductile-brittle slow-bend transition temperature (°F) and ϕ is in units of 10^{18} nvt. Harries et al.[14] found that Eq. 1 gave good agreement with the notch slow-bend tests of irradiated Ducol W-30 (see Table V-5) steel specimens. This equation has been plotted in Fig. 17 to compare it with the data obtained by ORNL. It can be readily seen that the equation does not correlate the impact test data for integrated doses greater than 2×10^{18} nvt.

Two expressions for the mean data of the limiting curves of Fig. 17 were calculated:

$$\Delta TT = 50 + 27 \log_{10} \phi/2 \times 10^{18} \qquad (T < 500°\text{F},\ \phi = 10^{17} \text{ to } 2 \times 10^{18} \text{ nvt}) \qquad (2)$$

and

$$\Delta TT = 50 + 206 \log_{10} \phi/2 \times 10^{18} \qquad (T < 500°\text{F},\ \phi = 2 \times 10^{18} \text{ to } 10^{20} \text{ nvt}) \qquad (3)$$

where ΔTT is the rise in 10 ft-lb Charpy V ductile-brittle impact transition temperature (°F), ϕ is the time-integrated neutron flux (nvt > 1 Mev), and T is the irradiation temperature (°F).

In a more recent WAPD[19] report, Golik has replotted the data of many investigators (Fig. 18) for specimens irradiated at temperatures

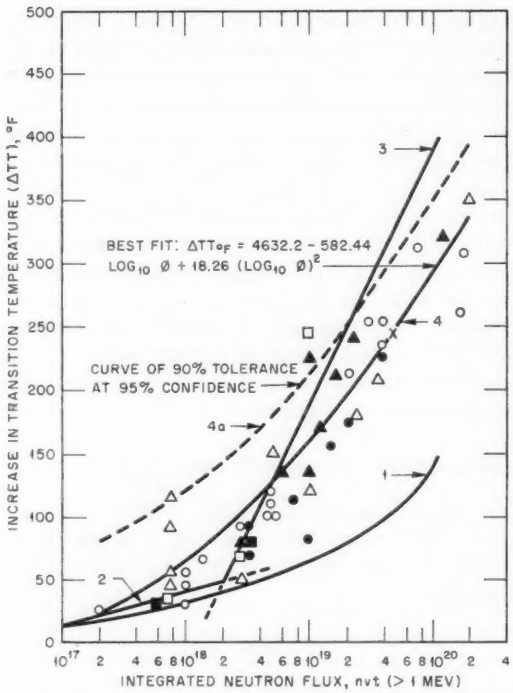

Figure 18 — Effect of neutron dosage on the impact transition temperature (statistical representation of published and unpublished data on the relation between neutron dosage (ϕ) and increase in transition temperature ($\Delta TT_{°F}$) for ferritic steels irradiated at 500°F or below).[19] ×, A-106. ●, A-201. ○, A-212B. ▲, E7016. □, SA-336. △, A-302B. ■, E9016. Curves 1 to 4 are the plots of Eqs. 1 to 4 shown in the text. Data points are from reference 19.

below 500° F. The "best fit" equation developed to express the relation indicated is

$$\Delta TT = 4632.2 - 582.44 \log_{10} \phi + 18.26 (\log_{10} \phi)^2 \quad (T < 500°F;\ \phi = 2 \times 10^{17} \text{ nvt to } 10^{20} \text{ nvt}) \quad (4)$$

where ΔTT is the rise in subsize Izod ductile-brittle impact transition temperature (° F), ϕ is the time-integrated neutron flux (nvt > 1 Mev), and T is the irradiation temperature (° F).

The data points plotted in Fig. 18 are a statistical representation of tests which use both sub-Izod and Charpy V-notch impact specimens.

Equations 1 to 4 have been plotted in Figs. 17 and 18 for comparison.

Present Status and Future Programs

The foregoing would indicate that one can now (with considerable uncertainty) predict the transition-temperature rise of commercial ferritic steels (including welds) with normal preirradiation heat-treatments and operating temperatures below 500° F, and that one can determine the upper limit for those materials when operating above this temperature. To clarify the remaining factors which affect the transition temperature, further irradiation impact testing is being carried out. At ORNL the objectives of the current program are to test further the effects of integrated flux, irradiation temperature, and postirradiation annealing. At Westinghouse Research Center, a program has been initiated[16] in which the following factors will be studied: (1) integrated flux; (2) temperature of irradiation; (3) neutron-flux intensity; (4) neutron-flux spectrum; (5) saturation behavior; (6) metallurgical differences due to preirradiation heat-treatment; (7) heat-to-heat damage response; and (8) postirradiation annealing effects (time and temperature) will be evaluated with respect to changes in brittle-fracture resistance and other mechanical properties.

Other general and summary data on steels for use in reactors and nuclear processing plants can be found in references 20 and 21.

Application to Reactor Vessels

Pressure vessels for nuclear-reactor applications are designed, fabricated, and inspected in accordance with the latest ASME Boiler and Pressure Vessel Code, Section VIII, Unfired Pressure Vessels,[22] and the latest ASME Boiler and Pressure Vessel Code Nuclear Cases, Revisions, and Addenda. These codes do not place any direct requirements on pressure vessels with regard to the increase of the NDT of the vessel material due to radiation, or with regard to the initial impact resistance of the vessel material.[22] No impact test is required on any (carbon or low-alloy steel pressure vessel) material for use at temperatures of −20° F and above or for use below that temperature when the temperature decrease is due to a lower seasonal atmospheric temperature.

Indirectly, the code requirements on pressure vessels correct for the effects of increasing NDT by eliminating notches in the vessels. Requirements are made as to welds used, the welding procedures, and inspection of materials and welds, which reduce very greatly the prob-

ability that notches will occur in the form of slag inclusions, weld undercutting, or other defects. In this respect the requirements for nuclear vessels are more stringent than for nonnuclear vessels. Nuclear pressure vessels, in accordance with Code Case 1273N,[23] are required to have pressure strength welds which are 100 per cent X-ray inspected and are of the double-butt welded type, or the equivalent, to eliminate defects.

Generally, builders and buyers of nuclear pressure vessels have taken it on themselves to correct for increases in the NDT by requiring that materials used initially have a low NDT and by observing the change in NDT during operation. In the Tentative Structural Design Basis for Reactor Pressure Vessels and Directly Associated Components,[24] some operational requirements are suggested for nuclear pressure vessels which could be used to offset the effects of the increase of the NDT.

It is suggested that when the metal temperature is less than 60° F above the NDT, the maximum applied load (on the material), including internal pressure, shall be restricted to 20 per cent of the design value. When the metal temperature is more than 60° F above the NDT, there is no restriction upon the load due to considerations of brittle fracture.

It has been the practice of some reactor designers to provide for the incorporation of removable specimens of the reactor-vessel steel at points inside the vessel where the radiation intensity may be expected to be comparable to that at the vessel wall. The specimens can be removed for test periodically during the vessel life. This appears to be a worthwhile practice which should contribute to the understanding of the problem as well as to the safety of the vessel.

It is not easy to decide rationally how the tolerable upper limit of fast-neutron irradiation on the walls of reactor pressure vessels should be determined. Because of the rather large scatter of the experimental data and because of the rather poor understanding of the relation between the test results and the pressure-vessel behavior, one would prefer a limit which provides a large safety factor against brittle fracture. At first glance, the plots of experimental data (Figs. 17 and 18) give the impression of an upward break in the rate of damage at an irradiation level of about 2×10^{18} nvt, and thus one may be tempted to choose an exposure limit in this vicinity. However, this characteristic is a result of the semilogarithmic plot. If the curves are plotted to a linear scale, as in Fig. 19, the existence of a real discontinuity of slope appears

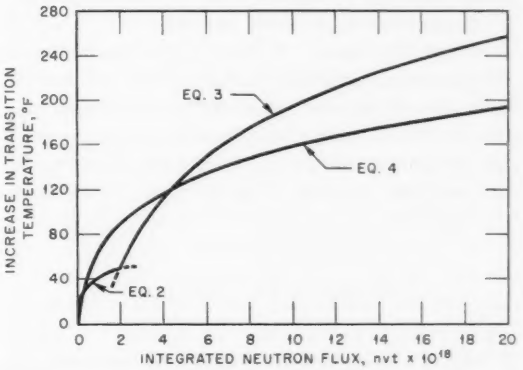

Figure 19 — Linear plot of the curves that fit the data of Figs. 17 and 18.

improbable; indeed, the curves show a saturation behavior which is characteristic of many radiation-damage effects. It therefore does not seem possible to arrive at an exposure criterion from semiqualitative considerations. Probably the only reasonable approach is to set, on the basis of whatever arbitrary decisions are necessary, an upper limit for the ductile-brittle transition temperature, or for the NDT, over the life of the vessel. To observe this limitation the designer would have to estimate the permissible lifetime exposure level on the basis of the existing experimental data, with a suitable safety factor, and provide the corresponding amount of fast-neutron shielding for the walls.

For water-cooled reactors, the atmospheric boiling temperature might define a "natural" choice for the permissible upper limit of the ductile-brittle transition temperature. Below this temperature no pressure stresses are applied by the vapor pressure of the contained water, and the probability of rapid cooling of the vessel, which might generate high thermal stresses, is greatly reduced. Furthermore, if the ductile-brittle transition is sufficiently low that the vessel can safely be pressurized at, or slightly below, the atmospheric boiling point, hydrostatic tests of the vessel and its seals can be made without the presence of an important amount of stored energy in the vessel; this is usually desirable.

If permissible limits corresponding to a very low total lifetime irradiation level are set, the effect on reactor costs may be appreciable. A very rough estimate may serve to illustrate the situation. In a reactor having an effective core power density of 30 kw/liter, the average rate of production of fission neutrons is 2.3×10^{12} neutrons/(cm^3)(sec). If the reactor has a volume V (measured in cubic centimeters) and a surface area A (measured in square centimeters), and if a fraction L of the fission neutrons leaks out of the reactor as fast neutrons, the average fast-neutron current density out of the core $[\bar{J}(\text{core})]$ is

$$\bar{J}\,(\text{core}) = 2.3 \times 10^{12}\, L\, \frac{V}{A}$$

If the core is approximated, for convenience, as a sphere, the fraction $V/A = R/3$. If a core of radius $R = 100$ cm is considered and if the leakage fraction L of neutrons above 1 Mev in energy is taken as 0.02, then the leakage current becomes

$$\begin{aligned}\bar{J}\,(\text{core}) &= (2.3 \times 10^{12})(0.02)\,(100/3) \\ &= 1.5 \times 10^{12} \text{ fast neutrons/(cm}^2\text{)(sec)}\end{aligned}$$

If it were decided, for example, to limit the radiation exposure at the pressure-vessel wall to a maximum of 2×10^{18} fast neutrons/(cm^2)(sec) over a reactor lifetime of 20 equivalent full-power years, the maximum permissible fast-neutron flux at the wall would be 3.2×10^9 fast neutrons/(cm^2)(sec). The ratio of the current density from the core to the permissible flux density at the wall would be

$$\frac{\bar{J}(\text{core})}{\phi(\text{wall})} = \frac{1.5 \times 10^{12}}{3.2 \times 10^9} = 470$$

The actual fast-neutron flux at the vessel wall is larger by some small factor than the current into the wall; but, very roughly, this may be considered to be compensated by the geometrical attenuation of the flux, and it may be said, in round numbers, that a fast-neutron attenuation by shielding material, by a factor of 400 or 500, or about e^6, would be needed between the core surface and the vessel wall. If this shielding were to be provided primarily by water, the average attenuation length (distance for the neutron flux to decrease by a factor $1/e$) could hardly be much less than about 9 cm at operating temperature. The thickness of fast-neutron shield between the core and vessel wall would have to be about $6 \times 9 = 54$ cm, or about 21 in.; thus the vessel inside diameter would be 308 cm (10.1 ft). The ratio of the vessel inside diameter to the core diameter would be 1.54, and the ratio of pressure-vessel cross-sectional area to the cross-sectional area actually utilized for power production would be $(1.54)^2 = 2.4$.

On the other hand, if a lifetime exposure of 2×10^{19} fast neutrons were allowed, the required attenuation by the internal fast-neutron shield would fall to a factor of 40 or 50, or about e^4, and the required thickness of the internal shield would decrease by about 18 cm, or about 7 in. With this shield thickness, a reactor core of 118 cm (rather than 100 cm) radius could be accommodated in the 10.1-ft pressure vessel cited above. If the height of the core were increased in proportion and if the power density of 30 kw/liter were maintained, the ratio of the power output of the larger core to that of the smaller core would be $(1.18)^3 = 1.64$. Thus the postulation of the higher permissible radiation level has resulted in an increase of 64 per cent in the estimate of the power output attainable from a pressure vessel of given diameter.

The use of a very large pressure vessel to reduce the neutron exposure of the walls can introduce substantial cost increases, for not only does the cost of the vessel itself increase, but the cost of related structures may increase also. In particular, the pressure and/or volume requirement of the secondary containment structure will increase. Consequently, if further consideration indicates that conventional pressure-vessel steels can be exposed to only very low total fast-neutron doses, there will be a strong incentive in the design of large reactors to incorporate the most effective shield possible within the vessel and, possibly, to consider some of the alloy steels that have very low NDT as pressure-vessel materials.

For the design of a good shield against fast-neutron damage (or even for the specification, in any but the roughest terms, of the damaging dose received by the pressure-vessel walls), one needs to know the relation between the damage produced by a given number of neutrons and the energy of the neutrons. Experimental data of this kind are lacking.

The common practice in experimental work has been to specify the fast-neutron dose in terms of the flux of fast neutrons with energies

above 1 Mev. This apparently has been done as a matter of convenience, and the practice is by no means intended to imply that neutrons of energy less than 1 Mev have no damaging effect. So long as tests are made at roughly equivalent positions in reactors having similar compositions, the neutron energy spectra will not vary greatly, and the test results should be comparable. However, the spectrum near the pressure-vessel wall of a power reactor can be vastly different than that in either the core of the reactor itself or the core of the test reactor, and the spectrum at the wall can be affected greatly by the design of the shield between the core and the wall.

The fundamental process by which fast-neutron damage occurs in steel is the displacement of atoms from their normal sites in the crystal lattice.* Although the energy required to displace a single atom is only about 25 ev, a neutron, because of its low mass, transfers to an iron atom only about 3 per cent of its kinetic energy in the average collision; hence, on the average, a neutron must have about 1 kv of energy to displace a single iron atom. When neutrons with considerably higher energies collide with atoms in the steel, the atom suffering the collision (the primary knock-on atom) may gain sufficient energy that it collides with other atoms to cause further displacements. In almost all reactor cases, these secondary displacements far outnumber the primary ones and presumably account for almost all the radiation damage.

The total number of displacements produced per neutron collision increases with neutron energy, but at a rate somewhat less than linear. As the neutron energy is increased, the scattering becomes more "forward." That is to say, the neutron makes relatively fewer nearly head-on collisions with nuclei and relatively more glancing collisions; the average fractional energy transfer to the struck nucleus thus decreases with neutron energy. Furthermore, at a neutron energy of about 1 Mev (in iron), inelastic scattering becomes important, and neutrons, on the average, lose a fraction of their kinetic energy in exciting nuclei rather than in imparting kinetic energy. It has been estimated that 1-Mev neutrons, in iron, cause the displacement of about 390 iron atoms per average collision.[25]

At still higher energies, an additional process becomes important in determining the efficiency of displacement production. When the energy of the primary knock-on atom becomes sufficiently high, much of the energy is lost in electron excitation rather than in the production of secondary knock-ons. For iron, the energy at which this process becomes important is estimated to be about 56 kev.[25] This would correspond to a neutron energy of about 3 Mev.

Although the quantities discussed above, which relate the total number of displacements to the neutron flux and the neutron energy, are not known very precisely, they would be of great value in relating neutron damage to neutron energy and in deriving design criteria from experimental observations if it could be said that radiation damage is determined only by, or primarily by, the total number of displacements. This is not known to be true for the case of embrittlement of steel; nevertheless, until proven untrue, it would appear to be a more useful assumption than that which is tacitly made when damage effects are described simply as a function of the time-integrated neutron flux above some arbitrarily chosen energy level.

Figure 20 is a plot of the energy spectrum of fission neutrons, showing, as a function of energy, the relative number of neutrons $N(E)$ produced by fission in unit energy interval. Also plotted is $EN(E)$, the fractional distribution of energy in neutrons of various energies. It may be seen that, whereas a rather large fraction of the neutrons lies below the energy 1 Mev, almost all the energy content is included in those neutrons having energies above 1 Mev. In the core of a typical water-moderated reactor, the neutron-flux spectrum would be rather similar to the fission-neutron spectrum in the energy range above 1 Mev; the proportion of lower energy flux would, however, be higher. In the reflector, and near the pressure-vessel wall, the spectrum might be quite different. For example, if a thick steel thermal shield is placed quite near the vessel wall, the neutron spectrum at the wall may have a large component of relatively low-energy neutrons, made up of neutrons which have been inelastically scattered in the thermal shield and further moderated by whatever water lies between the thermal shield and the vessel wall. On the other hand, if the region

*Reference 25, from which the discussion of displacement production is derived, is a good review of the fundamental processes which produce radiation damage.

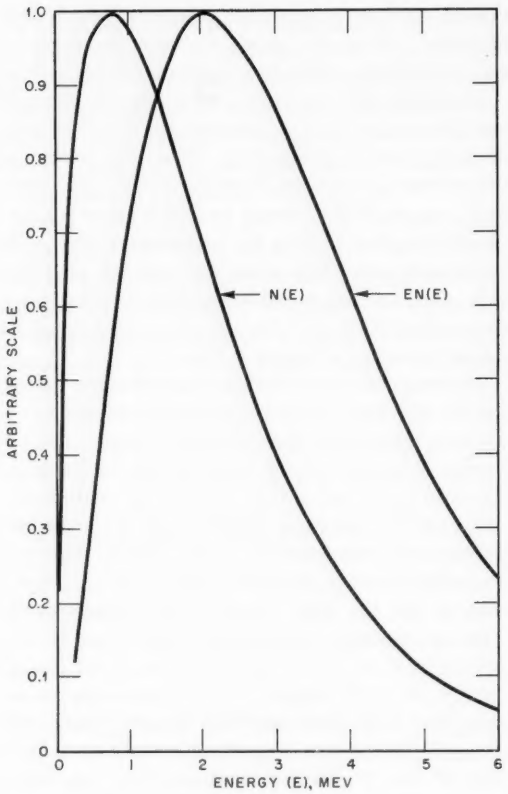

Figure 20 — Energy spectrum of fission neutrons. $N(E)$ is the number of neutrons in unit energy interval at energy E.

between the core and the vessel wall contains mostly water, the neutron spectrum at the wall may be appreciably "harder" than that in the core.

In assessing the present status of the embrittlement problem, it may be said that one of the most urgent needs is more consistent experimental data; for, whereas the average behavior of experimental specimens would indicate that reasonably high neutron exposures are tolerable, the behavior of the worst specimens is quite discouraging. It is not at all clear that this scatter is inherent in the phenomenon. It is quite possible that, when sufficient work has been done to standardize the tests and when the variables of sample composition and heat-treatment, neutron energy spectrum, and temperature of irradiation can be adequately controlled, the behavior will prove to be consistent.

References

1. Papers Prepared for Radiation Effects Review Meeting, Congress Hotel, Chicago, July 31–August 1, 1956, USAEC Report TID-7515(Pt. 2) (Del.), August 1956.
2. Earl R. Parker, *Brittle Behavior of Engineering Structures*, John Wiley & Sons, Inc., New York, 1957.
3. *ASTM Standards, Part 3, Metals Test Methods (Except Chemical Analysis)*, American Society for Testing Materials, Philadelphia, 1958.
4. J. C. Wilson, Effects of Irradiation on the Structural Materials in Nuclear Power Reactors, A/CONF.15/P/1978, Second United Nations International Conference on the Peaceful Uses of Atomic Energy, Geneva, 1958.
5. M. J. Makin et al., Mechanical Properties, Embrittlement, and Metallurgical Stability of Irradiated Metals and Alloys, A/CONF.15/P/80, Second United Nations International Conference on the Peaceful Uses of Atomic Energy, Geneva, 1958.
6. N. F. Pravdyuk et al., The Effect of Neutron Irradiation on the Mechanical Properties of Structural Materials, A/CONF.15/P/2052, Second United Nations International Conference on the Peaceful Uses of Atomic Energy, Geneva, 1958.
7. M. H. Bartz, Performance of Metals During Six Years Service in the Materials Testing Reactor, A/CONF.15/P/1878, Second United Nations International Conference on the Peaceful Uses of Atomic Energy, Geneva, 1958.
8. L. P. Trudeau, Effects of Neutron Irradiation on Mechanical Properties of Ferritic Steels and Irons, A/CONF.15/P/190, Second United Nations International Conference on the Peaceful Uses of Atomic Energy, Geneva, 1958.
9. J. C. Wilson et al., HRP Radiation Metallurgy, in Solid State Division Annual Progress Report for Period Ending August 31, 1958, USAEC Report ORNL-2614, p. 98, Oak Ridge National Laboratory, Nov. 20, 1958.
10. J. C. Wilson and O. Sisman, Radiation Metallurgy, in Solid State Division Annual Progress Report for Period Ending August 31, 1959, USAEC Report ORNL-2829, p. 207, Oak Ridge National Laboratory, Dec. 11, 1959.
11. L. P. Trudeau, The Status of Radiation Effects Research on Structural Materials and Implications to Reactor Design, a Paper Presented at the AEC Conference at Chicago, Oct. 15 and 16, 1959.
12. Norman E. Woldman, *Engineering Alloys (Revised)*, American Society for Metals, 1954.
13. Samuel L. Hoyt, ed., *ASME Handbook, Metals Properties*, Vol. 2, Sponsored by the Metals Engineering Handbook Board of the American Society of Mechanical Engineers, McGraw-Hill Book Company, Inc., New York, 1954.
14. D. R. Harries et al., The Effects of Neutron Irradiation on the Ductile-Brittle Transition Tem-

peratures of Weldable Structural Steel Plates, British Report AERE-M/R-2536, April 1958.

15. R. G. Berggren, The Status of Radiation Effects Research on Structural Materials and Implications to Reactor Design, a Paper Presented at the AEC Conference at Chicago, Oct. 15 and 16, 1959.
16. M. A. Golik, in Technical Progress Report, Materials Department, for the Period September 26, 1959 to December 25, 1959, USAEC Report WAPD-MRK-4, p. A-50, Westinghouse Electric Corp., Bettis Atomic Power Laboratory, Jan. 12, 1960. (Classified)
17. N. Balai, Embrittlement of Fine-Grained Ferritic Steels by Neutrons; Restoration of Impact Properties in Irradiated 3A-212B Steel by Thermal Heat Treatment, a Paper Presented at the AEC Conference at Chicago, Oct. 15 and 16, 1959.
18. A. H. Cottrell, Theory of Brittle Fracture in Steel and Its Application to Radiation Embrittlement, in *Brittleness in Metals, a Conference Held at R&D Branch, Culcheth Laboratory, 1 November 1957,* pp. 3–17, Risley, 1959.
19. M. A. Golik, in Technical Progress Report, Materials Department, for the Period December 26, 1959 to March 25, 1960, USAEC Report WAPD-MRK-5, p. A-22, Westinghouse Electric Corp., Bettis Atomic Power Laboratory, Apr. 5, 1960. (Classified)
20. B. Watkins, Steel for Reactors and Processing Plants, *Nuclear Eng.*, 4(40): 296–303 (July-August-September 1959).
21. D. R. Harries, Radiation Damage in Iron and Steel, *Nuclear Power*, 5(47): 97–99 (March 1960); Radiation Damage in Iron and Steel—2, *Nuclear Power*, 5(48): 142–145 (April 1960).
22. *Boiler and Pressure Vessel Code:* Section VIII, Unfired Pressure Vessels, American Society of Mechanical Engineers, New York, 1959.
23. ASME Boiler and Pressure Vessel Code, *Mech. Eng.*, 81(7): 92 (July 1959).
24. Tentative Structural Design Basis for Reactor Pressure Vessels and Directly Associated Components, Report PB-151987 (Revised Dec. 1, 1958).
25. G. J. Dienes and G. H. Vineyard, *Radiation Effects in Solids*, Interscience Publishers, Inc., New York, 1957.

Section VI

GAS-COOLED REACTORS

On Feb. 10 and 11, 1960, a symposium on gas-cooled reactors was sponsored jointly by the Franklin Institute and the Delaware Valley Section of the American Nuclear Society. The proceedings of this symposium[1] have recently been published.

The three sessions of the symposium covered the status of several major gas-cooled-reactor

Table VI-1 REACTORS REVIEWED AT GAS-COOLED-REACTOR SYMPOSIUM[1]

	Experimental Gas-Cooled Reactor (EGCR)	High-Temperature Gas-Cooled Reactor (HTGR)*	DRAGON Reactor Experiment	TURRET Reactor
Status	Operation by end of 1962	Completion in 1963	Completion in 1963	Criticality in 1962
Location	Oak Ridge, Tenn.	Peach Bottom, Pa.	Winfrith, U.K.	LASL
Power, Mw(t)	85	115	20	3
Gross, Mw(e)	29.5		None	None
Net, Mw(e)	22.0	40		
Turbine fluid	Steam	Steam		
Temp., °F/ pressure, psia	900/1300	1000/1450		
Coolant	Helium	Helium	Helium	Helium
Outlet temp., °F	1050	1380	1380	2400
Inlet temp., °F	510	660	660	1600
Pressure, psia	315	300	300	500
Fuel	$\frac{3}{4}$-in.-diameter UO_2 pellets in type 304 S.S. tubes of 20-mil wall thickness	Cylinders of graphite matrix with dispersed carbides of U^{235} and Th; 3.5 in. (diameter) by 12 ft (length)	U^{235} and thorium in graphite matrix; cylindrical, with fission-product vent system	Hollow graphite circular cylinder impregnated with U^{235}, $\frac{1}{2}$-in. ID by 1-in. OD by 5.875 in. long
Fuel channels	236; 8-in. lattice	810	37	312
Fuel assemblies	7-rod clusters 29 in. long; 1416 total		7-element clusters; 37 total	5 cylinders per channel
Fuel enrichment	2.5% U^{235}	13.8% U^{235} in Th	~14% U^{235} in Th	93% U^{235}
Specific power	7.5 Mw/ metric ton	83 Mw/ metric ton (U + Th)	~75 Mw/ metric ton (U + Th)	~430 Mw/metric ton (U^{235})
Fuel life	10,000 Mwd/ metric ton	75,000 Mwd/ metric ton (U + Th)	~70,000 Mwd/ metric ton (U + Th)	10 to 50% U burnup
Moderator	Graphite	Graphite	Graphite	Graphite
Reactor vessel diameter, ft	20	14		$12\frac{1}{3}$-ft-diameter sphere
Height, ft	46	34		
Wall thickness, in.	$2\frac{3}{4}$ (4-in. head)			2

*Philadelphia Electric Co.

Table VI-1 (Continued)

	Brown Boveri-Krupp Reactor (BBC-Krupp)	Sanderson & Porter Pebble-Bed Reactor (PBR)	Army Mobile Low-Power Reactor (ML-1)	Maritime Gas-Cooled Reactor (MGCR)
Status	Planned	Design study and fuel development program	Operation by mid-1961	Under development
Location			NRTS	
Power, Mw(t)		337	3	22,000 SHP and 60-kw auxiliary
Gross, Mw(e)	15	139		
Net, Mw(e)		125	0.3–0.5	
Turbine fluid	Steam	Steam	Nitrogen (closed cycle, core coolant)	Helium (closed cycle, core coolant)
Temp., °F/ pressure, psia	940/1065	1000/1450	1200/285	1300/739
Coolant	Helium or helium-neon	Helium	Nitrogen	Helium
Outlet temp., °F	1562	1233	1200	1300
Inlet temp., °F	392	550	800	753
Pressure, psia	142	965	310	740
Fuel	2.36-in.-OD graphite balls containing graphite-UC or graphite-ThC center	1.5-in.-OD spherical balls, coated Core: U^{233}, wt.% 0.60; Graphite, wt.% 93.10; Th, wt.% 6.30 Blanket: Graphite, wt.% 50; Th, wt.% 50	Concentric nest of curved plates or UO_2 or BeO-UO_2 pellets in $\frac{1}{4}$-in.-OD Hastelloy-X tubes (ref. design) of 30-mil wall thickness	~$\frac{1}{4}$-in.-OD S.S. tube containing UO_2 or UO_2-BeO or UO_2-Al_2O_3
Fuel channels	None (pebble-bed concept)	None (pebble-bed concept)	61	
Fuel assemblies	None	None	19-pin array of Hastelloy-X tubes	19-rod cluster
Fuel enrichment	20% U^{235}	(See Fuel)		5%
Specific power		4250 Mw/metric ton U^{233} (core)		
Fuel life		53,500 Mwd/metric ton U^{233} and Th^{232}	3000–10,000 hr	4 full-power years
Moderator	Graphite in balls and reflector	Graphite	H_2O	BeO
Reactor vessel diameter, ft		$13\frac{2}{3}$		15
Height, ft		21		10
Wall thickness, in.		5.5		

programs, recent work on fuel elements and materials, and component development and loop studies. The several gas-cooled reactors covered in the status reports are listed in Table VI-1, along with their principal characteristics. The papers on fuel elements and materials were perhaps the most significant, as indications of the progress that has been made on the fundamental problems of the gas-cooled concept, and highlights from those papers are summarized briefly in the following sections.

Fuel Elements for the Experimental Gas-Cooled Reactor

The fuel assemblies for the Experimental Gas-Cooled Reactor (EGCR) contain bundles of seven rod type elements. The rods are composed of UO_2 pellets in jackets of type 304 stainless steel. The length of a bundle is approximately 29 in.; each bundle is enclosed by a cylindrical graphite support sleeve which is

part of the assembly. Although the elements are superficially very similar to the uranium oxide elements that are used in many water-cooled reactors, study of the particular situation in the EGCR has shown that the problems and design criteria are different in a number of ways. To the extent that the problems are more difficult than the fuel problems in water-cooled reactors, the difficulty may be attributed primarily to the very considerably higher coolant temperature rather than to the circumstance that the coolant is a gas.

Because of the low strength of the steel jackets at their operating temperature, it does not appear reasonable to attempt to design for a free-standing jacket or to attempt to give the jacket appreciable strength as a "pressure vessel." Rather, it is expected that the jackets initially will collapse onto the UO_2 fuel under the external pressure of the coolant gas and that, whenever sufficient fission-product gas is released from the UO_2 to give an internal pressure substantially higher than the external coolant-gas pressure, the jackets will gradually enlarge through creep. It is considered probable that such a process will be the determining factor in the lifetime of EGCR fuel elements. Obviously, in such a case, the fuel element should be designed for the lowest possible fission-gas release (this requires that the UO_2 temperature be kept as low as possible), and an empty volume should be provided in the

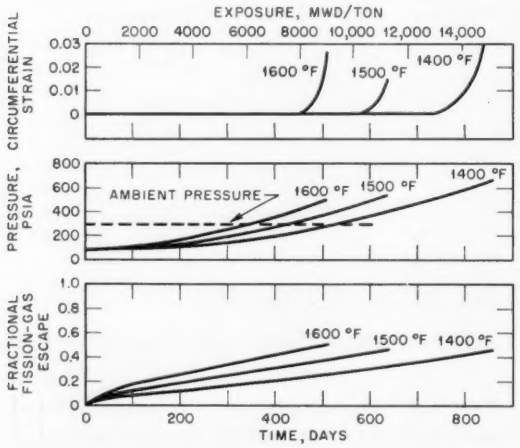

Figure 21—Calculated behavior of the EGCR fuel element with various constant surface temperatures, assuming that the gap remains constant as the cladding expands.[3] The cladding surface temperature is shown for each curve.

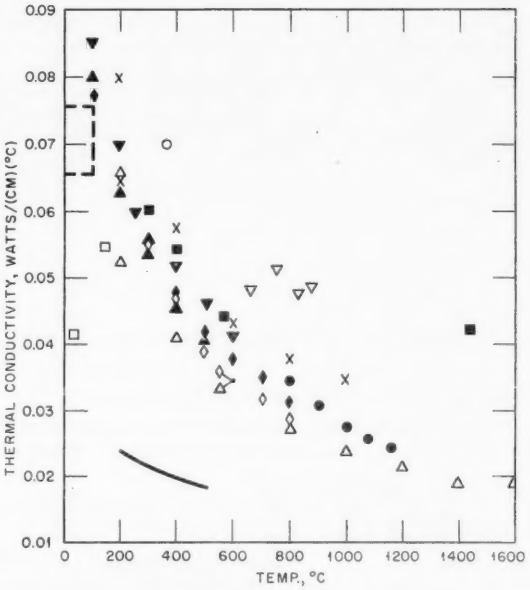

Figure 22—Compilation of reported conductivities of UO_2, extrapolated linearly to theoretical density.[4] ×, W. D. Kingery et al., *J. Am. Ceram. Soc.*, 37(2): 107–110 (1954). △, J. C. Hedge and I. B. Fieldhouse, USAEC Report AECU-3381, September 1956. ●, R. Scott, British Report AERE-M/R-2526, March 1958. □, M. Englander, French Report CEA-79, June 1951. ○, J. E. Flinta, USAEC Report TID-7546(Bk. 2), pp. 516–525, March 1958. ▲, ▼, ◊, and ♦, BMI-HAPO Samples 68, 1000, 70, and 65, respectively, USAEC Report BMI-1315, pp. 7–9, February 1959. ▽, H. Shapiro and R. M. Powers, UO_2 + 4 mole % Y_2O_3, USAEC Report SCNC-296, p. 28, May 1959 (Classified). ■, H. Shapiro and R. M. Powers, UO_2 + 1 mole % Y_2O_3, USAEC Report SCNC-296, p. 28, May 1959 (Classified). ——, J. D. Eichenberg, USAEC Report WAPD-200, September 1958. - - - -, A. M. Ross, Atomic Energy of Canada, Ltd., unpublished data. [It is important to recognize that the curve above is simply a convenient method of displaying the data on UO_2 conductivity from various sources; it is not intended to define the variation of conductivity with temperature. As reference 4 points out, the thermal conductivity varies with the method of fabrication, purity, stoichiometry, and irradiation effects. An informal communication from Hanford has emphasized the importance of the latter effects; recent Hanford data were cited which indicate that the decrease in conductivity produced by irradiation is not completely annealed out by heating to 300 to 500°C. We have been informed also of recent Hanford work that indicates the thermal conductivity of UO_2 to be much higher, at temperatures above 1400 to 1600°C, than one would deduce from extrapolation of the data plotted above. The high-temperature data are, of course, particularly important for gas-cooled reactors—Editor's Note.]

Table VI-2 PERCENTAGE OF FISSION-PRODUCT Xe^{133} EVOLVED IN LITR TESTS[4]

(Standard O/U Ratio Is 2.02 or Less; Density is 95 Per Cent Unless Noted Otherwise)

Center temp., °F	Burnup, Mwd/metric ton						
	4000	5000	6000	7000	11,000	13,000	14,000
1600–2100	0.01		0.01 (O/U ratio 2.03) 0.03 (O/U ratio 2.03)	0.01 (O/U ratio 2.03)	0.03		
2200						0.29 (bulk density 75%)	0.03
2300–2400					0.2	0.03	
2500–2600	9.0 (bulk density 85%; O/U ratio 2.13)			0.07 (O/U ratio 2.04)	1.3	0.04	0.06
3000		0.42 (bulk density 75%; O/U ratio 2.12)					
3100–3200		19.0 (bulk density 75%; O/U ratio 2.12)				15.9 (bulk density 85%; O/U ratio 2.08)	
3300	56.0 (O/U ratio 2.04)						

element to accommodate the gas that is released. These two features are approximated in the EGCR fuel element by the use of annular cylindrical UO_2 pellets rather than solid UO_2 cylinders.[2] The results of a theoretical estimate of the fission-gas pressure buildup and the resulting strain of the jacket are shown[3] in Fig. 21.* The effects are, of course, quite dependent on jacket temperature, since this temperature determines both the strength of the jacket and the maximum and average temperatures of the UO_2. The calculations are based on a heat-transfer rate of 31,500 Btu/hr per foot of fuel-element length. The results depend on the rate of diffusion of fission gases from the UO_2. An apparent diffusion coefficient of 10^{-9} sec^{-1} was assumed. The results of investigations of the various factors affecting the fuel-element life, most of which would enter a calculation of this kind, are summarized in other papers presented at the symposium.

The results of a number of measurements of the thermal conductivity of UO_2 were compiled in reference 4 and plotted as a function of UO_2 temperature. The plot is reproduced here as Fig. 22. The same reference presented the results of fission-gas release measurements derived from UO_2 irradiations in the Low Intensity Test Reactor (LITR). The experiments were made by irradiating encapsulated fuel pellets, collecting the Xe^{133} from the capsules after irradiation, and comparing the Xe^{133} concentration with the calculated equilibrium concentration. The results are shown in Table VI-2. The percentage of fission gas released increased with increasing temperature and, in general, was higher for those specimens with an oxygen-to-uranium ratio greater than 2.02. It was stated that the data are not yet sufficient to establish the effect of oxide density. Irradiation of prototype hollow UO_2 pellets in the Oak Ridge Research Reactor (ORR) yielded the fission-gas release data of Table VI-3. These irradiations were directed primarily toward determining the stability of the fuel in the capsule; the capsule was, in effect, a section of a prototype fuel element, including the type 304 stainless-steel jacket. The experiment was provided with a cadmium shutter that could be lowered and raised to produce severe thermal cycles in the capsules. It was reported that after removal from the reactor the capsules appeared to be in good shape. Gamma-ray scanning of the capsules indicated that fragmentation of the UO_2 was not greatly increased by the thermal

*Figures 21 and 22 and Tables VI-2 to VI-5 are reprinted here by permission from the *Journal of the Franklin Institute, Monograph No. 7.*

Table VI-3 FISSION-GAS RELEASE DATA FOR EGCR-ORR CAPSULES CONTAINING HOLLOW PROTOTYPE UO_2 PELLETS[4]

Capsule No.	Av.* bulk density, g/cm³	Cladding design temp., °F	Calculated burnup, Mwd/metric ton	Gas release, %
0-1	10.39	1300	1760	9.3
0-2	10.33	1600	1910	11.6
0-3	10.40	1300	1640	10.2
0-5	10.38	1600	3260	8.1

*Before irradiation.

cycling, and there was no detectable migration of the fuel along the capsule length. The possibility of migration, because of the empty space at the centers of the hollow pellets, had been feared.

The creep strength of type 304 stainless steel was measured, at 1500°F, in various atmospheres. The composition of the atmosphere had a marked effect. For example, after 900 hr at a stress of 3400 psi, the elongation was about 2 per cent in a CO_2 atmosphere, about 3.4 per cent in an air atmosphere, and about 6 per cent in a helium atmosphere.

Since it is expected that the steel jackets will collapse on the fuel, it is important that the initial diametral clearance between the fuel and jacket be sufficiently small to ensure that the jacket will collapse uniformly rather than buckle. As might be expected, the behavior is a function of the temperature of the steel. Table VI-4 shows the results of collapse tests

Table VI-4 RELATION OF DIAMETRAL CLEARANCE TO THE BUCKLING BEHAVIOR OF 0.020-IN.-WALL, TYPE 304 STAINLESS-STEEL JACKETS SUBJECTED TO 300 PSI EXTERNAL PRESSURE[4]

	Type of collapse for jackets having diametral clearance, in., as indicated				
Temp., °F	0.002	0.005	0.010	0.012	0.020
1300	Uniform	Nonuniform	Nonuniform	Nonuniform	Nonuniform
1500	Uniform	Uniform	Buckled		Buckled
1700	Uniform	Uniform	Uniform	Uniform	
1800	Uniform	Uniform	Uniform	Uniform	
1900	Uniform	Uniform	Uniform	Uniform	

at various temperatures for jackets having various diametral clearances.

A further problem in fuel elements of the EGCR type is that of longitudinal bowing due to the effects of nonuniform power distribution in the individual elements and nonuniform coolant-flow distribution over the coolant-flow area. The bowing tends to move the center of the fuel element in the direction of its hottest surface; this movement reduces the coolant-flow passage on the hot side and increases the temperature asymmetry and the bowing still further. Analysis of this problem indicated that bowing would probably be intolerable if the elements were unsupported over their full length[3] of 27.5 in. Spacers have therefore been added at the middle of the fuel-element cluster. These spacers, attached to the individual fuel-element jackets, bear against each other, and the outside ones bear against the graphite support sleeve.

Table VI-5 PROPOSED FUEL MATERIALS AND THEIR COMPATIBILITY WITH VARIOUS COOLANTS[4]

Fuel material	Coating or jacket	Max. compatible temp., °C, in the indicated coolant		
		CO_2	H_2	He
UC	Stainless steel	~800	>1000	>1000
UO_2 or UC	Be	600	600	600
UC-graphite	Graphite	500	>1000	>2000
UO_2-graphite	Graphite	500	>1000	>1000
UO_2-BeO	BeO*	1600	1600	1600
UO_2-Si-SiC	Si-SiC	1300	1300	1300

*Coolants must be very dry since BeO is volatile in the presence of moisture above 1200°C.

In a summary of the fuel-element tests to date, it was stated[3] that the results indicate that the design of a fuel element capable of a fuel lifetime of 10,000 Mwd/ton should be possible.

A brief discussion[4] was given of fuel elements and fuel materials which are under investigation for advanced gas-cooled reactors. Considerable interest centers around uranium carbide, primarily because of its higher thermal conductivity. Table VI-5 lists combinations of fuel materials and coating or jacket materials which are being tested or considered.

Materials for High-Temperature Gas-Cooled Reactors

There are presently under way a number of projects aimed toward reactor systems that ultimately could produce temperatures considerably in excess of 1000°F. Most of these

projects, including the High-Temperature Gas-Cooled Reactor (HTGR), the DRAGON Reactor Experiment, the Pebble-Bed Reactor (PBR), and the TURRET Reactor, are based on the use of completely nonmetallic elements or elements coated with silicon, and some leakage of fission products from the elements will probably be tolerated. The fuel elements for the Maritime Gas-Cooled Reactor (MGCR), however, will make use of the more conventional structural metals, and a high degree of fission-product retention will be sought, even though the goal is to produce coolant temperatures suitable for gas turbine use.[5] The currently planned fuel assembly consists of a bundle of 19 rods, each approximately $\frac{1}{4}$ in. in diameter and made up of UO_2 pellets in a tube of stainless steel or other metal. Dilution of the UO_2 with BEO or Al_2O_3 is also being considered.

One of the interesting results from the MGCR program[6] has been the observation of fission-product diffusion through nickel. For the test, fission products were introduced into A-nickel by irradiating sandwich specimens of enriched uranium foil between 5-mil A-nickel foils. After irradiation, the uranium was removed, and the A-nickel foils were pressure bonded at 800°C. After annealing the bonded foils for two weeks at 2000°F in an evacuated quartz tube, radioactive cerium and zirconium isotopes were found on the outside of the foil and on the inner surface of the quartz tube.

A second experiment of general interest investigated the deposition of fission products from a helium-gas stream. The experiment consisted of heating a small quantity of finely ground neutron-activated UO_2 in a flowing helium stream which then passed over a series of type 302 stainless-steel coupons. A temperature gradient was maintained throughout the length of the series of coupons. The results of this initial experiment indicated that:[6]

1. The deposition of fission products from the flowing gas stream occurred as if the stream were a saturated solution.
2. The gamma activity of Nichrome wires used to connect the coupons together was much more intense than that of the coupons.
3. Approximately 10 to 12 per cent of the radioactivity could be accounted for as plated out on the metal specimens.
4. The radioactive elements ruthenium, molybdenum, tellurium, and iodine were identified by gamma-spectrometer methods.
5. Significant plate-out occurred over the entire temperature range from 400 to 1700°F, although the maximum deposition occurred at different temperatures for the different fission products.

High-temperature reactors that do not rely on structural metallic jackets for fission-product containment fall into two classes: (1) those (HTGR and DRAGON) which tolerate some permeability of the fuel elements but attempt to control the fission-product level in the coolant stream by scavenging fission products from the elements themselves, and (2) those (typified by the PBR) which strive for a minimum degree of permeability of the fuel elements and accept whatever contamination of the coolant stream may result from an imperfect realization of this objective.

The HTGR fuel elements consist of cylinders made up of carbides of U^{235} and thorium dispersed in graphite.[5] These cylinders are surrounded by graphite sleeves which are analogous to the jackets of more conventional fuel elements. The fueled cylinder does not, however, contact the sleeve; heat is transferred from the cylinder to the sleeve by radiation and is removed from the outer surface of the sleeve by the coolant gas. A small flow of the helium coolant is drawn off from the annulus between the fuel cylinder and the sleeve and is passed through fission-product traps. The graphite sleeve is permeable, and therefore a flow of the scavenging helium is directed inward through the sleeve so as to counteract the diffusion of fission products outward through the sleeve. The fission-product trap currently under development is likely to be composed of activated charcoal. The initial stages of the trap are to be water cooled, and the final stage may be refrigerant cooled.

One objective of this HTGR fuel-element concept is the limitation of the activity buildup in the primary loop equipment to a level sufficiently low that fairly direct maintenance will be possible. Another objective is the limitation of the gaseous fission-product level in the primary helium coolant to such a value that accidental release of the coolant into the secondary containment will not result in serious difficulty or hazard. Thus the continuous release of activity to the site surroundings as a result of normal coolant leakage will not exceed permissible concentrations.

Even though the scavenging system is employed, it is, of course, desirable to use graphite of very low permeability for the fuel-element sleeve. The development of low-permeability graphite cans and sleeves by impregnation, by pyrolytic deposition of carbon, and by silicon carbide coatings is under way.[6]

The HTGR reports also summarized the results of experiments on the migration of the thorium and uranium carbides in the graphite matrix which is to be used in the fuel elements. At the high fuel temperatures used, diffusional processes could possibly give rise to migration of the fuel material from the hotter central regions to the cooler edges. The results of experiments appear to indicate that two diffusion processes are involved: (1) a shallow penetration having a steep concentration profile and (2) a deep penetration in which the uranium concentration is quite low. The first process appears to have a "volume" diffusion coefficient of 5×10^{-11} to 5×10^{-10} cm^2/sec at 2000°C, whereas the second process has a coefficient of the order 10^{-5} cm^2/sec.

Two fuel-element concepts have been studied under the PBR[7] program: uncoated and coated. The uncoated elements consist of dispersions of uranium oxide or uranium carbide in graphite spheres, the uranium being introduced either by infiltration or as an admixture. In the latter case the size of the carbide or oxide particles can be selected at will, and it would be expected that lower rates of fission-product leakage could be obtained. This was found to be the case. However, the investigations have indicated that the leakage rate of long-lived volatile fission products from uncoated fuel elements could be reduced by a maximum of about two orders of magnitude below the total production rate. Since this degree of reduction would still allow an activity level of a megacurie or more in the primary loop of the proposed PBR, the emphasis in the PBR fuel-element program has been shifted to methods of obtaining further retention through the use of coatings. These coatings could conceivably be applied either to the outside of the spherical fuel element or to the individual fuel particles which are dispersed in the graphite matrix. Of the possible surface coatings for the fuel element, the most promising has been siliconized silicon carbide. In one test of this type element, a leakage factor of 10^{-6} or lower was indicated. There was, however, some difficulty with cracking of the elements, which was attributed to initial defects. It is estimated that the top temperature of this type element will lie in the range 2200 to 2500°F due to the presence of free-phase silicon on the surface. Pyrolytically deposited carbon coatings which would not have this temperature limitation are also being investigated. Al_2O_3 coatings for the individual UO_2 particles, in postirradiation heating tests, reduced the fractional release of Xe^{133} by the order of 1000 below the release for uncoated UO_2 particles. However, chemical reaction between the Al_2O_3 and graphite was observed, which apparently was unimportant at 2500°F but became severe at 3000°F.

In connection with the basic problems of the reactors employing "unclad" fuels, reference 8 should be cited. It reports the results of a study, by an *ad hoc* group at ORNL, of the problems related to the release of fission products by fuel elements which are not designed to be completely impervious. The study considers three reactor designs: the HTGR, the PBR, and the HGCR-I; the HGCR-I is an Oak Ridge design utilizing graphite-covered fuel plates containing 200-μ particles of UO_2 dispersed in graphite. The report gives a good review of the existing information on fission-product release and removal and applies it to estimate the problems and costs of operation and maintenance of contaminated systems.

References

1. Gas-Cooled Reactors, A Symposium Sponsored Jointly by the Franklin Institute and the American Nuclear Society, Delaware Valley Section, February 10 and 11, 1960, *J. Franklin Inst., Monograph No. 7*, May 1960.
2. M. Bender, The Experimental Gas-Cooled Reactor Design, in Gas-Cooled Reactors, A Symposium Sponsored Jointly by the Franklin Institute and the American Nuclear Society, Delaware Valley Section, February 10 and 11, 1960, *J. Franklin Inst., Monograph No. 7*, pp. 67–78, May 1960.
3. G. Samuels, Fuel Elements for Gas-Cooled Reactors, in Gas-Cooled Reactors, A Symposium Sponsored Jointly by the Franklin Institute and the American Nuclear Society, Delaware Valley Section, February 10 and 11, 1960, *J. Franklin Inst., Monograph No. 7*, pp. 138–148, May 1960.
4. W. D. Manly and J. H. Coobs, Materials Development Program for the Gas-Cooled Reactor Project at the Oak Ridge National Laboratory, in Gas-Cooled Reactors, A Symposium Sponsored Jointly

by the Franklin Institute and the American Nuclear Society, Delaware Valley Section, February 10 and 11, 1960, *J. Franklin Inst., Monograph No. 7*, pp. 150–167, May 1960.

5. H. L. Browne, Maritime Gas-Cooled Reactors, in Gas-Cooled Reactors, A Symposium Sponsored Jointly by the Franklin Institute and the American Nuclear Society, Delaware Valley Section, February 10 and 11, 1960, *J. Franklin Inst., Monograph No. 7*, pp. 52–64, May 1960.
6. M. T. Simnad and W. P. Wallace, Materials and Fuel Element Development for the MGCR and HTGR Helium-Cooled Reactors, in Gas-Cooled Reactors, A Symposium Sponsored Jointly by the Franklin Institute and the American Nuclear Society, Delaware Valley Section, February 10 and 11, 1960, *J. Franklin Inst., Monograph No. 7*, pp. 171–189, May 1960.
7. L. D. Stoughton, Development of Spherical Uranium-Graphite Fuel Elements, in Gas-Cooled Reactors, A Symposium Sponsored Jointly by the Franklin Institute and the American Nuclear Society, Delaware Valley Section, February 10 and 11, 1960, *J. Franklin Inst., Monograph No. 7*, pp. 200-224, May 1960.
8. J. A. Lane et al., A Study of Problems Associated with Release of Fission Products from Ceramic Fuels in Gas-Cooled Reactors, USAEC Report ORNL-2851, Oak Ridge National Laboratory, Oct. 28, 1959.

Section VII

ORGANIC-MODERATED REACTORS: EVALUATION OF IRRADIATED EXPERIMENTAL FUEL ELEMENTS

Reference 1 gives the results of irradiation tests of experimental fuel elements in the Organic Moderated Reactor Experiment (OMRE). The initial results of the operation of the OMRE were summarized in the September 1958 issue of *Power Reactor Technology*, Vol. 1, No. 4. More recently, tests of experimental fuel elements for central-station organic-moderated reactors have been carried out in the OMRE.

The OMRE was originally fueled with plate type elements of stainless-steel-clad highly enriched UO_2–stainless steel cermet fuel. Elements of this type are not economically attractive for large power reactors. The first two experimental fuel elements irradiated in the reactor were of the plate type, with extended-surface (finned) aluminum cladding, bonded to a uranium alloy core. The design is similar to the one originally proposed for the City of Piqua organic-moderated reactor, presently under construction. The final Piqua fuel-element design utilizes the same materials but in a cylindrical configuration. The uranium alloy used for the experimental fuel plates was either uranium–3.5 wt.% molybdenum or uranium–3.5 wt.% molybdenum–0.5 wt.% silicon. The finned aluminum cladding was metallurgically bonded to the uranium alloy core with a thin intermediate nickel layer, which acts as a barrier to prevent interdiffusion of the aluminum and uranium. The aluminum jackets were provided with edge spacers so that five plates could be stacked together to form an assembly of nearly square cross section which was held together by stainless-steel clips. Each plate was about 12 in. long; consequently, a full-length fuel assembly consisted of three five-plate stacks placed end to end. However, only one of the experimental assemblies was a full-length assembly; the other assembly contained only the stack of fuel plates which would lie nearest the central plane of the reactor. Both assemblies contained some plates of the uranium-molybdenum alloy and some plates of the uranium-molybdenum-silicon alloy.

The experimental elements were loaded in the OMRE during July 1958. One of the assemblies (HB-1, which contained only the middle stack of plates and which originally contained uranium of 8 per cent enrichment) was removed on Oct. 29, 1958, because of high operating temperature, as indicated by thermocouples in the fuel plates, and because fission products had been detected in the reactor system. The second experimental element (HT-1, originally of 4 per cent enrichment) was removed on Nov. 13, 1958, after having been in the reactor for 384 Mwd of reactor operation. It also had shown excessive operating temperature just prior to its removal. The maximum burnups achieved were 0.23 at.% uranium in element HB-1 and 0.19 at.% uranium in element HT-1. Both elements were examined in the hot cell.

The following conclusions were derived from the irradiation and the subsequent examination:[1]

1. Particulate material in the OMRE coolant was trapped by the aluminum cladding fins at the inlet ends of both experimental fuel elements. This foreign material restricted the flow of coolant past the fuel plates and caused the fuel plates to overheat. The overheating caused partial melting of the aluminum cladding and some alloying of the aluminum with uranium from the core in four of the five plates in the higher enrichment HB-1 fuel element. Damage in the HT-1 fuel element was limited to a blister separation of the core and cladding on one fuel plate. Nothing was observed that would indicate the fuel elements would not have functioned properly in the same coolant, if free of particulate matter of sizes that could be trapped.

2. Under the irradiation conditions experienced by the measured plates, both the U–3.5% Mo and the U–3.5% Mo–0.5% Si alloy showed good dimen-

sional stability. Metallographic observations of the core microstructure in the blistered region, and the melting of the aluminum cladding, showed the localized temperature conditions experienced by the fuel plates to be considerably in excess of the 750°F design temperatures and the 780°F maximum thermocouple temperature. The lack of observable fuel swelling under these conditions is encouraging for the use of these alloys as OMR fuels at considerably higher burnups than those experienced in the test.

3. The 0.0005-in. nickel layer may be inadequate to prevent interdiffusion between the aluminum cladding and the uranium alloy core, particularly if fuel-surface temperatures exceed 750°F.

4. No gross reactions occurred between the organic coolant and the uranium alloy core materials at temperatures up to the melting point of aluminum. This conclusion, which is based on visual and metallographic examination, is substantiated by the fact that metallic fission products were not found in the coolant after the fission break.

The gist of the conclusions is that the failure of the experimental elements was due to the accumulation of foreign material at the inlet ends of the coolant passages, which restricted the coolant flow and caused the fuel plates to overheat. Aside from this difficulty, the performance of the elements was apparently encouraging. No discussion is given of the source of the foreign material or of the mechanism involved in its deposition.

It was stated, however, that the relatively low activity of the material indicated that it did not originate in the fuel element during failure. Chemical analysis of samples of the material showed that about 17 to 20 per cent could be extracted by solvents for polyphenyls; this extracted material did not contain a notably high fraction of high-boiler compounds. Fe^{59} and Cr^{51} accounted for the major amount of the identifiable activity present, and iron was identified, by an X-ray fluorescence determination, as the major metallic constituent present. Firing a sample resulted in 16 per cent ash.

Reference

1. J. H. Walter et al., Evaluation of Irradiated Experimental OMR Fuel Elements, USAEC Report NAA-SR-4670, Atomics International, Apr. 1, 1960.

Section VIII

NUCLEAR SUPERHEAT: THE BONUS REACTOR

It is generally recognized that the addition of integral nuclear superheat is one of the attractive possibilities for improving the economic performance of the boiling-water reactor. In the recent studies[1] made for the development of the 10-year Civilian Power Reactor Program, the estimate was made that integral nuclear superheat might account for a reduction of about 0.73 mill/kw-hr (about 10 per cent) in the potential cost of power from boiling-water reactors.

The expected sources of economic benefit from integral nuclear superheat are a decrease of fuel cost and an increase of electrical generating capacity per unit of reactor capacity (due to improved thermal efficiency) and a reduction in cost of the power-conversion equipment (due to the elimination of the moisture problem and to the use of more conventional steam conditions). These expected sources of benefit result from improvements in the conversion of heat into electricity; naturally, they will yield a net economic gain only if the superheating of boiling-water-reactor steam can be done without a large increase in the cost of heat production. In accomplishing this objective, it would appear that the reactor designer must pay particular attention to the following considerations:

1. The characteristic simplicity of the boiling-water-reactor system should be preserved.
2. The over-all power density of the boiler-superheater reactor should not be very much lower than that characteristic of the boiling-water reactor.
3. The neutron economy should not be allowed to deteriorate much relative to that of the boiling-water reactor.

Probably these objectives can be only approximated. Some complication of the reactor proper appears necessary in order to accomplish the more complex function of boiling and superheating the steam. Furthermore, the poorer heat-transfer and heat-transport performance of superheated steam relative to liquid water or boiling water tends to decrease the attainable power density. Finally, there does not presently appear to be an economically attractive alternative to the use of stainless steel as a structural material in the superheater region of the reactor. Unless the neutron losses to steel are minimized, the neutron economy — and, hence, the net fuel cost — will suffer.

Among the more basic problems of integral superheat development are, of course, the problems of materials and fuel-element performance which are common to all reactors but which have their characteristic aspects in the case of superheated steam. The question of whether the deposition of material on superheater fuel-element surfaces will be a problem is also a rather fundamental one; although the problem, if it exists, can certainly be reduced by the provision of effective means of drying the steam before it enters the superheater section of the reactor. Another rather basic problem is the question of carry-over of radioactivity by the superheated steam. Although it has been shown that this problem is not serious in the conventional direct-cycle boiling-water reactor, it may be more significant when radioactive material originates in a superheater because, in such a case, there is no large decontamination factor available through vaporization of the water. To date, no integral superheater reactor has been proposed which does not feed steam directly from the superheater section to the turbine.

Among what may be classified as problems of design for boiler-superheater reactors are several problems of neutron physics, as well as the more obvious mechanical ones. The maintenance

of the proper power split under various operating conditions between the boiler and the superheater sections of the reactor over the lifetime of the reactor core is one such problem; another problem is that of minimizing the reactivity change that would occur if the fuel elements, which normally act as superheaters, were flooded with water, either accidentally or intentionally. Problems related to the latter consideration are those of starting up the reactor and of supplying shutdown and emergency cooling for the superheater section.

The Pathfinder nuclear power plant, for which one of the design goals is nuclear superheat, was reviewed in the June 1959 issue of *Power Reactor Technology*, Vol. 2, No. 3, pp. 51–54. Reference 2 is a later report on this project. More recently, the Preliminary Design Study and Hazards Summary Report for another integral superheat boiling-water reactor, the Boiling Nuclear Superheater (BONUS) Power Station, has been published.[3] The following description of the plant is compiled from that report.

The preliminary design of the BONUS plant was developed by the General Nuclear Engineering Corporation under a subcontract to the Puerto Rico Water Resources Authority. The Authority was the prime contractor with the AEC for a study to determine the technical feasibility of, and to prepare a comprehensive preliminary design of, a small integral boiler-superheater reactor. Upon the completion of the preliminary design study, the Authority and the AEC jointly have undertaken the construction of the BONUS plant at the proposed Punta Jigüero site near Rincón, P. R. General Nuclear, under a prime contract with the AEC, is developing the detailed design of the plant, which is scheduled to begin operation in December 1962.

The net electrical output of the BONUS plant is nominally 15,000 kw. The main features of the reactor proper are shown in the cutaway drawing, Fig. 23, and the design characteristics of the plant are summarized in Table VIII-1.

The core of the reactor consists of two distinct zones: (1) a central forced-circulation boiler region which produces saturated steam at 900 psig and 534°F and (2) a peripheral four-pass steam-cooled region which superheats the steam to 900°F. The steam passes directly to a conventional turbine which operates at throttle conditions of 850 psig and 900°F. The total heat output of the reactor is 50 Mw; the gross electric output of the generator is 17,300 kw, giving a gross efficiency of 34.6 per cent.

The forced-circulation boiler zone consists of 64 square fuel assemblies on a 4.36-in.-square lattice containing 2.81 tons of uranium element. Each boiler fuel assembly is made up of 32 Zircaloy-2 tubes which have an outside diameter of 0.50 in. and which contain 0.445-in.-diameter UO_2 pellets over their 4.54-ft active length. An average specific power of 13.2 Mw(t) per ton of uranium, an average core power density of 33 kw(t) per liter of core, and an average coolant power density of 103 kw(t) per liter of coolant are obtained.

The superheater zone consists of 32 fuel assemblies arranged in four groups of eight assemblies around the square boiler zone and contains 1.79 tons of uranium element. Each superheater assembly contains 32 fuel elements mechanically arranged to yield eight parallel paths and four series passes for the steam. Each fuel element is a stainless-steel-clad, UO_2 (3.5 per cent U^{235}) pellet, rod type element. The fuel rod is surrounded by a stainless-steel tube to form the steam coolant annulus, and this, in turn, is surrounded by a stainless-steel pressure tube which provides a thermal insulating gap between the coolant tube and the surrounding water moderator. The superheater core is divided into eight zones, each of which can be monitored for exit temperature, flow, and fuel-element failure. An average specific power of 7.25 Mw(t) per ton of uranium, a core power density of 12 kw(t) per liter of core, and a coolant power density of 83 kw(t) per liter of coolant are obtained.

Seventeen 2 wt.% boron–stainless steel control-rod elements are used. Nine 7-in.-wide and $\frac{1}{8}$-in.-thick cruciform rods are in the boiler zone, and eight 12-in.-wide and $\frac{1}{4}$-in.-thick slabs are located between the boiler zone and the superheater zone. These rods can control a total of 19 per cent Δk and yield a shutdown margin of 2.4 per cent Δk in the cold clean condition without fixed poison shims; with poison shims, the shutdown margin is 5.2 per cent Δk. All rods are actuated by rack-and-pinion drive mechanisms located on the top of the pressure vessel.

Water is circulated through the boiler portion of the reactor core at a rate of about 7500 gal/min by means of two forced-circulation pumps. Before being withdrawn from the reactor vessel, this recirculating coolant is mixed with 354°F

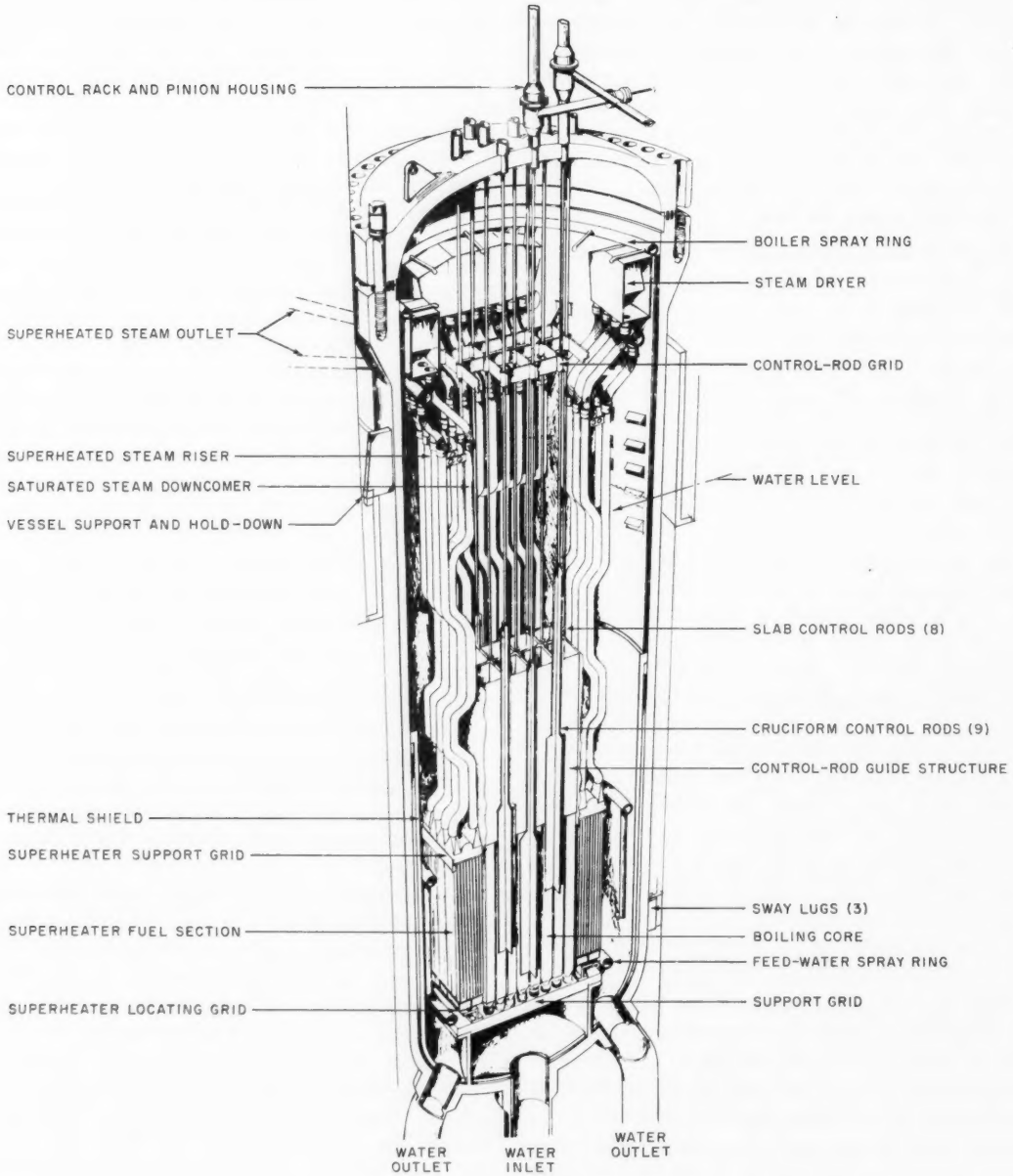

Figure 23—BONUS reactor perspective.

Table VIII-1 SUMMARY OF DESIGN AND PERFORMANCE DATA,* BONUS INTEGRAL SUPERHEATER REACTOR

General	
Reactor type	Thermal neutron, heterogeneous, H_2O moderated
Reactor heat-transfer system	Integral boiler-superheater within pressurized vessel
Reactor coolant	Water and steam (H_2O)
Reactor fuel	Uranium dioxide, natural and slightly enriched
Reactor coolant circulation, gal/min	Forced, 7500
Plant steam cycle	Direct, superheat
Gross electric output, kw(e)	17,300
Gross heat output, kw(t)	50,000
Thermal power to boiling, kw(t)	38,600
Thermal power to superheating, kw(t)	11,400
Gross cycle efficiency, %	34.6
Total reactor steam flow, lb/hr	152,000
Total reactor water flow, gal/min	7500
Reactor nominal operating pressure, psig	900
Saturated steam temp., °F	534
Superheated steam temp., °F	900
Turbine throttle steam pressure, psig	850
Feed-water temp., °F	354
Average steam voids in reactor core water, vol.%	13
Reactor Core Boiler Region	
Size and geometry of active region (including one-half of the water channel between the boiler and superheater zone)	35.5 in. square, 54.6 in. high
Volume of active region, liters	1126
Net heat generation in fuel, Mw(t)	37.0
Heat loss to moderator from gamma and neutron heating, Mw(t)	1.1
Net heat transfer to coolant, Mw(t)	35.9
Uranium content in boiler region, tons of uranium element	2.81
Uranium enrichment, wt.%	1.85 and 0.71
Average specific power, Mw(t) per ton of uranium	13.2
Average region power density, kw(t) per liter of region	32.9
Steam generation in boiler region, lb/hr	142,770
Structural metal in active region	Zircaloy-2
No. of fuel assemblies	64
Fuel assembly lattice	4.365 in. square
Fuel assembly dimensions	3.927 in. square, 54.6 in. active height
No. of fuel rods per assembly	32
Average heat flux, Btu/(hr)(sq ft)	102,000
Maximum heat flux, Btu/(hr)(sq ft)	323,000
Maximum fuel-centerline temp., °F	4400
Control rods in boiler region	Nine; 2 wt.% boron–stainless steel cruciforms
Control cruciforms dimensions	7-in. blade span, $\frac{1}{8}$ in. thick
Control-rod lattice	8.73 in. square
Reactor Core Superheater Region	
Size and geometry of active region (including one-half of the water channel between the boiler and superheater zone)	Four slabs, located adjacent to vertical faces of boiler region; 8.95- by 34.9-in. rectangle, 54.6 in. high (each)
Volume of active region, liters	1118
Net heat generation in fuel, Mw(t)	13.0
Heat loss to moderator from gamma and neutron heating, Mw(t)	0.4
Total heat entering coolant, Mw(t)	12.6
Thermal insulation heat loss to moderator, Mw(t)	1.2
Net heat transfer to coolant, Mw(t)	11.4
Uranium content in superheater region, tons of uranium element	1.79
Uranium enrichment, wt.%	3.5
Average specific power, Mw(t) per ton of uranium	7.25
Average region power density, kw(t) per liter of region	11.6
Total steam flow through region, lb/hr	152,000
Structural metal in active region	Stainless steel
Fuel assembly lattice	4.365- by 8.664-in. rectangle
No. of fuel assemblies	32
No. of fuel rods per assembly	32
Coolant flow geometry within active region	256 parallel flow channels; each channel makes four vertical passes through active core
Parallel flow channels per pass	8
No. of passes per assembly	4
No. of fuel rods per parallel flow channel in each pass	1
Parallel flow channel geometry	0.710-in.-OD by 0.542-in.-ID annulus
Average heat flux, Btu/(hr)(sq ft)	65,000
Maximum heat flux, Btu/(hr)(sq ft)	237,000

(Table continues)

Table VIII-1 (Continued)

Maximum cladding surface temp., °F	1140
Control rods at superheater-boiler region boundary	Eight; 2 on each vertical face; 2 wt.% boron–stainless steel slabs
Control slab dimensions	12 in. wide by ¼ in. thick
Reactor Core Moderator	
Heat transfer to moderator from boiler region, Mw(t)	1.1
Heat transfer to moderator from superheater region, Mw(t)	1.6
Steam generation in moderator, lb/hr	9230
Total water flow to moderator, lb/hr	283,000
Inlet temp. of water, °F	525
Reactor Vessel and Circulation Loops	
Pressure-vessel dimensions	7 ft ID, 27.5 ft high
Reactor pressure-vessel weight, tons	57
No. of reactor water circulation loops	2
Reactor water circulation pumps	Two; single stage, centrifugal
Flow rate per circulation loop, gal/min	3750
Power Plant	
Turbine	One; ASME-AIEE preferred standard, single flow, single casing, 3600 rpm
Turbine rating	16,500 kw at 3.5 in. Hg abs., 3% makeup
Main condenser	One, deaerating with divided hot well
Main condenser capacity	129,500 lb/hr at 2.0 in. Hg abs.
Generator	One, 13.8 kv, 3 phase, 50 cycles/sec, H_2 cooled
Generator maximum terminal output	17,300 kw at 2 in. Hg abs.
Plant Containment Building	
Description	Cylindrical concrete wall, roofed with hemispherical dome and floored with concrete slab
Diameter, ft	165
Height above ground, ft (approx.)	116
Maximum design pressure, psig	4.6

*For more detailed data, see USAEC Report TID-8524 (Vol. 4), Appendix C, pp. 260–270.

feed water injected into the lower part of the pressure vessel by a sparging ring. The slightly subcooled (9°F) water passes from the pressure vessel through two 16-in.-diameter pipes to two pumps located in a room beneath the reactor. Discharge pipes from the two pumps merge into a single 18-in.-diameter pipe which leads back to the reactor.

The amount of coolant flowing from the plenum at the bottom of the pressure vessel to each fuel assembly is determined by orifices that distribute the flow in proportion with the expected power output. The slightly subcooled water is heated as it rises through the boiler assemblies and reaches its boiling point after traversing about 22 per cent of the height of the core. Thereafter, steam bubbles begin to accumulate progressively until these bubbles occupy 50 per cent of the coolant-channel area as the steam-water mixture emerges from the top of the fuel assemblies. This corresponds to a steam weight fraction (quality) of about 5.6 per cent at the top of the core.

The steam-water mixture emerging from the top of the core continues upward through the cells of the superstructure. In the region above the superstructure, gravitational separation of water from the steam takes place. The steam then passes through a dryer before reaching the superheater inlet pipes.

The total flow of steam from the boiler region is 152,000 lb/hr. This corresponds to an average inlet velocity of 71 ft/sec at the beginning of the first pass of the superheater assemblies. Each superheater fuel assembly is orificed to make the amount of steam flowing into that assembly proportional to the expected heat output of that assembly.

Exhaust steam from the 32 superheater assemblies is collected in 11 separate pipes leading to the outside of the reactor shield, where monitoring of temperature, flow, and radioactivity is performed. Seven of the pipes collect steam from seven identical groups of four superheater assemblies. The other four pipes collect steam from individual superheater as-

semblies in the remaining group of four assemblies. In this way the performance of the four individual elements in a typical group can be monitored while the groups consisting of four assemblies each can be compared with each other.

Maintaining a constant steam outlet temperature, irrespective of changes in over-all reactor heat output required to accommodate variations in electric load, is one of the major problems in designing an integral boiler-superheater reactor. Reductions in over-all heat output can be readily accomplished by inserting control rods, but it is difficult to do this without distorting the ratio of the heat output of the boiler to the heat output of the superheater. The insertion of control rods in the boiler zone must be paralleled by the insertion of rods in the superheater by amounts such that the power ratio, as indicated by steam outlet temperature, remains constant. Since perfection is not expected in this manipulation of control rods, the steam outlet temperature of BONUS will be allowed to vary slightly, as necessary, within the range 900 to 950°F. The temperature will be reduced to 900°F before the steam reaches the turbine by controlled injection of the required amount of feed water into the steam in an external attemperator.

The reactor core is contained in a 7-ft-ID carbon-steel pressure vessel which has a 2.75-in. nominal base metal thickness and an over-all height of 27.5 ft and which is clad internally with $\frac{1}{4}$-in.-thick stainless steel. The reactor vessel is designed for a pressure of 1100 psig and a temperature of 600°F, but it will operate at a nominal presure of 900 psig and a temperature of 534°F.

The turbine-generator unit is an ASME-AIEE preferred standard single-flow single-casing 3600-rpm machine which produces 17,300 kw at 2-in. Hg backpressure. The unit will operate with inlet steam conditions of 151,300 lb/hr, 850 psig, and 900°F. The generator output will be at 13,800 volts, 3 phase, 60 cycles/sec. The turbine admission valves are reactor-pressure regulated to maintain the reactor pressure constant. Initially, this plant will not function as a demand station, but it will put out electrical power as dictated by the reactor power.

Four feed-water heaters are used to preheat the feed water to 354°F at full-power operation of the reactor.

The main turbine condenser and attached desuperheater are sized to condense the full-power steam output of the reactor when the turbine bypass valves are opened. Cooling for the main condenser is provided by sea water.

A continuous flow of 15 gal/min of reactor water through a system of filters and ion-exchange columns keeps the total impurity content of reactor water below 1 ppm. Oversize heat exchangers are used to reduce the temperature of the water to 120°F before it reaches the ion-exchange resins. These exchangers are also used to remove fission-product decay heat and to maintain the reactor water at low temperature for refueling operations.

The nuclear design of the superheater section of the reactor is such that flooding of the superheater passages by water causes only a very small change in reactivity, provided the reactor water is at operating temperature. This characteristic is obtained by a proper choice of fuel-to-water ratio, which compensates the extra neutron absorption of the flooding water by an equivalent (reactivitywise) decrease in the neutron loss due to resonance absorption and leakage. At room temperature, however, the effect of total flooding is to decrease reactivity by approximately 0.9 per cent k_{eff}. In order to avoid the possibility of a rapid reactivity increase, through flooding and subsequent emptying of the superheater channels, operation of the reactor is prohibited at room temperature; an interlock system prevents the withdrawal of control rods at temperatures below 500°F, and an auxiliary electric heater is provided for raising the reactor water temperature initially to the 500°F level. The startup procedure is to heat the reactor water with the auxiliary heater until the reactor has pressurized itself to a pressure of 850 psig. The superheater passages are then emptied by slowly opening the main steam stop valve and allowing the steam-water mixture from the superheater assemblies to flow to the main turbine condenser through a turbine bypass valve. This steam flow is maintained by the use of the auxiliary heater while the control rods are being withdrawn and the reactor is being made critical and brought up to a power level at which it will generate steam to feed the superheater passages.

The BONUS plant uses a large low-pressure containment building to house the entire power

plant, including both the turbine and the control room. A 165-ft-diameter hemispherical steel dome is attached to a steel-lined cylindrical concrete wall which, in turn, is sealed to a concrete slab floor. The maximum pressure that could result from blowdown of the entire hot-water system is calculated as 4.6 psig or less. The required thickness of steel in the dome is about $\frac{3}{8}$ in.

References

1. Civilian Power Reactor Program. Part II: Economic Potential and Development Program as of 1959, USAEC Report TID-8517, 1960.*
2. Allis-Chalmers Mfg. Co., Boiling Water Reactor with Internal Superheater, Pathfinder Atomic Power Plant Final Feasibility Report, USAEC Report ACNP-5917, Aug. 31, 1959.
3. Puerto Rico Water Resources Authority and General Nuclear Engineering Corp., Boiling Nuclear Superheater (BONUS) Power Station, Preliminary Design Study and Hazards Summary Report, Part A: Hazards Evaluation; Part B: Site Description, USAEC Report TID-8524(Vol. 4) (PRWRA-GNEC-2), June 1960.

*This report is available from the Superintendent of Documents, U. S. Government Printing Office, Washington 25, D. C., for $0.70.

Section IX

THE NEW PRODUCTION REACTOR

In the summer of 1957 the AEC was authorized to expend $3 million for design studies on a large-scale single- or dual-purpose plutonium production reactor. In August 1958 the AEC was authorized to proceed with detailed design and construction of a large production reactor estimated to cost $145 million. The reactor, an improved version of the Hanford graphite-moderated water-cooled reactor, is being designed by the General Electric Company, Hanford. The heat dissipation plant is being designed by Burns & Roe, Inc. Unlike the existing production reactors, however, the new reactor will have coolant temperatures and pressures sufficiently high to produce secondary steam, and facilities are to be included in the reactor to provide for conversion, at some future date, to either dual-purpose (plutonium plus power) operation or power-only operation. Preliminary construction of the reactor is under way, and initially the secondary steam energy will be dumped, through an exchanger, to the Columbia River. The scheduled completion date for the facility is Oct. 1, 1962. This convertible reactor is called the New Production Reactor (NPR).

About $25 million of the NPR design and construction costs will be required to facilitate its conversion to the dual-purpose or power-only operation. These costs are caused by the inclusion of heavy-walled zirconium process tubes and the necessary pumps, piping, and steam generators suitable for use under the temperature and pressure conditions resulting from dual-purpose or power-only operation. With respect to power-only operation, it should be mentioned that the plan is to operate the NPR for at least two years as a plutonium-only reactor, until conversion is authorized. After conversion, the reactor would be operated at full power to maximize the production of weapons plutonium; however, electric power would be generated. After conversion to power-only operation at an indefinite date, until the useful life of the reactor is exhausted, the reactor plant would be operated on the basis that the NPR would be available for power generation exclusively, and any plutonium production would be incidental and credited at the prevailing market value. This is termed "power-only" operation.

In May 1959 the AEC requested the Federal Power Commission (FPC) to make a comprehensive study of the economics of power generation at the NPR. The study investigated the need for power in the potential market area of the NPR, the ability to integrate NPR power production with existing networks, and the economics of NPR power production relative to fossil-fired plants and hydroelectric plants. The results of this study are discussed in reference 1; Volume II, which is classified, has also been published.

The NPR is a large graphite-moderated reactor, cooled by light water passing through 1004 Zircaloy-2 process tubes which house the fuel. The fuel is slightly enriched uranium metal clad in zirconium. After the coolant passes through the reactor, it is split into five parallel loops, each of which contains two heat exchangers. In these secondary heat exchangers, steam is generated at 87 psia, and this is the steam condensed by the river, although for power operation the secondary steam would be used to drive a turbine.

Conversion to dual-purpose operation would consist of adding from two to four large turbine-generators, plus minor changes in instrumentation and controls. Steam pressure could be increased by changing from five to seven coolant loops and/or operating the reactor at reduced power to permit an increase in the primary coolant exit temperature. A total of 24 different cases was studied, ranging from an electrical

capacity of 388 to 848 Mw(e) without coal-fired superheat and to 1186 Mw(e) with coal-fired superheat.

During the dual-purpose operation, the capital and operating costs assigned to power generation were only those incurred by reason of constructing and operating the export electric power producing facilities; the reactor operating and fuel costs would be charged to plutonium production. During the power-only phase, all costs of operating the NPR plant (but not interest and amortization of the original reactor investment) would be charged to power generation, as would the costs incurred by the export power facilities. Annual fixed charges were computed on the basis of three different interest rates: 2.5 and 4.0 per cent for federal financing and 4.5 per cent for public nonfederal financing. Three alternative fuel prices were utilized in computing fuel costs; these are as follows:

1. The published uranium price schedule and the plutonium fuel value equal to $12 per gram
2. A projection of future uranium production costs with the plutonium fuel value equal to $12 per gram (Forecast No. 1)
3. A projection of future uranium production costs coupled with a reduced plutonium value (Forecast No. 2)

Unfortunately, reference 1 does not give the projected costs of uranium and the reduced plutonium value used in the study since the data are classified. Table IX-1 gives the total NPR power production costs for four of the cases studied. These cases, which appeared to be the more attractive ones, are described more fully in Table IX-2.

The penalty paid by the low plant factor during the dual-purpose operation is substantial; if an 80 per cent plant factor could be realized during this time period, the energy costs would be less than 2 mills/kw-hr. The reason for the low 40 per cent factor during dual-purpose operation is the excess of hydroelectric power available in the summer months in the Pacific Northwest Pool, expected to persist for a number of years in the future.

Table IX-1 AT-SITE UNIT POWER PRODUCTION COSTS OF NPR*

(Rate of Financing, 4%; Published Fuel Costs Plant Factors: Dual Purpose, 40%, and Power Only, 70%; Total Energy Costs Are in Mills/Kw-Hr)

NPR plant case	Dual purpose	Power only
KK	3.28	4.42
EE	3.45	4.75
F	3.42	4.68
U	3.60	4.87

*These data are taken from Volume II of reference 1.

The costs of hydroelectric power and fossil-fuel electric power were developed for comparison purposes. Although the data are pertinent only to the Pacific Northwest region, the methods employed indicate the complexity necessary to compare competing sources of electric power production. For example, it was necessary to make a charge against the NPR for an increase in the reserve capacity of the system required because of the size and scheduled outage rate of the NPR. A comparison of the nuclear versus fossil-fuel and/or hydroelectric power, assuming eight years for dual-purpose operation and the remaining life for power-only operation, indicated that nuclear power was not economically attractive under any conditions if published fuel costs were used. If Forecast No. 1 fuel costs were realized, the nuclear plant was economically feasible for case KK, and if Forecast No. 2 fuel costs were realized, case KK was feasible when compared to fossil-fuel plants but

Table IX-2 POWER AND INVESTMENT FOR THE VARIOUS CASES OF NPR[1]

	Dual-purpose period			Power-only period		
		Investment*			Total investment*	
Case	Initial production, Mw net	Millions of dollars	Dollars per kilowatt	Ultimate production, Mw net	Millions of dollars	Dollars per kilowatt
KK	636	101.1	158.9	735	104.6	142.4
EE	400	66.9	167.3	618	99.9	161.7
F	848	122.3	144.2	848	122.3	144.2
U	420	74.1	176.5	553	91.2	164.8

*Based on 4.0 per cent interest during construction.

unfeasible when compared to a mix including hydroelectric power through 1972 and fossil-fuel electric power thereafter. Economic feasibility of the several cases would be enhanced by operating the plant dual-purpose for a period longer than eight years.

References

1. Federal Power Commission, Bureau of Power, San Francisco Regional Office, New Production Reactor Power Plant, Economic Feasibility Study, USAEC Report TID-5762(Vol. I), February 1960.

Index

VOLS. 1–3

Included in this issue is a cumulative index for Volumes 1 to 3 of *Power Reactor Technology*. Future indexes for this quarterly will be prepared annually and will appear in the final (Number 4) issue. In this index the bold numbers denote volumes, the numbers in parentheses denote issues, and the other numbers denote pages.

A

AB Atomenergi Laboratory, exponential experiments, **3**(4), 13
Activation experiments, **1**(2), 11
Advanced Gas-Cooled Reactor, design, **2**(1), 28–9
Air, corrosion of beryllium, **2**(4), 69
Air Force Nuclear Engineering Test Reactor
  See Reactor (Air Force Nuclear Engineering Test)
Aircraft Reactor Experiment, control rods, **3**(3), 45
Alkanex, radiation effects, **1**(4), 38
Alkylbenzene, radiation effects, **1**(4), 38
Alloys, radiation effects, **3**(4), 38–57
Aluminum, corrosion by carbon dioxide, **1**(1), 33
  corrosion by polyphenyls, **1**(4), 44–5
  corrosion by water, **1**(1), 18; **1**(2), 39; **3**(4), 29–30
  electrocladding of fuel elements, **2**(2), 34
  neutron absorption, **3**(3), 34
  pressure tubes for Gas-Cooled Reactor Experiment, **2**(3), 61
  properties, **1**(4), 23, 25
  radiation effects, **1**(3), 28; **1**(4), 40–1
  reactions with uranium dioxide, **1**(4), 25
  shielding properties, **2**(2), 30
  solubility in liquid bismuth, **1**(3), 50
  welding, **2**(2), 33
Aluminum (liquid), coolant properties, **1**(2), 40
Aluminum (sintered powder), corrosion by carbon dioxide, **1**(1), 33
Aluminum alloys, corrosion by carbon dioxide, **1**(1), 33
  corrosion by high-temperature water, **1**(2), 40
  corrosion by phosphates, **1**(2), 40
  radiation effects, **1**(4), 40
Aluminum-iron alloys, radiation effects, **3**(1), 37–8
Aluminum-nickel alloys, corrosion by water, **1**(3), 37–8
  properties, **1**(4), 25
  radiation effects, **1**(3), 33, 37–8
Aluminum-plutonium alloys
  See Plutonium-aluminum alloys
Aluminum-silicon systems, pressure-tube construction, **2**(1), 34
Aluminum-silicon-uranium systems, diffusion, **1**(2), 30–1
Aluminum-uranium alloys
  See Uranium-aluminum alloys
Aluminum-zirconium alloys, corrosion by uranyl sulfate, **1**(2), 52
Amber, radiation effects, **1**(3), 40
Americium-241, neutron cross sections, **1**(3), 13
APS-1 Reactor
  See Reactor (Obninsk)
Aqueous homogeneous reactors
  See Reactors (homogeneous)
ARBOR Reactor, design, **1**(2), 64–5
Argon, reactor cooling, **1**(4), 57–8
Argonaut Reactor
  See Reactor (Argonaut)
Argonne Boiling-Water Reactor
  See Reactor (ARBOR)
Argonne Low-Power Reactor
  See Reactor (ML-1)
Argonne National Laboratory, critical and exponential experiments, **3**(4), 13
Army Mobile Low-Power Reactor
  See Reactor (ML-1)
Army Package Power Reactor
  See Reactor (SM-1)
Asbestos, radiation effects, **1**(4), 38
Atomic Energy Research Establishment, critical and exponential experiments, **3**(4), 14, 15
Atomics International, exponential experiments, **3**(4), 15, 16

B

Babcock and Wilcox Co., critical experiments, **3**(4), 15
Barium uranate, melting point, **1**(2), 28
Barytes concrete, shielding properties, **2**(2), 31
Belgian reactors
See Reactor (Belgonucleaire); Reactor (BR-3)
Belgonucleaire Reactor
See Reactor (Belgonucleaire)
Beloyerski Urals Reactor
See Reactor (U.S.S.R. Superheater)
Berkeley Reactor (British), refueling, **2**(4), 60, 64–5
Beryllium, **2**(4), 67–71
compatibility with uranium, **2**(4), 70
compatibility with uranium dioxide, **2**(4), 70
corrosion by air, carbon dioxide, hydrogen, nitrogen, and oxygen, **2**(4), 69–70
costs, **2**(4), 71
fabrication and production, **2**(4), 67
moderation of liquid-metal-fuel reactors, **1**(3), 46
physical properties, **1**(1), 32
properties, **2**(4), 67–8, 69
radiation effects, **1**(1), 32; **1**(4), 40–1; **2**(4), 70
shielding properties, **2**(2), 30
thermal properties, **2**(4), 67, 69
toxicity, **2**(4), 70–1
Beryllium oxide, properties, **2**(4), 67
Beryllium oxide–thorium oxide systems, properties, **1**(2), 31
Beryllium oxide–thorium systems, properties, **1**(2), 31
Beryllium oxide–uranium dioxide systems, properties, **1**(2), 31
Beryllium–uranium dioxide systems, properties, **1**(2), 31
Bettis Atomic Power Laboratory, critical experiments, **3**(4), 14
Biphenyl, coolant properties, **2**(4), 42
nucleate boiling, **3**(1), 19
properties, **1**(4), 46
Bismuth, physical properties, **1**(3), 45
shielding properties, **2**(2), 30
Bismuth (liquid), coolant properties, **1**(2), 40
dissolution of aluminum, copper, iron, magnesium, molybdenum, nickel, niobium, tantalum, and tungsten, **1**(3), 50
physical properties, **1**(3), 48
Bismuth alloys (liquid), corrosion of steels, **1**(3), 51
Bismuth-graphite systems, neutron moderation, **2**(2), 10
Bismuth-lead alloys (liquid), coolant properties, **1**(2), 40
Boilers, Loeffler type, **3**(2), 13–14
Boiling, bubble formation, **1**(3), 20–1
burnout, **1**(3), 13, 17–18; **1**(4), 7–8; **3**(2), 36–7, 39
criticality effects in reactors, **1**(3), 20–1; **3**(4), 34–5
heat transfer, **3**(2), 35–7, 39
mathematical analysis, **1**(4), 8
steam slip, **3**(4), 28–9
Boiling (nucleate), biphenyl, **3**(1), 19
departure from, definition of, **3**(4), 27
heat transfer, **3**(1), 19; **3**(4), 27–8
organic-cooled and -moderated reactors, **3**(1), 19–21
polyphenyls, **3**(1), 19
Boiling reactors
See Reactors (boiling, heavy-water); Reactors (boiling-water)
BONUS Reactor
See Reactor (BONUS)
BORAX Reactors
See Reactor (BORAX)
Borides, applications as control materials, **3**(3), 40
Boron, applications as control material, **1**(2), 34
melting point, **1**(2), 28
nuclear properties, **3**(3), 32
radiation effects, **1**(2), 34
shielding properties, **2**(2), 30
Boron-10, effectiveness for reactor control, **1**(2), 34
nuclear properties, **3**(3), 32
Boron carbide, radiation effects, **1**(1), 30–1
Boron glass, neutron absorption, **3**(3), 36
Boron-hafnium systems, applications as control materials, **1**(2), 34–5
Boron-iron systems, control-rod design, **1**(3), 34
Boron-iron systems (stainless-steel-clad), control rods in SM-1 Reactor, **3**(3), 40
Boron–stainless steel systems, control-rod applications, **3**(3), 34, 38–40
corrosion by water, **3**(3), 39
properties, **3**(3), 38–40
radiation effects, **1**(1), 30; **2**(4), 71; **3**(3), 39
Boron-steel systems, neutron absorption, **3**(3), 33–40
Boron-titanium systems, corrosion by water, **3**(3), 41
properties, **3**(3), 40
radiation effects, **1**(1), 30; **3**(3), 40–1
Boron–Zircaloy-2 systems, radiation effects, **1**(1), 30
Boron-zirconium systems, corrosion by water, **3**(3), 41
properties, **3**(3), 40
radiation effects, **1**(1), 30; **3**(3), 40–1
Boron-zirconium systems (Zircaloy-2-clad), radiation effects, **1**(2), 34
BR-3 Reactor
See Reactor (BR-3)
Bradwell Reactors
See Reactor (Bradwell)
Breeder Reactors
See Reactors (Breeder)
Breeding, **3**(2), 21–9
conferences, **3**(2), 27–9
fast-breeder reactors, **3**(2), 25
Fast-Reactor Core Test Facility, **3**(2), 67
fluid-fuel reactors, **3**(1), 56
liquid-metal-fuel reactors, **1**(3), 42–5
Shippingport Pressurized-Water Reactor, **1**(3), 6–7

Breeding (Continued)
thermal-breeder reactors, **3**(2), 25–7, 52; **3**(3), 4
water-cooled and -moderated reactors, **2**(1), 17–19
British reactors
See Reactor (Berkeley); Reactor (Bradwell); Reactor (Dounreay); Reactor (Dragon); Reactor (Hinkley Point); Reactor (Hunterston); Reactor (Trawfynydd); Reactor (Zeus)
Brookhaven National Laboratory, exponential experiments, **3**(4), 13, 15
Brown-Boveri-Krupp Reactor, design, **3**(4), 59
Bubbles, formation, **1**(3), 20–1
Buckling, **1**(2), 1–7
heavy-water lattices, **3**(2), 30–1
heavy-water-moderated reactors, **1**(4), 2
measurement, **1**(2), 11; **3**(2), 30–1
reactor core lattices, **1**(3), 1–6
Savannah River Reactors, **1**(3), 1–2
Bulk Shielding Reactor, shielding experiments, **3**(2), 40
Burnable poisons, **1**(3), 13; **2**(2), 28–9
Burnout, boiling effects, **1**(3), 13, 17–18; **1**(4), 7–8; **3**(2), 36–7, 39
boiling-water reactors, **3**(3), 10
fuel elements at high pressure, **2**(4), 39–42
Homogeneous Reactor Experiment-II, **3**(3), 60–1
MTR-ETR fuel elements at low pressure, **2**(4), 36–9
polyphenyls, **2**(3), 20–1
pressurized-water reactors, **2**(4), 39–42
rectangular channels, **3**(3), 9–10
supercritical water reactors, **1**(3), 18
swirl flow effects, **3**(4), 25–7

C

Cadmium, applications as control material, **1**(2), 34; **3**(3), 41–3
epithermal neutron-absorption cross sections, **1**(3), 10–11
neutron absorption, **3**(3), 33–4
neutron cross sections, **1**(3), 13
nuclear properties, **3**(3), 32
radiation effects, **1**(1), 31
shielding properties, **2**(2), 30
Cadmium-113, neutron cross sections, **3**(4), 16
nuclear properties, **3**(3), 32
Cadmium alloys, applications in control rods, **3**(3), 41–3
Cadmium-indium-silver alloys, applications in control rods, **3**(3), 41–3
corrosion by water, **3**(3), 41
neutron absorption, **3**(3), 41
properties, **3**(3), 41–3
radiation effects, **3**(3), 41
Calcium uranate, melting point, **1**(2), 28
Calder Hall Reactors
See Reactor (Calder Hall)
Canadian reactors
See Reactor (NPD-2); Reactor (NRU)
Capacitors, radiation effects, **1**(4), 39
Carpenter 20-Cb, corrosion by nitrogen, **2**(4), 81
Carbon, shielding properties, **2**(2), 30
Carbon dioxide, coolant in gas-cooled heavy-water-moderated reactors, **2**(3), 57–8
coolant properties, **3**(4), 24
corrosion of aluminum, aluminum alloys, cast iron, magnesium, magnesium alloys, and steels, **1**(1), 33
corrosion of beryllium, **2**(4), 69–70
corrosion of stainless steel, **1**(1), 33; **1**(4), 28
corrosion of zirconium and Zircaloy-2, **2**(2), 39–40
oxidation of uranium dioxide, **3**(2), 50
reactor cooling, **1**(1), 33; **1**(4), 28, 57–8; **2**(2), 39–40; **2**(3), 57–9; **2**(4), 67–70; **3**(2), 50; **3**(4), 24
Carbon dioxide–graphite systems, moderator-coolant efficiency, **2**(3), 59
Carbon dioxide–helium systems, corrosion of zirconium and Zircaloy-2, **2**(2), 39–40
Carbon dioxide–water systems, coolant-moderator efficiency, **2**(3), 59
Carbon dioxide–zirconium hydride systems, coolant-moderator efficiency, **2**(3), 59
Carbon monoxide, reactor cooling, **1**(4), 57–8
Cast iron, corrosion by carbon dioxide, **1**(1), 33
Catalytic recombination, deuterium-oxygen systems, **1**(2), 46–8, 56–7
hydrogen-oxygen systems, **1**(2), 48–9, 56–7
Cements
See Concretes
Ceramic materials, radiation effects, **1**(4), 37
Cerium-cobalt-plutonium alloys, fuel for Fast-Reactor Core Test Facility, **3**(2), 68
Cerium oxide–thorium oxide systems, properties, **1**(2), 31
Cerium oxide–uranium dioxide systems
See Uranium dioxide–cerium oxide systems)
Cerium-zirconium alloys, corrosion by uranyl sulfate solutions, **1**(2), 52
Cesium (vapor), thermionic energy converters, **3**(1), 9–11
Chalk River Laboratory, critical experiments, **3**(4), 13
Channels (circular), heat transfer in laminar and turbulent flow, **3**(4), 25
Channels (hot)
See Hot-channel factors
Channels (parallel), two-phase fluid flow, **3**(4), 31–2
Channels (rectangular), burnout, **3**(3), 9–10
Channels (triangular), heat transfer, **3**(4), 24–5
Chlorine, shielding properties, **2**(2), 30
Chromium, nuclear and thermal properties, **1**(2), 39
Chromium–nickel–uranium dioxide systems (Nichrome-V-clad), reactions with water during irradiation, **1**(1), 18–19
Chromium-uranium alloys
See Uranium-chromium alloys

Chromium-zirconium alloys, corrosion by uranyl sulfate solutions, **1**(2), 52
Chugach Power Reactor
See Reactor (Sodium Deuterium)
Cobalt, neutron absorption, **3**(3), 35
Cobalt alloys, radiation effects, **1**(4), 40
Cobalt-cerium-plutonium alloys, fuel for Fast-Reactor Core Test Facility, **3**(2), 68
Coefficient of reactivity, **1**(1), 11–12; **3**(3), 3–4
effects on reactor stability, **1**(1), 13–14
Experimental Boiling-Water Reactor, **1**(1), 14–16
Experimental Breeder Reactor-I, **1**(1), 12–14
Pressurized Test Reactor, **3**(3), 3–4
uranium (Zircaloy-2-clad), **3**(3), 3–4
Columbium
See Niobium
Commissariat à l'Énergie Atomique, critical experiments, **3**(4), 15
Concretes, heat absorption, **1**(1), 20
radiation effects, **2**(2), 31–2
shielding properties, **2**(2), 31–2; **2**(4), 46–7
Conferences, Conference on the Physics of Breeding, Argonne National Lab., Oct. 19–21, 1959, **3**(2), 27–9
Conference on Transfer Functions and Reactor Stability, Argonne National Lab., May 2–3, 1960, **3**(4), 33–7
Second International Conference on the Peaceful Uses of Atomic Energy, Geneva, September 1958, **2**(1), 1–9
Symposium on Gas-Cooled Reactors Sponsored by the Franklin Institute and the Delaware Valley Section of the American Nuclear Society, Philadelphia, Feb. 10–11, 1960, **3**(4), 58–65
Containment, **1**(1), 17–21; **1**(4), 15–17; **2**(3), 22–37; **3**(3), 12–14
See also Reactor safety
Air Force Nuclear Engineering Test Reactor, **2**(3), 26
design of structures, **2**(3), 30; **2**(4), 44–5
Dresden Power Reactor, **2**(3), 27
economics, **2**(3), 29–30
effects of reactor rupture on vessels, **1**(1), 20–1
Elk River Power Reactor, **2**(3), 27
Enrico Fermi Fast-Breeder Reactor, **2**(3), 27
Experimental Boiling-Water Reactor, **2**(3), 25–6; **3**(3), 64
Experimental Breeder Reactor-II, **1**(3), 53; **2**(3), 25, 27
General Electric Test Reactor, **2**(3), 26
Homogeneous Reactor Experiment-II, **2**(3), 27
Humboldt Bay Power Reactor, **3**(3), 12
Indian Point Power Reactor, **2**(3), 26
liquid-metal-fuel reactors, **1**(3), 52
Livermore Pool Test Reactor, **2**(3), 26
MIT Reactor, **2**(3), 26
NASA Research Reactor, **2**(3), 26
N.S. *Savannah* Reactor, **2**(3), 26
Organic-Moderated Reactor Experiment, **1**(4), 42–51; **2**(3), 27
Pathfinder Power Reactor, **2**(3), 27
Piqua Power Reactor, **2**(3), 27
Plutonium Recycle Test Reactor, **2**(3), 27; **3**(3), 54–6
S1G Reactor, **2**(3), 27
Shippingport Pressurized-Water Reactor, **2**(3), 26
SM-1 Reactor, **2**(3), 26
Sodium Graphite Reactor, **2**(3), 27
Sodium Reactor Experiment, **2**(3), 27
underground location of reactors, **2**(3), 33–4
Vallecitos Boiling-Water Reactor, **2**(3), 27
Westinghouse Test Reactor, **2**(3), 26
Yankee Power Reactor, **2**(3), 26
Control, **1**(1), 11–17
Aircraft Reactor Experiment, **3**(3), 45
Calder Hall Reactors, **3**(3), 30, 45
compression springs, **1**(2), 45
control-rod design, **1**(3), 9–13, 34
Dresden Power Reactor, **3**(3), 45
Enrico Fermi Fast-Breeder Reactor, **3**(3), 45
Experimental Boiling-Water Reactor, **3**(3), 28–31, 45
fast reactors, **1**(3), 8–9
homogeneous reactors, **1**(2), 54–6
Indian Point Power Reactor, **3**(3), 45
liquid-metal-fuel reactors, **1**(3), 48–9
ML-1 Reactor, **3**(3), 45
Organic-Moderated Reactor Experiment, **3**(3), 45
Pathfinder Power Reactor, **2**(3), 52
Plutonium Recycle Test Reactor, **3**(3), 53–6
power-distribution effects, **1**(3), 11
pressurized-water reactors, **1**(2), 62–3; **2**(4), 85
principles of application, **3**(3), 26–8
reflectors, **1**(3), 12–13
S1G Reactor, **3**(3), 45
Shippingport Pressurized-Water Reactor, **3**(3), 45
SM-1 Reactor, **3**(3), 40, 45
Sodium Reactor Experiment, **3**(3), 30, 45
Swedish reactor for heating, **3**(3), 30
Vallecitos Boiling-Water Reactor, **3**(3), 45
Veronezh Reactor, **2**(1), 23–4
Yankee Power Reactor, **3**(3), 45
Control materials, **1**(1), 30; **1**(2), 34–5; **3**(3), 26–47
borides, **3**(3), 40
boron, **1**(2), 34; **3**(3), 32
boron-hafnium systems, **1**(2), 34–5
boron-iron systems, **1**(3), 34, 37
boron–stainless steel systems, **3**(3), 34, 38–40
boron-steel systems, **3**(3), 33–40
burnable poisons, **1**(3), 13; **2**(2), 28–9
burnup, **3**(3), 36–7
cadmium, **3**(3), 32, 33–4
cadmium-indium-silver alloys, **3**(3), 41
cobalt, **3**(3), 35
corrosion by water, **3**(3), 40–1
costs, **3**(3), 44
dysprosium, **1**(2), 34; **3**(3), 32, 43–4
dysprosium oxide, **3**(3), 35
epithermal absorption cross section, **1**(3), 10–11

Control materials (Continued)
erbium, **3**(3), 32
erbium oxide, **3**(3), 35
europium, **1**(2), 34; **3**(3), 32, 43–4
europium oxide, **3**(3), 35
europium oxide–stainless steel systems, **3**(3), 34, 40
gadolinium, **3**(3), 32, 43–4
gadolinium oxide, **3**(3), 35
gadolinium-tantalum alloys, **3**(3), 34
gamma heating, **1**(3), 12; **3**(3), 37–8
gold, **3**(3), 35
hafnium, **3**(3), 32, 33–5, 42, 43
Haynes-25, **3**(3), 34
holmium oxide, **3**(3), 35
indium, **3**(3), 32, 34–5
iridium, **3**(3), 32
lithium, **3**(3), 32
lutetium, **3**(3), 32
lutetium oxide, **3**(3), 35
mercury, **3**(3), 32
rare earths, **3**(3), 43–4
rhenium, **3**(3), 32
rhodium, **3**(3), 32
samarium, **1**(2), 34; **3**(3), 32, 43–4
samarium oxide, **3**(3), 35
samarium oxide–stainless steel systems, **3**(3), 34
silver, **3**(3), 32, 34–5
tantalum, **3**(3), 34–5
terbium oxide, **3**(3), 36
thulium oxide, **3**(3), 36
titanium, **3**(3), 34
tungsten, **3**(3), 36
variation in worth, **1**(3), 12
ytterbium oxide, **3**(3), 36
Convection (forced), heat transfer, **3**(4), 25–7
steam slip in boiling water, **3**(4), 28–9
supercritical water reactors, **1**(3), 18
Coolant contamination, BORAX-IV Reactor, **2**(1), 22–3
Experimental Boiling-Water Reactor, **2**(1), 22
Coolant flow, Engineering Test Reactor, **3**(2), 34–5
Gas-Cooled Reactor Experiment, **2**(4), 79–80
Coolant purification, Experimental Boiling-Water Reactor, **2**(1), 22–3
gas-cooled reactors, **2**(1), 32
Organic-Moderated Reactor Experiment, **1**(4), 44
Shippingport Pressurized-Water Reactor, **2**(4), 74–6
Coolants, aluminum (liquid), **1**(2), 40
biphenyl, **2**(4), 42
bismuth (liquid), **1**(2), 40
bismuth-lead alloys (liquid), **1**(2), 40
carbon dioxide, **1**(1), 33; **1**(4), 28, 57–8; **2**(2), 39–40; **2**(3), 57–9; **2**(4), 69–70; **3**(2), 50; **3**(4), 24
carbon monoxide, **1**(4), 57–8
decomposition in Organic-Moderated Reactor Experiment, **3**(2), 70
deuterium oxide, **3**(3), 53–6
dissociation in water-cooled reactors, **2**(1), 21–2
gallium (liquid), **1**(2), 40
gas-cooled reactors, **1**(4), 57–8
helium, **1**(4), 25, 57–8; **2**(3), 55–6, 59–61; **2**(4), 83–5; **3**(2), 38
helium-graphite systems, **2**(3), 59
hydrogen, **1**(4), 57–6
liquid metals, **1**(2), 40
neon, **1**(4), 57–8
nitrogen, **1**(4), 57–8; **2**(3), 61; **2**(4), 79–81
nitrogen-graphite systems, **3**(4), 24
organic-moderated reactors, **1**(4), 45–8
physical properties, **1**(3), 48
Santowax M, **3**(1), 19
Santowax O, **3**(1), 19
Santowax O-M, **1**(4), 45; **2**(4), 42
Santowax R, **2**(4), 42
Copper, heat transfer, **1**(1), 6
radiation effects, **1**(4), 40
shielding properties, **2**(2), 30
solubility in liquid bismuth, **1**(3), 50
welding, **2**(2), 33
Copper-uranium alloys, properties, **1**(2), 28
Critical assemblies, core physics, **3**(1), 15–17
graphite-moderated beryllium-reflected, **1**(3), 6
Critical experiments, **3**(4), 12–16
Criticality, **1**(4), 5
boiling effects, **1**(3), 20–1; **3**(4), 34–5
Cross sections
See Neutron cross sections
Czechoslovakia Gas-Cooled Reactor, refueling, **2**(4), 61

D

Danger coefficient, **1**(2), 11
Decontamination, fuel-element surfaces, **3**(3), 24–5
Shippingport Pressurized-Water Reactor, **2**(4), 76–7
Departure from nucleate boiling, definition, **3**(4), 27
Deuterium, determination in deuterium oxide–water systems, **2**(2), 45–6
Deuterium oxide, Plutonium Recycle Test Reactor cooling, **3**(3), 53–6
Deuterium oxide–water moderated systems, neutron age, **1**(2), 4–5
Deuterium oxide–water systems, deuterium determination, **2**(2), 45–6
neutron moderation, **2**(2), 10
Deuterium-oxygen systems, catalytic recombination, **1**(2), 46–8, 56–7
Doppler coefficient, measurement in Physical Constants Testing Reactor, **3**(2), 31–2
uranium-238, **2**(2), 13–14
Dounreay Reactor, core design, **1**(4), 24
Dowtherm-A, radiation effects, **1**(4), 38
Dragon Reactor, design, **3**(4), 58
Dresden Power Reactor
See Reactor (Dresden Power)
Dural, heat transfer, **1**(1), 6

Dutch-Norwegian Establishment for Nuclear Energy Research, exponential experiments, **3**(4), 13
Dysprosium, applications as control material, **1**(2), 34; **3**(3), 32, 43–4
Dysprosium-164, nuclear properties, **3**(3), 32
Dysprosium oxide, melting point, **1**(2), 28
neutron absorption, **3**(3), 35

E

East Central Nuclear Group–Florida West Coast Nuclear Group Reactor
See Reactor (Florida Power)
Economics of nuclear power, **1**(1), 4; **2**(3), 1–12; **2**(4), 1–30; **3**(2), 1–12
beryllium costs, **2**(4), 71
boiling-water reactors, **2**(4), 2, 3, 4, 11–16; **3**(2), 1–2, 4, 7, 8, 10
containment costs, **1**(4), 16–17; **2**(3), 29–30
control-rod costs, **3**(3), 44
enriched-uranium costs, **1**(1), 1; **3**(2), 19
fast-breeder reactors, **3**(2), 2, 4
fuel elements, **1**(2), 18–19
fuel reprocessing, **1**(1), 2
gas-cooled reactors, **1**(4), 53–5; **3**(2), 2, 3–4
heavy-water reactors, **2**(2), 44–8; **2**(4), 2, 3, 4, 22–30; **3**(2), 2, 4, 52–8
homogeneous reactors, **1**(2), 59–60; **3**(2), 2, 4
industrial process heat, **2**(3), 4–5
liquid-metal-fuel reactors, **1**(3), 53–4
marine reactors, **2**(2), 1–6; **2**(3), 13–16; **3**(2), 13–18
New Production Reactor, **3**(4), 75–7
organic-cooled and -moderated reactors, **2**(4), 2, 3, 16–21; **3**(2), 2–3, 4, 7–9
Organic-Moderated Reactor Experiment, **1**(4), 49–50
pressurized-water reactors, **2**(4), 2, 3, 4–11, 14–15; **3**(2), 1–2, 4, 9–10
Sodium Deuterium Reactor, **3**(2), 56–7
sodium graphite reactors, **3**(2), 2–3, 4
test reactors, **1**(4), 64
waste problems, **3**(4), 1–11
Elastomers, radiation effects, **1**(4), 37, 39
Electrical components, radiation effects, **1**(3), 40; **1**(4), 38–9
Electrical insulation, **1**(4), 39
Electrochemical power, direct conversion of nuclear energy, **3**(3), 48–50
Electrocladding, fuel elements with aluminum, **2**(2), 34
Electrons, effect on glycerine, **1**(4), 38
Elk River Power Reactor, containment, **2**(3), 27
Embrittlement, radiation effects, **3**(4), 38–57
Engineering Test Reactor
See Reactor (Engineering Test)
Engines, radiation effects, **1**(4), 39
Engines (nuclear gas, reciprocating), **2**(3), 62–3
Enrico Fermi Reactor
See Reactor (Enrico Fermi Fast Breeder)
Erbium, nuclear properties, **3**(2), 32
Erbium oxide, neutron absorption, **3**(3), 35
Europium, application as control material, **1**(2), 34; **3**(3), 32, 43–4
neutron cross sections, **1**(3), 13
Europium-151, nuclear properties, **3**(3), 32
Europium-155, neutron cross sections, **3**(4), 16
Europium oxide, melting point, **1**(2), 28
neutron absorption, **3**(3), 35
Europium oxide (stainless-steel-clad), applications as control material, **3**(3), 34
fabrication, **1**(2), 34
Europium oxide–stainless steel systems, neutron absorption, **3**(3), 34
Europium oxide–stainless steel systems (stainless-steel-clad), control rods in SM-1 Reactor, **3**(3), 40
Evaporators, waste-disposal applications, **1**(2), 45
Experimental Boiling-Water Reactor
See Reactor (Experimental Boiling-Water)
Experimental Breeder Reactors
See Reactor (Experimental Breeder)
Exponential experiments, **3**(4), 12–16

F

Fast-fission factor, definition, **1**(1), 4
Fast-Reactor Core Test Facility
See Reactor (Fast, Core Test Facility)
Ferrite, radiation effects, **3**(1), 37–8
Finned fuel elements, Calder Hall Reactors, **1**(1), 5
Finned tubes
See Tubes (finned)
Fission gas
See also Fission products
release from uranium dioxide fuel, **1**(1), 25–6; **1**(2), 24
Fission-neutron age, indium, **2**(4), 31–3
Fission products
See also Fission gas; Reactor wastes
buildup in recycled fuels, **1**(4), 19; **2**(2), 42–3
decay energy, **1**(4), 5; **2**(4), 34; **3**(4), 2–5
neutron cross sections, **3**(4), 16
reactor poisoning, **3**(4), 12, 16–19
release from fluid-fuel reactors, **1**(4), 14–15
release from uranium dioxide fuel elements, **1**(4), 25, 28
release from uranium dioxide–silicon carbide–silicon fuel elements, **1**(2), 24
release from uranium fuel elements, **1**(4), 26–7, 29
from uranium-235, **3**(3), 15
Fissium-molybdenum-uranium alloys, nuclear properties, **1**(4), 29
Fissium-uranium alloys
See Uranium-fissium alloys
Fissium-uranium-plutonium alloys, nuclear properties, **1**(1), 25
Fixation, reactor wastes, **3**(4), 7–8
Florida Power Reactor, **3**(2), 54

Fluid flow, **3**(1), 18–23; **3**(2), 34–9; **3**(3), 7–11; **3**(4), 22–32
See also Gas flow
parallel-channel flow of two-phase, **3**(4), 31–2
Fluid flow (laminar), heat transfer in circular channels, **3**(4), 25
Fluid flow (turbulent), heat transfer, **3**(3), 8–9
heat transfer in circular channels, **3**(4), 25
Fluid-fuel reactors
See Reactors (fluid-fuel)
Fluidized-bed reactors, design, **3**(1), 61–3
Fluorides (fused), corrosion of Hastelloy B, Hastelloy W, Inconel, and Inconel X, **1**(3), 39
Fluorine, shielding properties, **2**(2), 30
Formex, radiation effects, **1**(4), 38
Friction coefficients, gases, **3**(2), 38
Fuel breeding
See Breeding
Fuel cells, direct conversion of nuclear energy, **3**(3), 48–50
Fuel cycles, **1**(4), 19–21; **3**(3), 15–23
Homogeneous Reactor Experiment-II, **1**(2), 51
liquid-metal-fuel reactors, **1**(3), 47
uranium-236 problems, **2**(2), 42
Fuel elements, **1**(2), 18–33; **1**(3), 24–36; **1**(4), 22–35; **2**(3), 40–50
bonding with lead, **2**(2), 34
BORAX-IV Reactor, **1**(4), 12, 30
burnout, **1**(3), 17–18; **1**(4), 7–8; **2**(4), 39–42
Calder Hall Reactors, **1**(4), 32
damage in Sodium Reactor Experiment, **3**(2), 60–4
decontamination of surfaces, **3**(3), 24–5
design, **1**(1), 21–9
economics, **1**(1), 1–2, 21–9; **1**(2), 18–19
electrocladding with aluminum, **2**(2), 34
Experimental Boiling-Water Reactor, **1**(4), 31; **3**(3), 62
Experimental Breeder Reactor-II, **1**(2), 22–4
Experimental Gas-Cooled Reactor, **2**(3), 55–6; **3**(4), 59–62
fabrication methods, **1**(2), 27–8; **1**(3), 24–5; **3**(2), 42–4, 45
Fast-Reactor Core Test Facility, **3**(2), 68
fast reactors, **1**(2), 67; **1**(4), 32
fission-product buildup in recycled, **1**(4), 19; **2**(2), 42–3
fission-product release, **1**(4), 25–9
fluidized-bed reactors, **3**(1), 61–2
Gas-Cooled Reactor Experiment, **2**(3), 61; **2**(4), 79, 80–1
gas-cooled reactors, **1**(4), 27–8, 31–2, 55–7
handling of irradiated, **2**(4), 55
heat transfer and burnout at high pressure, **2**(4), 39–42
heat transfer and burnout in MTR-ETR type, **2**(4), 36–9
heavy-water reactors, **3**(2), 52–8
homogeneous reactors, **1**(2), 47–8, 49–50, 52–3
isotope buildup in recycled, **1**(4), 19; **2**(2), 42–3
lead bonding, **1**(4), 30
limitations of Magnox cladding, **1**(4), 32
materials, **1**(1), 17–20, 27
melting in MTR, **1**(4), 15
melting in S1W Reactor, **1**(4), 15
melting in SM-1 Reactor, **1**(4), 15
MTR-ETR type hydrodynamic characteristics, **3**(1), 18–19
Pathfinder Power Reactor, **2**(3), 52
pebble-bed reactors, **2**(3), 40–2, 56–7
plutonium, **1**(2), 42–3
plutonium-aluminum alloys (Zircaloy-2-clad), **1**(3), 28
plutonium-cerium-cobalt alloys, **3**(2), 68
plutonium-iron alloys, **3**(2), 68
plutonium-reactivity, lifetime, **3**(3), 15–20
Plutonium Recycle Test Reactor, **3**(3), 53–6
radiation effects, **1**(1), 20; **3**(2), 43–4, 45, 59; **3**(4), 66–7
reactions with water during irradiation, **1**(1), 18–19
reactivity lifetime, **3**(3), 15
reenrichment by blending of recycled, **1**(4), 20–1
rupture in high-temperature water, **1**(2), 31
Shippingport Pressurized-Water Reactor, **1**(4), 31; **2**(2), 34
Sodium Graphite Reactor, **3**(2), 59–60
specifications for SM-1 Reactor, **1**(3), 40
stainless-steel cladding, **1**(3), 39; **1**(4), 30
temperature coefficient of reactivity, **3**(3), 3–4
thermal conductivity of uranium dioxide, **3**(2), 44–5, 46–9
thermal-neutron-flux distribution, **3**(2), 32
thorium oxide, **1**(4), 30
TURRET Reactor, **2**(4), 83
uranium alloy type, **1**(4), 29
uranium-bismuth alloys, **1**(3), 42–55
uranium dioxide–sodium potassium slurries, **1**(2), 44
uranium dioxide–thorium oxide systems (aluminum-nickel alloy clad), **1**(3), 33
uranium dioxide type, **1**(2), 67; **1**(4), 25, 28, 30, 32; **2**(3), 55–6; **3**(2), 42–4, 45; **3**(4), 59–62
uranium-graphite systems, **2**(3), 40–7
uranium-magnesium alloys, **2**(3), 47–50
uranium type, **1**(4), 26, 27, 31–2
uranium-zirconium alloys, **3**(2), 59–60
uranium-zirconium alloys (Zircaloy-clad), **1**(4), 31
Veronezh Reactor, **2**(1), 23–4
welding, **2**(2), 33–4
Zircaloy cladding, **1**(4), 30
Fuel elements (aluminum-clad), fabrication, **1**(2), 39
Fuel elements (finned), Calder Hall Reactors, **1**(1), 5
Fuel elements (magnesium-alloy-clad), limitations, **1**(4), 32
Fuel elements (pellets), erosion by high-temperature water, **1**(2), 31
Fuel elements (plates), hydrodynamic characteristics, **3**(1), 18–19
Fuel elements (rods), buckling, **1**(3), 1–5
corrosion by high-temperature water, **1**(2), 32
resonance absorption in uranium, **1**(3), 9

Fuel elements (stainless-steel-clad), dissolution, **1**(2), 39
Fuel elements (tubes), heat transfer, **3**(1), 22–3
hydrodynamic characteristics, **3**(1), 22–3
Fuel reprocessing, costs, **1**(1), 2
homogeneous reactors, **1**(2), 48, 50–2
liquid-metal-fuel reactors, **1**(3), 49–50
S1W Reactor, **1**(2), 31
Thorex Process, **1**(2), 51
TURRET Reactor, **2**(4), 83
Fuel rods
See Fuel elements (rods)
Fuel tubes
See Fuel elements (tubes)
Fuels
See Fuel elements
Fused fluoride salts
See Fluorides (fused)
Fused-salt-fuel reactors, **1**(2), 69
design, **3**(1), 54

G

G2 Reactor, refueling, **2**(4), 60, 64
G3 Reactor, refueling, **2**(4), 60, 64
Gadolinium, applications as control material, **1**(2), 34; **3**(3), 32, 43–4
neutron cross sections, **1**(3), 13; **3**(4), 16
Gadolinium oxide, melting point, **1**(2), 28
neutron absorption, **3**(3), 35
Gadolinium oxide–stainless steel systems, radiation effects, **1**(1), 31
Gadolinium oxide–titanium systems, radiation effects, **1**(1), 31
Gadolinium-tantalum alloys, neutron absorption, **3**(3), 34
Gallium (liquid), coolant properties, **1**(2), 40
Gamma heating, control rods, **1**(3), 12; **3**(3), 37–8
Gamma radiation, effects on glycerine, **1**(4), 38
Gas-cooled heavy-water-moderated reactors, design, **2**(1), 29–30; **2**(3), 57–8
Gas-Cooled Reactor Experiment
See Reactor (Gas-Cooled, Experiment)
Gas-cooled reactors
See Reactors (gas-cooled)
Gas flow
See also Fluid flow
heat transfer from finned tubes, **1**(1), 5–11; **3**(2), 38
Gas Suspension Coolant Project, **3**(4), 22–4
Gases, heat transfer, **2**(2), 23–7; **3**(2), 37–8; **3**(4), 22–4
properties, **2**(2), 26–7
Generators (magnetohydrodynamic), applications to nuclear power, **3**(3), 48–50
Germanium-uranium alloys
See Uranium-germanium alloys
Glass (boron), neutron absorption, **3**(3), 36
Glazes, corrosion, **1**(3), 38–9
Glycerine, radiation effects, **1**(4), 38
Gold, neutron absorption, **3**(3), 35
welding, **2**(2), 33
Gold-197, neutron cross sections, **1**(3), 13
Graphite, impregnation with uranium, **2**(3), 41–2
lattice buckling, **1**(2), 5–7; **1**(3), 5–6
moderating properties, **2**(2), 10; **3**(3), 1–3
moderation of liquid-metal-fuel reactors, **1**(3), 46
neutron cross sections, **2**(2), 36
nuclear properties, **1**(1), 31
physical properties, **1**(1), 3
properties, **2**(2), 36–7
radiation effects, **2**(2), 37–8
temperature effects in lattices, **1**(3), 6–7
Graphite-bismuth systems, neutron moderation, **2**(2), 10
Graphite–carbon dioxide systems, moderator-coolant efficiency, **2**(3), 59
Graphite-helium systems, moderator-coolant efficiency, **2**(3), 59
Graphite-moderated reactors
See Reactors (graphite-moderated)
Graphite-moderated systems, neutron age, **1**(2), 5–7
Graphite-moderated water-cooled reactors
See Reactors (graphite-moderated water-cooled)
Graphite-nitrogen systems, coolant properties, **3**(4), 24
Graphite–uranium dioxide systems, radiation effects, **1**(2), 26
Graphite-uranium systems
See Uranium-graphite systems

H

Hafnium, applications as control material, **1**(2), 34; **3**(3), 32, 33–5, 42, 43
neutron cross sections, **1**(3), 10–11, 13
Halden Reactor, refueling, **2**(4), 57
Hanford Atomic Products Operation, critical and exponential experiments, **3**(4), 13, 14, 15, 16
Hanford Production Reactors, fuel-element rupture tests, **1**(2), 31
Hastelloy 8286, corrosion by nitrogen, **2**(4), 81
Hastelloy B, corrosion by fused fluorides, **1**(3), 39–40
Hastelloy R-235, corrosion by nitrogen, **2**(4), 81
Hastelloy W, corrosion by fused fluorides, **1**(3), 39
Hastelloy X, corrosion by nitrogen, **2**(4), 81
Haynes-25, neutron absorption, **3**(3), 34
Health physics, radiation tolerances, **2**(4), 47–8
Heat exchangers
See also Boilers
liquid-metal-fuel reactors, **1**(3), 53
Heat transfer, **1**(1), 5–11; **1**(3), 17–19; **1**(4), 7–9; **2**(4), 36–43; **3**(1), 18–23; **3**(2), 34–9; **3**(3), 7–11; **3**(4), 22–32
burnout in rectangular channels, **3**(3), 9–10
burnout limits of polyphenyls, **2**(3), 20–1
Calder Hall Reactors, **1**(1), 5–11
gas-cooled systems, **2**(2), 23–7
liquid-metal-fuel reactors, **1**(3), 47–8

Heat transfer (Continued)
pressure vessels, 1(1), 20
vortex flow, 3(4), 25–7
Heavy hydrogen
See Deuterium
Heavy water
See Deuterium oxide
Heavy-Water Components Test Reactor, 3(2), 54–5
Heavy-water-moderated reactors
See Reactors (heavy-water-cooled and -moderated)
Helium, coolant in Experimental Gas-Cooled Reactor, 2(3), 55–6
coolant in Maritime Gas-Cooled Reactor, 2(3), 59–61
coolant in TURRET Reactor, 2(4), 83–5
heat transfer, 3(2), 38
reactor cooling, 1(4), 25, 57–8
Helium–carbon dioxide systems
See Carbon dioxide–helium systems
Helium-graphite systems, coolant-moderator efficiency, 2(3), 59
High-Temperature Gas-Cooled Reactor
See Reactor (Peach Bottom)
Hinkley Point Reactors
See Reactor (Hinkley Point)
Holmium oxide, neutron absorption, 3(3), 35
Homogeneous Reactor Experiment-II
See Reactor (Homogeneous Experiment-II)
Homogeneous Reactor Test
See Reactor (Homogeneous Experiment-II)
Homogeneous reactors
See Reactors (homogeneous)
Hot-channel factors, 2(4), 42–3
Engineering Test Reactor, 3(3), 7
Gas-Cooled Reactor Experiment, 3(4), 30–1
Human tissue, radiation effects, 1(4), 37
Humboldt Bay Power Reactor, containment, 3(3), 12
Hunterston Reactors, refueling, 2(4), 61, 65
Hydrocarbons, radiation effects, 1(4), 39
Hydrofluoric acid–nitric acid systems, corrosion of stainless steel, 1(2), 39
Hydrofluoric acid–nitric acid–water systems, decontamination efficiency, 3(3), 24–5
Hydrogen, corrosion of beryllium, 2(4), 69
neutron cross sections, 1(3), 13
reactor cooling, 1(4), 57–8
shielding properties, 2(2), 30
Hydrogen-oxygen systems, catalytic recombination, 1(2), 48–9, 56–7

I

Inconel, corrosion by fused fluorides, 1(3), 39
Inconel 702, corrosion by nitrogen, 2(4), 81
Inconel X, corrosion by fused fluorides, 1(3), 39
Indian Point Power Reactor
See Reactor (Indian Point Power)
Indium, application as control material, 3(3), 32, 34–5
fission-neutron age, 2(4), 31–3
neutron cross sections, 1(3), 13
Industrial process heat, economics of nuclear power, 2(3), 4–5
reactor applications, 3(1), 1–5
Insulation (electrical), radiation effects, 1(3), 40; 1(4), 39
Insulation (thermal), Gas-Cooled Reactor Experiment, 2(4), 81–2
Refrasil, 2(4), 82
Thermoflex, 2(4), 82
Iridium, nuclear properties, 3(3), 32
Iridium-191, nuclear properties, 3(3), 32
Iridium-193, nuclear properties, 3(3), 32
Iron, neutron cross sections, 2(2), 10
neutron interactions, 3(2), 40
shielding properties, 2(2), 30
solubility in liquid bismuth, 1(3), 50
Iron-aluminum alloys, radiation effects, 3(1), 37–8
Iron-boron systems
See Boron-iron systems
Iron limonite concrete, shielding properties, 2(4), 46
Iron-nickel alloys, radiation effects, 3(1), 37–8
Iron-plutonium alloys, fuel for Fast-Reactor Core Test Facility, 3(2), 68
Iron-silicon systems, radiation effects, 3(1), 37–8
Iron-uranium alloys
See Uranium-iron alloys
Irradiated fuels
See Fuel elements

K

Kaiser Gas-Cooled Reactor
See Reactor (Experimental Gas-Cooled)
Kinetic Experiment on Water Boilers
See Reactor (Kinetic Experiments on Water Boilers)
Knolls Atomic Power Laboratory, critical experiments, 3(4), 14

L

LAMPRE, 3(2), 65–9
Lattices, buckling, 1(3), 1–6
design, 1(2), 1–15
Experimental Boiling-Water Reactor, 3(3), 62
exponential measurements on biphenyl-moderated, 1(3), 14
theory, importance of accuracy, 1(1), 3–5
Lattices (graphite-moderated), buckling, 1(2), 5–7; 1(3), 5–6
measurements for uranium dioxide rods, 2(3), 18–19
measurements for uranium rods, 2(3), 18–19

Lattices (graphite-moderated) (Continued)
Organic-Moderated Reactor Experiment, I(4), 42–4
temperature effects, I(3), 6–7
Lattices (heavy-water-moderated), I(2), 1–5
buckling measurements, I(2), 2–4; I(4), 2; 3(2), 30–1
gas-cooled heavy-water-moderated reactors, 2(3), 57–8
physics, 2(3), 17–19
Lead, bonding of fuel elements, 2(2), 34
neutron interactions, 3(2), 40
properties, I(4), 25
shielding properties, 2(2), 30
Lead-bismuth alloys, coolant properties, I(2), 40
Leak detection, heavy-water reactors, 2(2), 46
Leather, radiation effects, I(4), 39
Lenin Reactor, design, 2(2), 3
Lid Tank Shielding Facility, neutron-cross-section determinations, 2(2), 30
Liquid Metal Fuel Reactor, design, 3(1), 54
Liquid Metal Fuel Reactor Experiment, design, I(3), 42–4, 54–5
Liquid-metal-fuel reactors
See Reactors (liquid-metal-fuel)
Liquid metals
See Metals (liquid)
Lithium, nuclear properties, 3(3), 32
shielding properties, 2(2), 30
Lithium (liquid), coolant properties, I(2), 40
Lithium chloride–potassium chloride systems (fused), physical properties, I(3), 48
Lithium hydride, radiation effects, I(1), 31
shielding properties, I(1), 31
Lithium sulfate, inhibition of uranyl sulfate corrosion of stainless steel and Zircaloy-2, I(2), 53
Livermore Pool Test Reactor, containment, 2(3), 26
Loeffler boilers, 3(2), 13–14
Los Alamos Molten Plutonium Reactor Experiment, 3(2), 65–9
Los Alamos plasma thermocouple, 3(1), 11–13
Los Alamos Scientific Laboratory, critical experiments, 3(4), 16
Lucite, radiation effects, I(4), 37
Lutetium, nuclear properties, 3(3), 32
Lutetium oxide, neutron absorption, 3(3), 35

M

Magnesium, corrosion by carbon dioxide, I(1), 33
corrosion by polyphenyls, I(4), 44–5
physical properties, 2(3), 47
properties, I(4), 23
solubility in liquid bismuth, I(3), 50
welding, 2(2), 33
Magnesium (liquid), coolant properties, I(2), 40
Magnesium alloys
See also Magnox
corrosion by carbon dioxide, I(1), 33
radiation effects, I(4), 40
Magnesium oxychloride cement, radiation effects, I(1), 31
shielding properties, I(1), 31
Magnesium uranate, melting point, I(2), 28
Magnesium-uranium alloys
See Uranium-magnesium alloys
Magnesium-zirconium couples, diffusion, I(2), 30
Magnetic materials, radiation effects, 3(1), 37–8
Magnetite concrete, shielding properties, 2(4), 46
Magnetite limonite concrete, shielding properties, 2(4), 46
Magnetohydrodynamic generators, applications to nuclear power, 3(3), 48–50
Magnox, heat transfer, I(1), 5–11
limitations as fuel-element cladding material, I(4), 32
Magnox A-12, properties, I(4), 23, 27
Magnox C, corrosion by carbon dioxide, I(1), 33
radiation effects, I(1), 32–3
Magnox E, corrosion by carbon dioxide, I(1), 33
radiation effects, I(1), 32–3
Maintenance procedures, Homogeneous Reactor Experiment-II, I(2), 58–9
homogeneous reactors, I(2), 57–9
liquid-metal-fuel reactors, I(3), 52
Pennsylvania Advanced Reactor, I(2), 59
Manganese-uranium alloys, properties, I(2), 28
Marine reactors
See Reactors (marine)
Martin Power Reactor, core physics, 3(1), 15
Materials Testing Reactor
See Reactor (Materials Testing)
Maxwell-Boltzmann neutron energy spectrum, I(3), 14
Merchant vessel power plants
See Reactors (marine)
Mercury, coolant properties, I(2), 40
nuclear properties, 3(3), 32
Metals, radiation effects, I(4), 37
Metals (liquid), coolant properties, I(2), 40
heat transfer, 3(1), 21–2
reactions with water, I(1), 18; 3(1), 30–3
Metaterphenyl, nucleate boiling, 3(1), 19
Microswitches, radiation effects, I(4), 39
MIT Reactor, containment, 2(3), 26
ML-1 Reactor
See Reactor (ML-1)
Moderators, beryllium, I(3), 46
bismuth-graphite systems, 2(2), 10
carbon dioxide–water systems, 2(3), 59
carbon dioxide–zirconium hydride systems, 2(3), 59
control in pressurized-water reactors, 2(4), 85
deuterium oxide in Plutonium Recycle Test Reactor, 3(3), 53–6
deuterium oxide–water systems, I(2), 4–5; 2(2), 10
graphite, I(1), 31; I(3), 46; 2(2), 10; 3(3), 1–3
graphite-helium systems, 2(3), 59
homogeneous reactors, I(2), 48
materials, I(2), 35–8

Moderators (Continued)
physical properties, 1(1), 31
power flattening by variation of properties, 3(3), 4–5
radiation effects, 1(1), 31
water, 2(2), 9–10
zirconium hydride, 1(3), 37
Molten fluoride reactors
See Reactors (fused-salt-fuel)
Molybdenum, nuclear properties, 1(2), 39
radiation effects, 1(4), 40
solubility in liquid bismuth, 1(3), 50
thermal properties, 1(2), 39
Molybdenum-fissium-uranium alloys, nuclear properties, 1(4), 29
Molybdenum–thorium oxide systems, thermal properties, 1(2), 28, 30
Molybdenum-uranium alloys
See Uranium-molybdenum alloys
Molybdenum–uranium dioxide systems, properties, 1(2), 31

N

NaK, coolant properties, 1(2), 40
NASA Research Reactor, containment, 2(3), 26
National Reactor Test Station, critical experiments, 3(4), 14
Neon, reactor cooling, 1(4), 57–8
Neptunium-237, neutron cross sections, 1(3), 13; 2(2), 16
Neutron age, calculation methods, 2(2), 15–16
deuterium oxide–water moderated systems, 1(2), 4–5
graphite-moderated systems, 1(2), 5–7
Neutron cross sections, 2(2), 16
americium-241, 1(3), 13
cadmium, 1(3), 10–11, 13; 3(3), 34
cadmium-113, 3(4), 16
cadmium-indium-silver alloys, 3(3), 41
determination in fission-product mixtures, 3(4), 12–19
europium, 1(3), 13
europium-155, 3(4), 16
fission products of uranium-235, 3(4), 16
gadolinium, 1(3), 13
gadolinium-155, 3(4), 16
gadolinium-157, 3(4), 16
gold-197, 1(3), 13
graphite, 2(2), 36
hafnium, 1(3), 10–11, 13
hydrogen, 1(3), 13
indium, 1(3), 13
iron, 2(2), 10
Lid Tank Shielding Facility, 2(2), 30
Maxwell–Boltzmann neutron energy spectrum, 1(3), 14
measurement, 1(2), 11–12
neptunium-237, 1(3), 13; 2(2), 16
plutonium-239, 1(3), 13; 2(2), 17
plutonium-240, 1(3), 13; 1(4), 4–5; 2(2), 16
plutonium-241, 1(3), 13; 1(4), 5
samarium-149, 1(3), 13; 2(2), 16; 3(4), 16
stainless steel, 2(2), 10
uranium-233, 1(3), 13; 2(2), 17
uranium-234, 1(3), 13
xenon-135, 1(3), 13; 3(4), 16
Neutron economy, liquid-metal-fuel reactors, 1(3), 46–7
Neutron energy spectra, thermal-energy range, 1(2), 6–9; 1(4), 5
Neutrons
See also Radiation effects
absorption by aluminum, 3(3), 34
delayed, in reactors, 3(1), 24–5
distribution prediction in shields, 3(2), 40
distribution of thermal in fuels, 3(2), 32
distribution of thermal in Physical Constants Test Reactor, 3(3), 1–3
economy in heavy-water reactors, 1(1), 38–40
flux-distribution determination, 3(3), 5
interactions in iron, lead, nitrogen, and oxygen, 3(2), 40
moderation, 2(2), 7–10
resonance escape calculation for uranium, uranium dioxide, thorium, and thorium oxide, 1(1), 4
resonance escape probability, 1(2), 9–10
thermalization theory, 1(2), 8–9
New Production Reactor, design and economics, 3(4), 75–7
Nichrome-V–Water systems, chemical reactions during irradiation, 1(1), 18–19
Nickel, properties, 1(2), 39
shielding properties, 2(2), 30
solubility in liquid bismuth, 1(3), 50
welding, 2(2), 33
Nickel alloys, corrosion by nitrogen, 2(4), 81
radiation effects, 1(4), 40
Nickel-aluminum alloys
See Aluminum-nickel alloys
Nickel–chromium–uranium dioxide systems (Nichrome-V-clad), reactions with water during irradiation, 1(1), 18–19
Nickel-iron alloys, radiation effects, 3(1), 37–8
Nickel-uranium alloys
See Uranium-nickel alloys
Niobium, properties, 1(2), 39; 1(4), 23, 29
reactions with uranium, 1(4), 29
solubility in liquid bismuth, 1(3), 50
Niobium oxide–uranium dioxide systems, thermal conductivity, 3(2), 49
Niobium–thorium oxide systems, properties, 1(2), 31
Niobium-uranium alloys
See Uranium-niobium alloys
Niobium–uranium dioxide systems, properties, 1(2), 31
Niobium-uranium-zirconium alloys
See Uranium-niobium-zirconium alloys

Niobium-zirconium alloys, corrosion by uranyl sulfate solutions, **1**(2), 52
Nitric acid–hydrofluoric acid systems, corrosion of stainless steel, **1**(2), 39
Nitric acid–hydrofluoric acid–water systems, decontamination efficiency, **3**(3), 24–5
Nitrogen, coolant in Gas-Cooled Reactor Experiment, **2**(3), 61; **2**(4), 79–81
corrosion of beryllium, **2**(4), 69
corrosion of Carpenter 20-Cb, Hastelloy 8286, Hastelloy R-235, Hastelloy X, Inconel 702, and nickel alloys, **2**(4), 81
corrosion of stainless steel, **3**(1), 38–40
neutron interactions, **3**(2), 40
reactor cooling, **1**(4), 57–8
Nitrogen-graphite systems, coolant properties, **3**(4), 24
Nondestructive testing, Zircaloy-2 tubing, **1**(2), 45
NPD Reactor, refueling, **2**(4), 58–63
NRU Reactor, refueling, **2**(4), 58–63
Nuclear data, **1**(4), 5
Nuclear energy, direct conversion to useful power, **3**(3), 48–50
Nuclear gas engines, **2**(3), 61–2
Nuclear physics
See Reactor physics
Nuclear power, evaluation of various reactor designs, **3**(3), 51–2
Nuclear radiation
See Radiation effects; specific types of nuclear radiation
Nuclear superheaters
See Superheaters (Nuclear)
Nucleate boiling
See Boiling (nucleate)
Nylon, radiation effects, **1**(4), 37

O

Oak Ridge National Laboratory, critical experiments, **3**(4), 14, 16
Obninsk Reactor, refueling, **2**(4), 59
Organic materials, radiation effects, **1**(3), 40
Organic-moderated reactors
See Reactors (organic-cooled and -moderated)
ORNL Graphite Reactor, shielding, **2**(2), 31
Orthoterphenyl, nucleate boiling, **3**(1), 19
Oxygen, corrosion of beryllium, **2**(4), 69
neutron interactions, **3**(2), 40
shielding properties, **2**(2), 30
Oxygen-deuterium systems, catalytic recombination, **1**(2), 46–8, 56–7
Oxygen-hydrogen systems, catalytic recombination, **1**(2), 48–9, 56–7

P

PAR
See Reactor (Pennsylvania Advanced)
Parr Shoals Reactor, **3**(2), 54
Pathfinder Power Reactor
See Reactor (Pathfinder Power)
PCTR
See Reactor (Physical Constants Testing)
Peach Bottom Reactor, design, **3**(4), 58
Pebble Bed Reactor, design, **2**(3), 56–7; **3**(4), 59
Pennsylvania Advanced Reactor
See Reactor (Pennsylvania Advanced)
Pentalene, radiation effects, **1**(4), 38
Perspex, radiation effects, **1**(3), 40
Phosphates, corrosion of aluminum alloys, **1**(2), 40
Phosphorus pentoxide–uranium systems, melting point, **1**(2), 28
Physical Constants Testing Reactor
See Reactor (Physical Constants Testing)
Piqua Power Reactor, containment, **2**(3), 27
Plastics, radiation effects, **1**(3), 40; **1**(4), 37
Platinum, welding, **2**(2), 33
Plexiglas, radiation effects, **1**(4), 37
Plutonium, production in New Production Reactor, **3**(4), 75–7
reactivity lifetimes in fuel elements, **3**(3), 15–20
reactor fuels, **1**(2), 42–3
recycle in sodium graphite reactors, **3**(3), 18–20
Plutonium-239, neutron cross sections, **1**(3), 13; **2**(2), 17
Plutonium-240, neutron cross sections, **1**(3), 13; **1**(4), 4–5; **2**(2), 16
Plutonium-241, neutron cross sections, **1**(3), 13; **1**(4), 5
Plutonium-aluminum alloys, radiation effects, **1**(3), 27–8
rod buckling, **1**(3), 4
Plutonium-aluminum alloys (Zircaloy-2-clad), fabrication into fuel elements, **1**(3), 28
fuel in Plutonium Recycle Test Reactor, **3**(3), 53–6
Plutonium-cerium-cobalt alloys, fuel for Fast-Reactor Core Test Facility, **3**(2), 68
Plutonium-iron alloys, fuel for Fast-Reactor Core Test Facility, **3**(2), 68
Plutonium Recycle Test Reactor
See Reactor (Plutonium Recycle Test)
Plutonium-uranium alloys, radiation effects, **1**(2), 22–5
Plutonium-uranium-fissium alloys, nuclear properties, **1**(1), 25
Polyethylene, radiation effects, **1**(4), 37
Polyethylene terephthalate, radiation effects, **1**(3), 40
Polymers, radiation effects, **1**(3), 40
Polymethylmethacrylate, radiation effects, **1**(4), 37
Polyphenyls, burnout limits in reactors, **2**(3), 20–1
corrosion of aluminum, magnesium, stainless steels, and steels, **1**(4), 44–5
nucleate boiling, **3**(1), 19
properties, **1**(4), 45–9
Polystyrene, radiation effects, **1**(3), 40; **1**(4), 37
Polytetrafluorethene, radiation effects, **1**(3), 40
Potassium chloride–lithium chloride systems, physical properties, **1**(3), 48

Potassium-sodium alloys, coolant properties, 1(2), 40
Potassium–sodium–uranium dioxide systems (slurries), temperature effects on fuel suspension, 1(2), 44
Potassium uranate, melting point, 1(2), 28
Power oscillation, 1(2), 12–13
Pressure drop, calculations in pressurized-water reactors, 3(2), 39
Pressure-tube reactors, refueling, 2(4), 62
Pressure tubes, aluminum-silicon systems, 2(1), 34
gas-cooled heavy-water-moderated reactors, 2(3), 56, 58
Gas-Cooled Reactor Experiment, 2(3), 61
Plutonium Recycle Test Reactor, 3(3), 53, 55
Pressure vessels, Experimental Breeder Reactor-II, 1(3), 56–7
heat transfer, 1(1), 20
homogeneous reactors, 1(2), 57
liquid-metal-fuel reactors, 1(3), 53
radiation effects, 3(4), 38–57
Pressurized Test Reactor, temperature coefficient of reactivity, 3(3), 3–4
Pressurized-Water Reactors
See Reactors (pressurized-water)
Process heat, economics of nuclear power, 2(3), 4–5
reactor applications, 3(1), 1–5
Process heat reactors
See Reactors (process heat)
Pumps, homogeneous reactors, 1(2), 57
liquid-metal-fuel reactors, 1(3), 52–3
PWR
See Reactor (Shippingport Pressurized-Water)

R

Radiation (gamma), attenuation and heating codes, 3(2), 41
Radiation effects, 1(4), 40; 2(4), 72; 3(2), 59
Alkanex, 1(4), 38
alkylbenzene, 1(4), 38
alloys, 3(4), 38–57
aluminum, 1(3), 28; 1(4), 40–1
aluminum alloys, 1(4), 40
aluminum-iron alloys, 3(1), 37–8
aluminum-nickel alloys, 1(3), 33; 3(1), 37–8
amber, 1(3), 40
asbestos, 1(4), 38
beryllium, 1(1), 32; 1(4), 40–1; 2(4), 70
boron, 1(2), 34
boron carbide, 1(1), 30–1
boron–stainless steel systems, 1(1), 30; 2(4), 71; 3(3), 39
boron-titanium systems, 1(1), 30; 3(3), 40–1
boron–Zircaloy-2 systems, 1(1), 30
boron-zirconium systems, 1(2), 34; 3(3), 40–1
boron-zirconium systems (Zircaloy-2-clad), 1(2), 34
cadmium, 1(1), 31
cadmium-indium-silver alloys, 3(3), 41
capacitors, 1(4), 39
ceramic materials, 1(4), 37
cobalt alloys, 1(4), 40
compacts, 1(2), 19–20
concretes, 2(2), 31–2
control-rod springs, 1(2), 45
copper, 1(4), 40
Dowtherm-A, 1(4), 38
elastomers, 1(4), 37, 39
electrical components, 1(3), 40; 1(4), 38–9
electrical insulation, 1(4), 39
engines, 1(4), 39
ferrite, 3(1), 37–8
Formex, 1(4), 38
fuel elements, 1(1), 20; 3(2), 43–4, 45, 59; 3(4), 66–7
gadolinium oxide–stainless steel systems, 1(1), 31
gadolinium oxide–titanium systems, 1(1), 31
Gas-Cooled Reactor Experiment fuel elements, 2(4), 81–2
glycerine, 1(4), 38
graphite, 2(2), 37–8
human tissue, 1(4), 37
hydrocarbons, 1(4), 39
iron-nickel alloys, 3(1), 37–8
iron-silicon systems, 3(1), 37–8
leather, 1(4), 39
lithium hydride, 1(1), 31
magnesium alloys, 1(4), 40
magnesium oxychloride cement, 1(1), 31
magnetic materials, 3(1), 37–8
Magnox C, 1(1), 32–3
Magnox E, 1(1), 32–3
mathematical analysis, 3(4), 51–7
mechanisms of damage, 1(4), 36–7
metals, 1(4), 37
microswitches, 1(4), 39
moderators, 1(1), 31
molybdenum, 1(4), 40
nickel alloys, 1(4), 40
nylon, 1(4), 37
organic materials, 1(3), 40
Organic-Moderated Reactor Experiment fuel elements, 3(4), 66–7
pentalene, 1(4), 38
Perspex, 1(3), 40
plastics, 1(3), 40; 1(4), 37
plutonium-aluminum alloys, 1(3), 27–8
polyethylene, 1(4), 37
polyethylene terephthalate, 1(3), 40
polymers, 1(3), 40
polymethylmethacrylate, 1(4), 37
polystyrene, 1(3), 40; 1(4), 37
polytetrafluorethene, 1(3), 40
pressure vessels, 3(4), 38–57
reactor vessels, 3(4), 38–57
Refrasil, 2(4), 82
resistors, 1(4), 39
rubber (natural), 1(4), 37
selsyn motors, 1(4), 39
semiconductors, 1(4), 37; 3(1), 37

Radiation effects (Continued)
shielding, 1(1), 31; 2(4), 47–8
silicones, 1(4), 38; 3(1), 37
Sodium Graphite Reactor fuel elements, 3(2), 59
stainless steel, 1(4), 40; 2(3), 56; 2(4), 72
steels, 1(4), 40; 3(4), 38–57
tantalum, 1(4), 40
Thermoflex, 2(4), 82
thorium, 1(2), 24–5
thorium (aluminum-clad), 1(3), 29
thorium oxide, 1(2), 31
titanium, 1(4), 40
tungsten, 1(4), 40
uranium, 1(2), 19–20; 1(3), 25; 1(4), 26, 31–2; 3(2), 59
uranium (depleted), 1(2), 19
uranium (zirconium-clad), 1(3), 25
uranium alloys, 1(2), 32; 1(4), 29
uranium-aluminum alloys, 1(1), 29; 1(3), 33–4
uranium dioxide, 1(2), 24; 1(4), 25, 28, 38; 3(2), 43–4, 45
uranium dioxide (stainless-steel-clad), 2(3), 56
uranium dioxide (Zircaloy-2-clad), 1(1), 26–7; 1(3), 28–33
uranium dioxide–graphite systems, 1(2), 26
uranium dioxide–silicon carbide–silicon systems, 1(2), 24
uranium dioxide–thorium oxide systems, 1(1), 28; 1(2), 24, 26
uranium dioxide–thorium oxide systems (aluminum-nickel alloy clad), 1(3), 33
uranium-fissium alloys, 1(2), 22
uranium-germanium alloys, 1(2), 32
uranium-graphite systems, 2(3), 44–5
uranium hydride compacts, 1(2), 19–20
uranium-iron alloys, 1(2), 32
uranium-magnesium alloys, 1(2), 28; 2(3), 48–50
uranium-molybdenum alloys, 1(2), 19–21, 32; 1(3), 25–7
uranium-niobium alloys, 1(2), 19–20; 1(3), 27
uranium-niobium-zirconium alloys, 1(2), 21
uranium-plutonium alloys, 1(2), 22–5
uranium-silicon systems, 1(2), 19–21, 32
uranium–stainless steel alloys, 1(1), 29
uranium-thorium alloys, 1(2), 24–5, 32
uranium-titanium alloys, 1(2), 20–1, 32
uranium-vanadium alloys, 1(2), 32
uranium-zirconium alloys, 1(1), 29; 1(2), 26, 27, 32; 1(3), 25, 34; 3(2), 59
welds, 3(4), 41–2
Zircaloy, 1(1), 29
Zircaloy-2, 1(1), 26–7; 1(2), 34; 1(3), 25–7, 29–33
zirconium, 1(3), 25, 34; 1(4), 40
zirconium diboride, 1(1), 30
Radiation tolerances, 2(4), 47–8
Radioisotopes, safe handling, 2(3), 38–9
Rare-earth oxides, melting point, 1(2), 28
Rare earths, control-rod applications, 3(3), 43–4
Reactivity, coefficient of
See Coefficient of reactivity
Reactor (Advanced Gas-Cooled), design, 2(1), 28–9
Reactor (Air Force Nuclear Engineering Test), blast-effect studies, 1(2), 17
containment, 2(3), 26
Reactor (Aircraft, Experiment) (ARE), control rods, 3(3), 45
Reactor (APS-1)
See Reactor (Obninsk)
Reactor (ARBOR), design, 1(2), 64–5
Reactor (Argonaut), materials and operating characteristics, 1(1), 40–1
Reactor (Argonne Low-Power)
See Reactor (ML-1)
Reactor (Army Package Power)
See Reactor (SM-1)
Reactor (Belgonucleaire), design, 2(1), 5, 17
thermal-output characteristics, 2(1), 2
Reactor (Beloyerski Urals)
See Reactor (U.S.S.R. Superheater)
Reactor (Berkeley) (British), refueling, 2(4), 60, 64–5
Reactor (BONUS), design, 3(4), 68–74
superheater, 3(4), 68–74
Reactor (BORAX), coefficient of reactivity, 1(1), 15–16
stability, 1(1), 15–16
Reactor (BORAX-I), destructive experiment analysis, 1(2), 17
operating characteristics, 3(1), 49
self-limitation of power, 1(3), 20–1
Reactor (BORAX-II), operating characteristics, 3(1), 49
Reactor (BORAX-III), operating characteristics, 3(1), 49
Reactor (BORAX-IV), coolant contamination, 2(1), 22–3
core design, 1(4), 24
fuel-element bonding, 1(4), 30; 2(2), 34
fuel-element design, 1(4), 12
operating characteristics, 3(1), 49
stability, 1(2), 64; 2(1), 20; 3(1), 47–53
Reactor (BR-3), design and safety, 3(1), 41
Reactor (Bradwell), design, 1(4), 54; 2(1), 6
refueling, 2(4), 60
Reactor (Brown-Boveri-Krupp), design, 3(4), 59
Reactor (Bulk Shielding), shielding experiments, 3(2), 40
Reactor (Calder Hall), control rods, 3(3), 30, 45
core design, 1(4), 24
design, 1(1), 34–5; 1(4), 54
fuel-element design, 1(1), 5; 1(4), 32
graphite loss, 2(2), 36
heat transfer, 1(1), 5–11
refueling, 2(4), 60, 64
safety, 2(3), 28–9
specific power, 2(1), 26
Reactor (Chugach Power)
See Reactor (Sodium Deuterium)
Reactor (Czechoslovakia Gas-Cooled), refueling, 2(4), 61
Reactor (Dounreay), core design, 1(4), 24

Reactor (Dragon), design, **3**(4), 58
Reactor (Dresden Power), containment, **2**(3), 27
control rods, **3**(3), 45
core design, **1**(4), 24
design, **2**(1), 5, 17
refueling, **2**(4), 57
thermal-output characteristics, **2**(1), 2
Reactor (Elk River Power), containment, **2**(3), 27
Reactor (Engineering Test), **1**(4), 64
fuel-element burnout, **2**(4), 36–9
hot-channel factors, **3**(3), 7
thermal analysis, **3**(2), 34–5
Reactor (Enrico Fermi Fast Breeder), containment, **2**(3), 27
core design, **1**(4), 24
control rods, **3**(3), 45
dynamics, **3**(4), 36
refueling, **2**(4), 58, 64
Reactor (Experimental Boiling-Water), coefficient of reactivity, **1**(1), 14–16
containment, **2**(3), 25–6; **3**(3), 64
control rods, **3**(3), 28–31, 45
coolant contamination and purification, **2**(1), 22–3
core design, **1**(4), 24
design, **1**(1), 36–8
fuel elements, **1**(4), 31; **3**(3), 62
modifications, **3**(3), 62–4
physics, **2**(2), 11
radioactive contamination, **2**(1), 22–3
refueling, **2**(4), 57
safety, **3**(3), 62–4
stability, **2**(1), 20; **3**(1), 44–7, 51–3; **3**(4), 34–5
thermal-output characteristics, **2**(1), 2
turbine corrosion, **2**(2), 51
Reactor (Experimental Breeder-I), alpha-radiation determination, **1**(3), 9
analysis after meltdown, **1**(3), 22
coefficient of reactivity, **1**(1), 12–14
core damage from failure, **1**(2), 66
core design, **1**(4), 24
safety experiments, **3**(1), 28
stability, **1**(1), 12–13; **3**(4), 36
Reactor (Experimental Breeder-II), containment, **1**(3), 53; **2**(3), 25, 27
core design, **1**(4), 24
design, **1**(3), 56–8
dynamics, **3**(4), 36
fuel-element design, **1**(2), 22–4
refueling, **2**(4), 58, 63–4
Reactor (Experimental Gas-Cooled), core design, **1**(4), 24
design, **2**(1), 6, 28–9; **2**(3), 55–6; **3**(4), 58, 59–62
Reactor (Fast, Core Test Facility), breeding, **3**(2), 67
design, **3**(2), 65–9
superheater, **3**(2), 67
Reactor (Florida power), **3**(2), 54
Reactor (G2), refueling, **2**(4), 60, 64
Reactor (G3), refueling, **2**(4), 60, 64
Reactor (Gas-Cooled Experiment), **2**(4), 79–82
design, **2**(1), 6; **2**(3), 61–2
hot-channel factors, **3**(4), 30–1
radiation effects on fuel elements, **2**(4), 81–2
thermal analysis, **2**(4), 79–80, 81
Reactor (Gas-Cooled, Experiment-II), design, **2**(4), 82
Reactor (General Electric Test), containment, **2**(3), 26
Reactor (Halden), refueling, **2**(4), 57
Reactor (Hanford Production), fuel-element rupture tests, **1**(2), 31
Reactor (Heavy-Water Components Test), **3**(2), 54–5
Reactor (High-Temperature Gas-Cooled) *See* Reactor (Peach Bottom)
Reactor (Kinetic Experiments on Water Boilers), safety experiments, **3**(1), 28
stability, **3**(4), 33–4
Reactor (Lenin), design, **2**(2), 3
Reactor (Lid Tank Shielding Facility), neutron-cross-section determinations, **2**(2), 30
Reactor (Liquid Metal Fuel), design, **3**(1), 54
Reactor (Liquid Metal Fuel, Experiment), design, **1**(3), 42–4, 54–5
Reactor (Livermore Pool Test), containment, **2**(3), 26
Reactor (Los Alamos Molten Plutonium, Experiment), **3**(2), 65–9
Reactor (Maritime Gas-Cooled), design, **2**(3), 59–61; **3**(4), 59
Reactor (Martin Power), core physics, **3**(1), 15
Reactor (Materials Testing), **1**(4), 64
fuel-element burnout, **2**(4), 36–9
fuel-element melting, **1**(4), 15
Reactor (MIT), containment, **2**(3), 26
Reactor (ML-1), control rods, **3**(3), 45
design, **3**(4), 59
Reactor (NASA Research), containment, **2**(3), 26
Reactor (New Production), design and economics, **3**(4), 75–7
Reactor (NPD-2), refueling, **2**(4), 58, 63
Reactor (NRU), refueling, **2**(4), 58, 63
Reactor (N.S. *Savannah*), containment, **2**(2), 12; **2**(3), 26
core physics, **3**(1), 15
design, **2**(2), 3
Reactor (Obninsk), refueling, **2**(4), 59
Reactor (Organic-Moderated, Experiment), containment, **1**(4), 42–51; **2**(3), 27
control rods, **3**(3), 45
coolant decomposition, **3**(2), 70
coolant purification, **1**(4), 44
economics, **1**(4), 49–50
fuel-element temperatures, **3**(4), 31
radiation effects in fuel elements, **3**(4), 66–7
refueling, **2**(4), 59
safety, **1**(4), 44–5
Reactor (ORNL Graphite), shielding, **2**(2), 31
Reactor (Parr Shoals), **3**(2), 54
Reactor (Pathfinder Power), **2**(3), 51–6
control, **2**(3), 52

Reactor (Pathfinder Power) (Continued)
containment, **2**(3), 27
superheaters, **3**(4), 69
Reactor (Peach Bottom), design, **2**(1), 30–2; **3**(4), 58
Reactor (Pebble Bed), design, **2**(3), 56–7; **3**(4), 59
Reactor (Pennsylvania Advanced), design, **1**(2), 47
maintenance, **1**(2), 59
Reactor (Physical Constants Testing), buckling measurements, **3**(2), 30–1
Doppler coefficient measurements, **3**(2), 31–2
thermal-neutron distribution, **3**(3), 1–3
Reactor (Piqua Power), containment, **3**(3), 27
Reactor (Plutonium Recycle Test), **1**(2), 42–3
containment, **2**(3), 27; **3**(3), 54–6
design, **3**(3), 53–7
safety, **3**(3), 54–6
Reactor (Pressurized Test), temperature coefficient of reactivity, **3**(3), 3–4
Reactor (Russian Gas-Cooled Heavy-Water), design, **1**(1), 35–6
Reactor (S1G), containment, **2**(3), 27
control rods, **3**(3), 45
physics, **2**(4), 34
Reactor (S1W), fuel-element melting, **1**(4), 15
fuel reprocessing, **1**(2), 31
Reactor (Saclay EL-3), fuel-element welding, **2**(2), 33
Reactor (Savannah River), buckling, **1**(3), 1–2
Reactor (Shippingport Pressurized-Water), breeding, **1**(3), 6–7
containment, **2**(3), 26
control rods, **3**(3), 45
coolant purification, **2**(4), 74–6
core design, **1**(4), 24
decontamination, **2**(4), 76–7
fuel-cycle calculations, **3**(3), 21
fuel-element welding, **2**(2), 34
fuel elements, **1**(4), 31
nuclear analysis, **1**(4), 1–2
operating experience, **2**(4), 74–7
physics, **2**(2), 11
refueling, **2**(4), 56
spatial power oscillation, **3**(3), 35
thermal-output characteristics, **2**(1), 21
Reactor (Siberian), **2**(1), 7
design, **2**(1), 34
refueling, **2**(4), 59
Reactor (SM-1), containment, **2**(3), 26
control rods, **3**(3), 40, 45
core design, **1**(4), 24
fuel-element melting, **1**(4), 15
fuel-element specifications, **1**(3), 40
nuclear analysis, **1**(4), 3
refueling, **2**(4), 56
Reactor (Sodium Deuterium), **1**(4), 61–2
design, **3**(2), 54–7
economics, **3**(2), 56–7
Reactor (Sodium, Experiment), containment, **2**(3), 27
control rods, **3**(3), 30, 45
core design, **1**(4), 24
fuel-element damage, **3**(2), 60–4
shutdown, **3**(1), 33; **3**(2), 60–3
Reactor (Sodium Graphite), **3**(2), 59–64
containment, **2**(3), 27
power flattening, **3**(3), 4–5
Reactor (SPERT), operating behavior, **1**(2), 16–17; **1**(4), 14
stability, **3**(4), 34–5
Reactor (SPERT-I), safety experiments, **3**(1), 28
self-limitation of power, **1**(3), 20–1
Reactor (SPERT-II), safety experiments, **3**(1), 28
Reactor (SPERT-III), safety experiments, **3**(1), 28
Reactor (Submarine Intermediate)
See Reactor (S1G)
Reactor (Submarine Thermal)
See Reactor (S1W)
Reactor (Swedish, for heating), control-rod worth, **3**(3), 30
Reactor (Swimming Pool)
See Reactor (Bulk Shielding)
Reactor (Thorium Breeder), design, **1**(2), 49
Reactor (Transient, Test Facility), safety experiments, **3**(1), 29
Reactor (Trawfynydd), neutron-flux-distribution determination, **3**(3), 5
Reactor (TURRET), design, **2**(4), 83–5; **3**(4), 58
Reactor (Ural), refueling, **2**(4), 59
Reactor (U.S.S.R. Superheater), design, **2**(1), 7, 35–6
Reactor (Vallecitos Boiling-Water), containment, **2**(3), 27
control rods, **3**(3), 45
stability, **2**(1), 20
Reactor (Veronezh), design, **2**(1), 5, 17, 23–4
refueling, **2**(4), 57
thermal-output characteristics, **2**(1), 21
Reactor (Westinghouse Test), containment, **2**(3), 26
Reactor (Yankee Power), containment, **2**(3), 26
control rods, **3**(3), 45
core design, **1**(4), 24
core physics, **2**(2), 11–12; **3**(1), 15
design, **2**(1), 5, 17
refueling, **2**(4), 56
thermal-output characteristics, **2**(1), 21
Reactor (Zeus), stability, **3**(4), 36
Reactor constants, **2**(2), 7
Reactor control materials
See Control materials
Reactor control systems
See Control
Reactor core design, **1**(2), 1–15
Reactor core materials, water-cooled and -moderated reactors, **2**(1), 10–12
Reactor cores
See also Lattices
buckling, **1**(3), 1–6
Reactor dynamics, **1**(4), 10–18
Reactor fuel elements
See Fuel elements
Reactor fuel materials
See Fuel elements

Reactor fuel solutions
See Fuel elements
Reactor fuses, **2**(3), 34–5
Reactor kinetics, accident calculations, **3**(1), 25–6
delayed neutrons, **3**(1), 24–5
Reactor lattices
See Lattices
Reactor moderators
See Moderators
Reactor physics, **1**(1), 3–5; **1**(3), 1–16; **1**(4), 1–6; **2**(2), 7–22; **2**(3), 17–19; **2**(4), 31–5; **3**(2), 30–3; **3**(3), 1–6; **3**(4), 12–21
conferences, **3**(2), 27–9; **3**(4), 33–7
Experimental Boiling-Water Reactor, **2**(2), 11
homogeneous reactors, **1**(2), 47
kinetics and dynamics, **3**(1), 24–7
Martin Power Reactor, **3**(1), 15
N.S. *Savannah* Reactor, **3**(1), 15
SIG Reactor, **2**(4), 34
Shippingport Pressurized-Water Reactor, **2**(2), 11
water-cooled and -moderated reactors, **2**(1), 12–16; **3**(1), 15–17
Yankee Power Reactor, **3**(1), 15
Reactor reflectors, reactor control, **1**(3), 12–13
Reactor research centers, critical and exponential measurements, **3**(4), 12, 16–19
Reactor safety, **1**(3), 20–3; **1**(4), 10–18; **2**(3), 22–37; **2**(4), 44–5; **3**(1), 28–35
See also Containment
accident calculations, **3**(1), 25–6
BR-3 Reactor, **3**(1), 41
Calder Hall Reactors, **2**(3), 28–9
Experimental Boiling-Water Reactor, **3**(3), 62–4
Experimental Breeder Reactor-I, **1**(2), 66; **1**(3), 22; **3**(1), 28
experiments, **3**(1), 28–30
fast-breeder reactors, **3**(2), 22–4
homogeneous reactors, **1**(2), 54–6
marine reactors, **2**(2), 1–6
Organic-Moderated Reactor Experiment, **1**(4), 44–5
Plutonium Recycle Test Reactor, **3**(3), 54–6
Reactor shielding materials
See Shielding
Reactor stability
See Stability
Reactor structural materials, **1**(2), 38–40
radiation effects, **1**(1), 31–3
Reactor vessels, radiation effects, **3**(4), 38–57
Reactor wastes
See also Waste disposal
composition, **3**(4), 2, 4
heat generation, **1**(4), 5; **2**(4), 34; **3**(4), 2, 5
Reactors, criticality effects of boiling, **1**(3), 20–1; **3**(4), 34–5
delayed neutrons, **3**(1), 24–5
design evaluation, **3**(3), 51–2
direct conversion of power, **3**(3), 48–50
fission-product poisoning, **3**(4), 12, 16–19
hot-channel factors, **2**(4), 42–3
industrial process heat applications, **3**(1), 1–5
reflector control, **1**(3), 12–13
refueling machinery, **2**(4), 54–5
stability, **1**(1), 16–17; **1**(2), 12–15; **3**(4), 33–7
theoretical studies of oscillations, **1**(1), 13–14
Reactors (aqueous homogeneous)
See Reactors (homogeneous)
Reactors (boiling heavy-water), **3**(2), 54
See also Reactor (Halden)
Reactors (boiling-water), **1**(2), 64–5; **1**(4), 52; **3**(2), 13–14
See also Reactor (ARBOR); Reactor (Belgonucleaire); Reactor (BONUS); Reactor (BORAX); Reactor (Dresden Power); Reactor (Elk River); Reactor (Experimental Boiling-Water); Reactor (Humboldt Bay Power); Reactor (Kinetic Experiments on Water Boilers); Reactor (ML-1); Reactor (Pathfinder Power); Reactor (Vallecitos Boiling-Water)
advance designs, **3**(3), 64–7
burnout, **3**(3), 10
coefficient of reactivity, **1**(1), 15–16
criticality effects of boiling, **1**(3), 20–1; **3**(4), 34–5
design, **3**(2), 8
design for marine applications, **2**(2), 3
dynamics, **1**(3), 21–3
economics, **2**(4), 2, 3, 4, 11–16
evaluation, **3**(2), 1–2, 4, 7, 8, 10
heat transfer, **3**(2), 39
power distribution, **1**(2), 65; **1**(3), 21
process heat applications, **3**(1), 2–5
reference list, **2**(1), 2
self-sustained power oscillation, **3**(3), 35
stability, **1**(3), 22; **1**(4), 10–14; **3**(1), 42–53
thermal performance, **2**(1), 18–23
transfer function, **1**(4), 14
turbine corrosion and erosion, **2**(2), 49–51
Reactors (breeder)
See also Reactors (fast-breeder); Reactors (thermal-breeder)
burnable poisons, **2**(2), 29
fluid-fuel reactors, **3**(1), 56
liquid-metal-fuel reactors, **1**(3), 42–5
Reactors (fast), **1**(2), 66–7; **2**(4), 62
See also Reactors (fast-breeder)
control, **1**(3), 8–9
Doppler effect on criticality, **1**(3), 7–8
fuel elements, **1**(2), 67; **1**(4), 32
reference list, **2**(1), 3
stability, **3**(4), 35–6
Reactors (fast-breeder)
See also Reactor (Dounreay); Reactor (Enrico Fermi Fast Breeder); Reactor (Experimental Breeder); Reactors (breeder); Reactors (fast)
breeding efficiency, **3**(2), 25
evaluation, **3**(2), 2, 4
safety, **3**(2), 22–4
Reactors (fluid-fuel), **3**(1), 54–60; **3**(2), 64–9
See also Reactor (Fast, Core Test Facility); Reactor (Homogeneous, Experiment-II); Reactor (Liquid Metal Fuel); Reactor (Liquid

Reactors (fluid-fuel) (Continued)
Metal Fuel, Experiment); Reactor (Los Alamos Molten Plutonium Experiment); Reactor (Pennsylvania Advanced); Reactors (Homogeneous); Reactors (fused-salt-fuel); Reactors (liquid-metal-fuel)
breeding, **3**(1), 56
fission-product release, **1**(4), 14–15
uranium dioxide–sodium–potassium fuel slurries, **1**(2), 44
Reactors (fluidized-bed), design, **3**(1), 61–3
Reactors (fused-salt-fuel), **1**(2), 69
design, **3**(1), 54
Reactors (gas-cooled), **1**(4), 53–8; **2**(1), 26–32; **2**(3), 55–64; **3**(4), 58–65
See also Reactor (Advanced Gas-Cooled); Reactor (Berkeley); Reactor (Bradwell); Reactor (Brown-Boveri-Krupp); Reactor (Calder Hall); Reactor (Czechoslovakia Gas-Cooled); Reactor (Dragon); Reactor (Experimental Gas-Cooled); Reactor (G2); Reactor (G3); Reactor (Gas-Cooled, Experiment); Reactor (Hunterston); Reactor (Maritime Gas-Cooled); Reactor (ORNL Graphite); Reactor (Peach Bottom); Reactor (Pebble Bed); Reactor (Trawfynydd); Reactor (TURRET); Reactors (gas-cooled heavy-water-moderated)
conferences, **3**(4), 58–65
coolant purification, **2**(1), 32
coolants, **1**(4), 57–8
design, **1**(1), 33–6; **1**(2), 68
design for marine applications, **2**(2), 3
economics, **1**(4), 53–5
evaluation, **3**(2), 2, 3–4
fuel elements, **1**(4), 27–8, 31–2, 55–7
heat transfer, **2**(2), 23–7
materials for high temperature, **3**(4), 62–4
reference list, **2**(1), 2–3
refueling, **2**(4), 62
Reactors (gas-cooled heavy-water-moderated)
See also Reactor (Russian Gas-Cooled Heavy-Water); Reactors (gas-cooled)
design, **2**(1), 29–30; **2**(3), 57–8
Reactors (graphite-moderated), **2**(1), 33–7
See also specific reactors by name
lattice design, **1**(2), 5–7
nuclear analysis, **1**(4), 2–3
reference list, **2**(1), 2–3
Reactors (heavy-water-cooled and -moderated), **1**(4), 59–63; **3**(2), 52–8
See also Reactor (Florida Power); Reactor (Halden); Reactor (Heavy-Water Components Test); Reactor (Homogeneous, Experiment-II); Reactor (MIT); Reactor (NPD-2); Reactor (NRU); Reactor (Parr Shoals); Reactor (Physical Constants Testing); Reactor (Plutonium Recycle Test); Reactor (Saclay EL-3); Reactor (Savannah River); Reactor (Sodium Deuterium); Reactor (Thorium Breeder); Reactor (Swedish, for heating); Reactors (gas-cooled heavy-water-moderated); Reactors (organic-cooled heavy-water-moderated); Reactors (sodium-cooled heavy-water-moderated)
buckling measurements, **1**(2), 2–4; **1**(4), 2; **3**(2), 30–1
core physics, **2**(3), 17–19; **3**(2), 30–1
design, **2**(3), 56, 58; **2**(4), 22–30
deuterium oxide economy, **2**(2), 44–8
economics, **2**(4), 2–4, 22–30
evaluation, **3**(2), 2, 4, 52–8
fuel-element design, **3**(2), 52–8
lattice design, **1**(2), 1–5
leak detection, **2**(2), 46
light-water removal, **2**(4), 78
neutron economy, **1**(1), 38–40
oscillation experiments, **3**(1), 26
reactivity lifetime, **2**(2), 18–19
reference list, **2**(1), 3
tritium monitoring, **2**(2), 46–7
Reactors (homogeneous)
See also Reactor (Homogeneous, Experiment-II); Reactor (Pennsylvania Advanced); Reactor (Thorium Breeder)
control, **1**(2), 54–6
economics, **1**(1), 59–60
evaluation, **3**(2), 2, 4
features and general design, **1**(2), 46–61; **3**(1), 54–5
heavy-water-moderated, **3**(2), 54
maintenance, **1**(2), 57–9
pumps, **1**(2), 57
reference list, **2**(1), 3
safety, **1**(2), 54–6
Reactors (liquid-metal-fuel), **1**(3), 42–55
See also Reactor (Liquid Metal Fuel); Reactor (Liquid Metal Fuel, Experiment)
breeding, **1**(3), 42–5
containment, **1**(3), 52
control, **1**(3), 48–9
fuel reprocessing, **1**(3), 49–50
graphite moderators, **1**(3), 46
maintenance, **1**(3), 52
pressure vessels, **1**(3), 53
pumps, **1**(3), 52–3
Reactors (liquid-plutonium-fuel), **3**(2), 65–9
See also Reactor (Fast, Core Test Facility); Reactor (Los Alamos Molten Plutonium, Experiment)
Reactors (marine), **2**(2), 1–6; **2**(3), 13–16; **3**(2), 13–18
See also Reactor (Lenin); Reactor (Maritime Gas-Cooled); Reactor (N.S. *Savannah*); Reactors (organic-cooled and -moderated); Reactors (pressurized-water)
comparison of several concepts, **2**(3), 61
safety, **2**(2), 1–6
Reactors (organic-cooled heavy-water-moderated), **1**(4), 62–3
Reactors (organic-cooled and -moderated), **1**(2), 68; **3**(2), 14–17
See also Reactor (Organic-Moderated, Experiment)

Reactors (organic-cooled and -moderated) (Continued)
advance designs, **3**(3), 68–70
burnout limits of polyphenyls, **2**(3), 20–1
coolants, **1**(4), 45–8
design, **2**(4), 21; **3**(2), 8–9
design for marine applications, **2**(2), 3
economics, **2**(4), 2–3, 16–21
evaluation, **3**(2), 2–3, 4, 7–9
exponential measurements, **1**(3), 14
heat transfer, **2**(4), 42
nucleate boiling, **3**(1), 19–21
physics, **2**(2), 12
process heat applications, **3**(1), 2–5
reference list, **2**(1), 3
Reactors (pebble-bed)
See also Reactor (Pebble Bed)
fuel elements, **2**(3), 40–2
Reactors (power), evaluation, **3**(2), 1–12
Reactors (pressure-tube)
See also Reactor (Florida Power); Reactor (Obninsk); Reactor (Plutonium Recycle Test); Reactor (Siberian)
refueling, **2**(4), 62
Reactors (pressurized-water)
See also Reactor (BR-3); Reactor (Indian Point Power); Reactor (Lenin); Reactor (Martin Power); Reactor (New Production); Reactor (N.S. *Savannah*); Reactor (Parr Shoals); Reactor (Pressurized Test); Reactor (S1W); Reactor (Shippingport Pressurized-Water); Reactor (SM-1); Reactor (Ural); Reactor (Veronezh); Reactor (Yankee Power); Reactors (supercritical water)
burnout, **2**(4), 39–42
design, **2**(4), 4–11; **3**(2), 10
design for marine applications, **2**(2), 3
economics, **2**(4), 2, 3, 4–11, 14–15
evaluation, **3**(2), 1–2, 4, 9–10
hydrodynamic calculations, **3**(2), 39
moderator control, **2**(4), 85
physics, **2**(2), 11–12
process heat applications, **3**(1), 2–5
reference list, **2**(1), 2
shim control, **1**(2), 62–3
thermal cycle, **2**(4), 7
thermal design, **1**(2), 63
thermal performance, **2**(1), 18–23
Reactors (process heat), **2**(3), 4–5
See also Reactor (Halden); Reactor (Swedish, for heating)
design, **3**(1), 2–5
economics, **2**(3), 4–5
Reactors (sodium-cooled)
See also Reactor (S1G); Reactors (sodium-cooled heavy-water-moderated); Reactors (sodium graphite)
fuel elements, **1**(4), 29, 32
Reactors (sodium-cooled heavy-water-moderated), **3**(2), 54
See also Reactor (Sodium Deuterium)
Reactors (sodium graphite)
See also Reactor (Sodium, Experiment); Reactor (Sodium Graphite)
evaluation, **3**(2), 2–3, 4
plutonium fuel cycle, **3**(3), 18–20
reference list, **2**(1), 3
Reactors (solid-fuel), refueling methods, **2**(4), 49–66
transfer function, **3**(1), 26–7
Reactors (supercritical water), burnout, **1**(3), 18
Reactors (test), economics, **1**(4), 64
Reactors (thermal-breeder), **3**(2), 52
breeding efficiency, **3**(2), 25–7; **3**(3), 4
Reactors (water-cooled and -moderated), **2**(1), 10–25
breeding, **2**(1), 17–19
coolant dissociation, **2**(1), 21–2
core physics, **2**(1), 12–16; **3**(1), 15–17
fuel elements, **1**(4), 25–6, 30–1
physics, **2**(2), 11–13
Reciprocating nuclear gas engines, **2**(3), 62–3
Reflectors, reactor control, **1**(3), 12–13
Refractory materials, melting point, **1**(2), 26–7
Refrasil, radiation effects, **2**(4), 82
thermal insulating properties, **2**(4), 82
Resistors, radiation effects, **1**(4), 39
Resonance escape, **1**(1), 4
probability, **1**(2), 9–10
thorium, thorium oxide, uranium, and uranium dioxide, **1**(1), 4
Rhenium, nuclear properties, **3**(3), 32
Rhodium, nuclear properties, **3**(3), 32
Rubber (natural), radiation effects, **1**(4), 37
Russian Gas-Cooled Heavy-Water Reactor, design, **1**(1), 35–6
Russian Icebreaker Lenin, reactor design, **2**(2), 3
Russian reactors
See Reactor (Lenin); Reactor (Obninsk); Reactor (Russian Gas-Cooled); Reactor (Siberian); Reactor (Ural); Reactor (U.S.S.R. Superheater); Reactor (Veronezh)

S

S1G Reactor
See Reactor (S1G)
S1W Reactor
See Reactor (S1W)
Saclay Center for Nuclear Studies, critical experiments, **3**(4), 13
Saclay EL-3 Reactor, fuel-element welding, **2**(2), 33
Salts (fused)
See Fluorides (fused)
Samarium, application as control material, **1**(2), 34; **3**(3), 32, 43–4
Samarium-149, neutron cross sections, **1**(3), 13; **2**(2), 16; **3**(4), 16
nuclear properties, **3**(3), 32
Samarium oxide, melting point, **1**(2), 28
neutron absorption, **3**(3), 35

Samarium oxide–stainless steel systems, neutron absorption, **3**(3), 34
Santowax M, nucleate boiling, **3**(1), 19
Santowax O, nucleate boiling, **3**(1), 19
Santowax O-M, coolant properties, **2**(4), 42
properties, **1**(4), 45
Santowax R, coolant properties, **2**(4), 42
Savannah Reactor
See Reactor (N.S. *Savannah*)
Savannah River Laboratory, critical and exponential experiments, **3**(4), 13
Savannah River Reactors, buckling, **1**(3), 1–2
Sea disposal, reactor wastes, **3**(4), 9
Selsyn motors, radiation effects, **1**(4), 39
Semiconductors, radiation effects, **1**(4), 37; **3**(1), 37
Shielding, **1**(2), 38; **2**(2), 30–2; **2**(4), 46–8; **3**(1), 36; **3**(2), 40–1
aluminum, **2**(2), 30; **3**(3), 34
barytes concrete, **2**(2), 31
beryllium, **2**(2), 30
bismuth, **2**(2), 30
boron, **2**(2), 30
boron glass, **3**(3), 36
cadmium, **2**(2), 30
carbon, **2**(2), 30
chlorine, **2**(2), 30
concretes, **2**(2), 31–2; **2**(4), 46–7
copper, **2**(2), 30
experiments in Bulk Shielding Reactor, **3**(2), 40
fluorine, **2**(2), 30
hydrogen, **2**(2), 30
iron, **2**(2), 30
iron limonite concrete, **2**(4), 46
lead, **2**(2), 30
lithium, **2**(2), 30
lithium hydride, **1**(1), 31
magnesium oxychloride cement, **1**(1), 31
magnetite concrete, **2**(4), 46
magnetite limonite concrete, **2**(4), 46
neutron-distribution prediction, **3**(2), 40
nickel, **2**(2), 30
organic-moderated reactors, **3**(2), 15
ORNL Graphite Reactor, **2**(2), 31
oxygen, **2**(2), 30
radiation effects, **1**(1), 31
radiation tolerances, **2**(4), 47–8
sodium, **2**(2), 30
sulfur, **2**(2), 30
titanium, **2**(2), 30
tungsten, **2**(2), 30
Shippingport Pressurized-Water Reactor
See Reactor (Shippingport Pressurized-Water)
Siberian Reactor
See Reactor (Siberian)
Silicon-aluminum systems, pressure-tube construction, **2**(1), 34
Silicon-aluminum-uranium systems, diffusion, **1**(2), 30–1
Silicon carbide–silicon–uranium dioxide systems, radiation effects, **1**(2), 24
Silicon dioxide–thorium oxide systems, properties, **1**(2), 31
Silicon dioxide–uranium dioxide systems, properties, **1**(2), 31
Silicon-iron systems, radiation effects, **3**(1), 37–8
Silicon–thorium oxide systems, properties, **1**(2), 31
Silicon–uranium dioxide systems, properties, **1**(2), 31
Silicon-uranium systems
See Uranium-silicon systems
Silicon–uranium–Zircaloy-2 compacts, density, **1**(2), 31
Silicones, radiation effects, **1**(4), 38; **3**(1), 37
Silver, neutron absorption, **3**(3), 34–5
nuclear properties, **3**(3), 32
welding, **2**(2), 33
Silver-zirconium alloys, corrosion by uranyl sulfate solutions, **1**(2), 52
SM-1 Reactor
See Reactor (SM-1)
Sodium (liquid), coolant properties, **1**(2), 40
corrosion of uranium, **1**(4), 32
physical properties, **1**(3), 48
properties, **1**(4), 46
shielding properties, **2**(2), 30
Sodium-cooled reactors
See Reactors (sodium-cooled)
Sodium Deuterium Reactor
See Reactor (Sodium Deuterium)
Sodium Graphite Reactor
See Reactor (Sodium Graphite)
Sodium-potassium alloys (liquid), coolant properties, **1**(2), 40
Sodium–potassium–uranium dioxide systems (slurries), temperature effects on fuel suspension, **1**(2), 44
Sodium Reactor Experiment
See Reactor (Sodium, Experiment)
Sodium uranate, melting point, **1**(2), 28
Solid fixation, reactor wastes, **3**(4), 7–8
Soviet Icebreaker Lenin, reactor design, **2**(2), 3
Soviet reactors
for a list, *see* Russian reactors
SPERT Reactors
See Reactor (SPERT)
Springs, radiation effects on control-rod springs, **1**(2), 45
Stability, **1**(1), 13–14, 16–17; **1**(2), 12–13; **3**(4), 33–7
boiling-water reactors, **1**(3), 22; **1**(4), 10–14; **3**(1), 42–53; **3**(3), 35
BORAX Reactor, **1**(1), 15–16; **1**(2), 64; **2**(1), 20; **3**(1), 47–53
coefficient of reactivity effects, **1**(1), 13–14
conferences, **3**(4), 33–7
Experimental Boiling-Water Reactor, **2**(1), 20; **3**(1), 44–7, 51–3; **3**(4), 34–5
Experimental Breeder Reactor-I, **1**(1), 12–13; **3**(4), 36
fast reactors, **3**(4), 35–8

Stability (Continued)
Kinetic Experiments on Water Boilers, **3**(4), 33–4
Shippingport Pressurized-Water Reactor, **3**(3), 35
SPERT Reactors, **3**(4), 34–5
Vallecitos Boiling-Water Reactor, **2**(1), 20
Zeus Reactor, **3**(4), 36
Stainless steel, cladding for fuel elements, **1**(3), 39; **1**(4), 30
corrosion by carbon dioxide, **1**(1), 33; **1**(4), 28
corrosion by hydrofluoric acid–nitric acid systems, **1**(2), 39
corrosion by nitrogen, **3**(1), 38–40
corrosion by polyphenyls, **1**(4), 44–5
corrosion by uranyl sulfate, **1**(2), 52–3
dissolution, **1**(2), 39
heat transfer, **1**(1), 6
neutron cross sections, **2**(2), 10
nuclear properties, **1**(2), 39
properties, **1**(4), 25, 28, 29
properties of type 304, **1**(4), 23
radiation effects, **1**(4), 40–1; **2**(3), 56; **2**(4), 72
reactions with uranium, **1**(4), 29
reactions with uranium dioxide, **1**(4), 25
thermal properties, **1**(2), 39
welding, **2**(2), 33
Stainless steel–boron systems
See Boron–stainless steel systems
Stainless steel–europium oxide systems, neutron absorption, **3**(3), 34
Stainless steel–europium oxide systems (stainless-steel-clad), control rods in SM-1 Reactor, **3**(3), 40
Stainless steel–gadolinium oxide systems, radiation effects, **1**(1), 31
Stainless steel–uranium alloys, radiation effects, **1**(1), 29
Stainless steel–uranium carbide compacts, density, **1**(2), 31
Stainless steel–uranium nitride compacts, density, **1**(2), 31
Steam, corrosion of uranium dioxide, **3**(2), 49–50
corrosion of zirconium and Zircaloys, **2**(2), 39
Steam cycle, Pathfinder Power Reactor, **2**(3), 53–4
Steam slip, **3**(4), 28–9
Steel [Jessops (G1)], corrosion by carbon dioxide, **1**(1), 33
Steels, corrosion by bismuth alloys, **1**(3), 51
corrosion by carbon dioxide, **1**(1), 33
corrosion by polyphenyls, **1**(4), 44–5
heat transfer, **1**(1), 6
radiation effects, **1**(4), 40; **3**(4), 38–57
Strontium uranate, melting point, **1**(2), 28
Structural materials
See Reactor structural materials
Submarine Intermediate Reactor
See Reactor (S1G)
Submarine Thermal Reactor
See Reactor (S1W)
Sulfur, shielding properties, **2**(2), 30
Sulfuric acid, corrosion inhibition of uranyl sulfate corrosion of Zircaloy-2, **1**(2), 53
Supercritical water reactors, burnout, **1**(3), 18
Superheaters (fossil-fueled), **3**(2), 11–12
Superheaters (nuclear), BONUS Reactor, **3**(4), 68–74
evaluation, **3**(2), 3, 4
Fast-Reactor Core Test Facility, **3**(2), 67
heat transfer, **3**(4), 69–74
Pathfinder Power Reactor, **2**(3), 51–3; **3**(4), 69
Swedish reactor for heating, control-rod worth, **3**(3), 30
Swirl flow, heat transfer, **3**(4), 25–7
Symposia
See Conferences

T

Tantalum, neutron absorption, **3**(3), 34–5
radiation effects, **1**(4), 40
solubility in liquid bismuth, **1**(3), 50
Tantalum-gadolinium alloys, neutron absorption, **3**(3), 34
Temperature coefficients of reactivity
See Coefficient of reactivity
Temperature coefficient of resonance, thorium, **1**(1), 4
uranium-238, **1**(1), 4
Terbium oxide, neutron absorption, **3**(3), 36
Terphenyl, decomposition in Organic-Moderated Reactor Experiment, **3**(2), 70
Terphenyl, meta-
See Santowax M
Terphenyl, ortho-
See Santowax O
Thermal insulation
See Insulation (thermal)
Thermionic energy conversion
See also Thermocouples
cesium vapor-filled converters, **3**(1), 9–11
direct conversion of nuclear energy, **3**(3), 48–50
high vacuum converter performance, **3**(1), 8–9
Los Alamos plasma thermocouple, **3**(1), 11–13
theory and efficiency, **3**(1), 6–14
Thermocouples
See also Thermionic Energy Conversion
Organic-Moderated Reactor Experiment, **3**(4), 31
Thermocouples (Los Alamos plasma), **3**(1), 11–13
Thermoelectric power
See Thermionic energy conversion
Thermoflex, radiation effects, **2**(4), 82
thermal insulating properties, **2**(4), 82
Thermopiles
See Thermionic energy conversion
Thorex Process, homogeneous reactor fuel reprocessing, **1**(2), 51
Thorium, conversion to uranium-233 in water-cooled and -moderated reactor, **2**(1), 17–19
effective resonance integral, **1**(4), 4
radiation effects, **1**(2), 24–5
resonance escape of neutrons, **1**(1), 4
Thorium (aluminum-clad), radiation effects, **1**(3), 29
Thorium Breeder Reactor, design, **1**(2), 49

Thorium oxide, physical properties, 1(1), 27
radiation effects, 1(4), 30
resonance escape of neutrons, 1(1), 4
Thorium oxide–beryllium oxide systems, properties, 1(2), 31
Thorium oxide–beryllium systems, properties, 1(2), 31
Thorium oxide–cerium oxide systems, properties, 1(2), 31
Thorium oxide–molybdenum systems, thermal properties, 1(2), 28, 30
Thorium oxide–niobium systems, properties, 1(2), 31
Thorium oxide–silicon dioxide systems, properties, 1(2), 31
Thorium oxide–silicon systems, properties, 1(2), 31
Thorium oxide–uranium dioxide systems
See Uranium dioxide–thorium oxide systems
Thorium oxide–zirconium oxide systems, properties, 1(2), 31
Thorium oxide–zirconium systems, properties, 1(2), 31
Thorium-uranium alloys
See Uranium-thorium alloys
Thulium oxide, neutron absorption, 3(3), 36
Titanium, corrosion by uranyl sulfate, 1(2), 52
neutron absorption, 3(3), 34
nuclear properties, 1(2), 39
radiation effects, 1(4), 40
shielding properties, 2(2), 30
thermal properties, 1(2), 39
Titanium alloys, high-temperature properties, 1(2), 39
Titanium-boron systems
See Boron-titanium systems
Titanium–gadolinium oxide systems, radiation effects, 1(1), 31
Titanium-uranium alloys
See Uranium-titanium alloys
Titanium-vanadium alloys, high-temperature properties, 1(2), 39
Toxicology, beryllium, 2(4), 70–1
Transfer function, boiling-water reactors, 1(4), 14
conferences, 3(4), 33–7
Transient Reactor Test Facility, safety experiments, 3(1), 29
solid-fuel reactors, 3(1), 26–7
Transuranic elements, disposal, 1(4), 5, 7
Trawfynydd Reactor, neutron-flux-distribution determination, 3(3), 5
Tritium, monitoring, 2(2), 46–7
Tubes
See also Channels
heat transfer to gases, 3(2), 38
heat transfer in turbulent flow, 3(3), 8–9
Tubes (finned, roughened), heat transfer, 1(1), 9
Tubes (finned, smooth), heat transfer, 1(1), 9
Tubes (finned, transverse), heat transfer with axial gas flow, 1(1), 5–11
Tubes (pressure)
See Pressure tubes
Tungsten, neutron absorption, 3(3), 36
radiation effects, 1(4), 40
shielding properties, 2(2), 30
solubility in liquid bismuth, 1(3), 50
Turbines, corrosion and erosion in boiling-water reactors, 2(2), 49–51
TURRET Reactor, design, 2(4), 83–5; 3(4), 58

U

Ultrasonics, applications in welding, 1(2), 45
United Nations, Second International Conference on the Peaceful Uses of Atomic Energy, 2(1), 1–9
Ural Reactor, refueling, 2(4), 59
Uranium, compatibility with beryllium, 2(4), 70
corrosion by liquid sodium, 1(4), 32
effective resonance integral, 1(4), 3–4
electrocladding with aluminum, 2(2), 34
enrichment costs, 1(1), 1; 3(2), 19
extraction costs, 3(2), 21–2
fabrication into fuel elements, 1(3), 24–5
fission-product release from fuel elements, 1(4), 26–7, 29
fuel elements, 1(4), 26, 27, 31–2
fuel elements for Sodium Graphite Reactor, 3(2), 59–61
impregnation of graphite, 2(3), 41–2
nuclear properties, 1(1), 24; 1(2), 39
physical properties, 1(1), 23–4; 2(3), 47
properties, 1(2), 32; 1(4), 22, 26
radiation effects, 1(3), 25; 1(4), 26, 31–2; 3(2), 59
radiation effects in powder compacts, 1(2), 19–20
reactions with niobium, stainless steel, vanadium, and Zircaloy-2, 1(4), 29
reactions with water, 1(1), 18
resonance absorption in rods, 1(3), 9
resonance escape of neutrons, 1(1), 4
thermal properties, 1(2), 19, 39
welding, 2(2), 33
Uranium-233, neutron cross sections, 1(3), 13; 2(2), 17
Uranium-234, neutron cross sections, 1(3), 13
Uranium-235, fission products, 1(3), 13
reactivity lifetimes in fuel elements, 3(3), 15
Uranium-236, problems created in recycled fuels, 2(2), 42
Uranium-238, conversion to plutonium-239, 1(3), 6–7
Doppler coefficient, 2(2), 13–14
temperature coefficient of resonance, 1(1), 4
Uranium (depleted), radiation effects, 1(2), 19
Uranium (enriched), costs and supplies, 1(1), 1; 3(2), 19
Uranium (Zircaloy-2-clad), temperature coefficient of reactivity, 3(3), 3–4
Uranium (zirconium-clad), fabrication into fuel elements, 1(3), 25
radiation effects, 1(3), 25

Uranium alloys, fuel elements, 1(4), 29
properties, 1(2), 32; 1(4), 29
radiation effects, 1(2), 32; 1(4), 29
Uranium-aluminum alloys, fuel-element fabrication, 1(2), 26
properties, 1(2), 28
radiation effects, 1(1), 29; 1(3), 33–4
thermal properties, 1(2), 29, 30
Uranium-bismuth alloys (liquid), reactor cooling, 1(3), 42–55
Uranium borides, thermal properties, 1(2), 29
Uranium carbide–stainless steel compacts, density, 1(2), 31
Uranium carbide–Zircaloy-2 compacts, density, 1(2), 31
Uranium carbides, corrosion resistance, 1(2), 27
properties, 1(2), 28
thermal properties, 1(2), 29
Uranium-chromium alloys, properties, 1(2), 32
radiation effects, 1(2), 32
Uranium-copper alloys, properties, 1(2), 28
Uranium dioxide, compatibility with beryllium, 2(4), 70
corrosion by steam, 3(2), 49–50
effective resonance integral, 1(4), 3–4
erosion by high-pressure water, 1(2), 31
fabrication into fuel elements, 3(2), 42–4, 45
fission-gas release, 1(1), 25–6; 1(2), 24
fission-product release from fuel elements, 1(4), 25, 28
fuel applications in fast reactors, 1(2), 67
fuel elements, 1(4), 25, 28, 30, 32
melting point, 1(2), 26–7
oxidation by carbon dioxide, 3(2), 50
physical properties, 1(1), 25; 2(3), 47
properties, 1(2), 28; 1(4), 22, 28
radiation effects, 1(2), 24; 1(4), 25, 28, 38; 3(2), 43–4, 45
reactions with aluminum, stainless steel, and Zircaloy-2, 1(4), 25
resonance escape of neutrons, 1(1), 4
thermal conductivity, 3(2), 44–5, 46–9
Uranium dioxide (stainless-steel-clad), Experimental Gas-Cooled Reactor fuel elements, 2(3), 55–6; 3(4), 59–62
radiation effects, 2(3), 56
Uranium dioxide (Zircaloy-2-clad), radiation effects, 1(1), 26–7; 1(3), 28–33
thermal properties, 1(3), 29–33
Uranium dioxide (zirconium-clad), corrosion by high-temperature water, 1(2), 32
Uranium dioxide–beryllium oxide systems, properties, 1(2), 31
Uranium dioxide–beryllium systems, properties, 1(2), 31
Uranium dioxide–cerium oxide systems, properties, 1(2), 31
thermal conductivity, 3(2), 49
Uranium dioxide–chromium–nickel systems (Nichrome-V-clad), reactions with water during irradiation, 1(1), 18–19
Uranium dioxide–graphite systems, radiation effects, 1(2), 26
Uranium dioxide–molybdenum systems, properties, 1(2), 31
Uranium dioxide–niobium oxide systems, thermal conductivity, 3(2), 49
Uranium dioxide–niobium systems, properties, 1(2), 31
Uranium dioxide–silicon carbide–silicon systems, radiation effects, 1(2), 24
Uranium dioxide–silicon dioxide systems, properties, 1(2), 31
Uranium dioxide–silicon systems, properties, 1(2), 31
Uranium dioxide–sodium–potassium systems (slurries), temperature effects on fuel suspension, 1(2), 44
Uranium dioxide–thorium oxide systems, radiation effects, 1(1), 28; 1(2), 24, 26
rod buckling, 1(3), 4–5
Uranium dioxide–thorium oxide systems (aluminum-nickel alloy clad), fabrication into fuel elements, 1(3), 33
radiation effects, 1(3), 33
Uranium dioxide–yttrium oxide systems, thermal conductivity, 3(2), 49
Uranium dioxide–zirconium oxide systems, properties, 1(2), 31
Uranium dioxide–zirconium systems, properties, 1(2), 31
Uranium-fissium alloys, nuclear properties, 1(4), 29
radiation effects, 1(2), 22
Uranium-fissium-molybdenum alloys, nuclear properties, 1(4), 29
Uranium-germanium alloys, properties, 1(2), 32
radiation effects, 1(2), 32
Uranium-graphite systems, fuel elements, 2(3), 40–7
properties, 2(3), 42
radiation effects, 2(3), 44–5
temperature effects, 2(3), 41
Uranium hydride, radiation effects in powder compacts, 1(2), 19–20
Uranium-iron alloys, properties, 1(2), 28, 32
radiation effects, 1(2), 32
thermal properties, 1(2), 29
Uranium-magnesium alloys, fuel-element characteristics, 2(3), 47–50
radiation effects, 2(3), 48–50
Uranium-magnesium alloys (Zircaloy-2-clad), radiation effects, 1(1), 29
Uranium-manganese alloys, properties, 1(2), 28
Uranium-molybdenum alloys, nuclear properties, 1(1), 24; 1(4), 29
properties, 1(2), 32
radiation effects, 1(2), 19–21, 32; 1(3), 25–7
reactions with water, 1(1), 18
Uranium-molybdenum alloys (Zircaloy-2-clad), radiation effects, 1(3), 26–7
Uranium-nickel alloys, properties, 1(2), 28
thermal properties, 1(2), 29

Uranium–nickel–Zircaloy-2 compacts, density, **1**(2), 31
Uranium-niobium alloys, nuclear properties, **1**(1), 24
radiation effects, **1**(2), 19–20; **1**(3), 27
Uranium-niobium-zirconium alloys, reactions with water, **1**(1), 18
nuclear properties, **1**(1), 24
radiation effects, **1**(2), 21
Uranium nitride, corrosion by 680°F water, **1**(2), 27
properties, **1**(2), 28
thermal properties, **1**(2), 29
Uranium nitride–stainless steel compacts, density, **1**(2), 31
Uranium oxides
See also Uranium dioxide
effect of oxygen content on fuels, **3**(2), 45–6
Uranium oxycarbide, properties, **1**(2), 28
Uranium–phosphorus pentoxide systems, melting point, **1**(2), 28
Uranium-plutonium alloys, radiation effects, **1**(2), 22–5
Uranium-plutonium-fissium alloys, nuclear properties, **1**(1), 25
Uranium resources, consumption, **2**(3), 10–11
Uranium silicides, thermal properties, **1**(2), 29, 30
Uranium-silicon-aluminum systems, diffusion, **1**(2), 30–1
Uranium-silicon systems, nuclear properties, **1**(1), 24
properties, **1**(2), 28, 32
radiation effects, **1**(2), 19–20, 21, 32
Uranium–silicon–Zircaloy-2 compacts, density, **1**(2), 31
Uranium–stainless steel alloys, radiation effects, **1**(1), 29
Uranium sulfides, thermal properties, **1**(2), 29
Uranium-thorium alloys, properties, **1**(2), 32
radiation effects, **1**(2), 24–5, 32
Uranium-titanium alloys, properties, **1**(2), 28, 32
radiation effects, **1**(2), 20–1, 32
Uranium–titanium–Zircaloy-2 compacts, density, **1**(2), 31
Uranium-vanadium alloys, properties, **1**(2), 32
radiation effects, **1**(2), 32
Uranium-zirconium alloys, corrosion by water, **1**(2), 21–2
dissolution, **1**(2), 31
fuel elements for Sodium Graphite Reactor, **3**(2), 59–60
nuclear properties, **1**(1), 24
properties, **1**(2), 32
radiation effects, **1**(1), 29; **1**(2), 26, 27, 32; **3**(2), 59
Uranium-zirconium alloys (Zircaloy-clad), fuel elements, **1**(4), 31
Uranium-zirconium alloys (Zircaloy-2-clad), radiation effects, **1**(3), 25
Uranium-zirconium alloys (zirconium-clad), radiation effects, **1**(3), 34
reactions with water during irradiation, **1**(1), 18–19
Uranyl sulfate–water systems, corrosion of stainless steel, titanium, zirconium, and zirconium alloys, **1**(2), 52–3
homogeneous reactor fuels, **1**(2), 52–3
U.S.S.R. Reactors
for a list, *see* Russian reactors
U.S.S.R. Superheater Reactor, design, **2**(1), 7, 35–6

V

Vallecitos Boiling-Water Reactor
See Reactor (Vallecitos Boiling-Water)
Vanadium, high-temperature properties, **1**(2), 38–9
nuclear properties, **1**(2), 39
properties, **1**(4), 23, 29
reactions with uranium, **1**(4), 29
thermal properties, **1**(2), 39
Vanadium alloys, high-temperature properties, **1**(2), 38–9
Vanadium-titanium alloys, high-temperature properties, **1**(2), 39
Vanadium-uranium alloys
See Uranium-vanadium alloys
Veronezh Reactor
See Reactor (Veronezh)
Vessels (pressure)
See Pressure vessels
Vessels (reactor), radiation effects, **3**(4), 38–57
Vortex flow, heat transfer, **3**(4), 25–7

W

Waste disposal, economics, **3**(4), 4, 6–7
evaporators, **1**(2), 45
fixation, **3**(4), 7–8
oceans, **3**(4), 9
transuranic elements, **1**(4), 5–7
Water, corrosion of aluminum, **1**(1), 18; **1**(2), 39; **3**(4), 29–30
corrosion of aluminum alloys, **1**(2), 40
corrosion of aluminum-nickel alloys, **1**(3), 37–8
corrosion of boron–stainless steel systems, **3**(3), 39
corrosion of boron-titanium systems, **3**(3), 41
corrosion of boron-zirconium systems, **3**(3), 41
corrosion of cadmium-indium-silver alloys, **3**(3), 41
corrosion of control rods, **3**(3), 40–1
corrosion of fuel elements in high temperature, **1**(2), 32
corrosion of uranium dioxide (zirconium-clad), **1**(2), 32
corrosion of uranium nitride, **1**(2), 27
corrosion of uranium-zirconium alloys, **1**(2), 21–2
corrosion of Zircaloys, **2**(2), 38–9
corrosion of zirconium, **1**(2), 32; **2**(2), 38–9
erosion of fuel pellets, **1**(2), 31
fuel-element rupture in high temperature, **1**(2), 31
neutron moderation, **2**(2), 9–10

Water (Continued)
physical properties, 1(3), 48
properties, 1(4), 46
reactions with fuels during irradiation, 1(1), 18–19
reactions with uranium, 1(1), 18
reactions with uranium-molybdenum alloys, 1(1), 18
reactions with uranium-niobium-zirconium alloys, 1(1), 18
reactions with uranium-zirconium alloys, 1(1), 18–19
Water–carbon dioxide systems, coolant-moderator efficiency, 2(3), 59
Water–hydrofluoric acid–nitric acid systems, decontamination efficiency, 2(3), 24–5
Water-metal systems, chemical reactions, 1(1), 18–19; 3(1), 30–3
Welding, electron-beam process, 2(2), 33–4
nonferrous metals, 2(2), 33
Saclay EL-3 Reactor fuel elements, 2(2), 33
stainless steel, 2(2), 33
ultrasonic techniques, 1(2), 45
Welds, radiation effects, 3(4), 41–2
Westinghouse Reactor Evaluation Center, critical and exponential experiments, 3(4), 14
Westinghouse Test Reactor, containment, 2(3), 26
Wolfram
See Tungsten

X

Xenon-133, presence in irradiated uranium dioxide–silicon carbide–silicon fuel elements, 1(2), 24
Xenon-135, neutron cross sections, 1(3), 13; 3(4), 16

Y

Yankee Power Reactor
See Reactor (Yankee Power)
Ytterbium oxide, neutron absorption, 3(3), 36
Yttrium oxide–uranium dioxide systems, thermal conductivity, 3(2), 49
Yttrium-zirconium alloys, corrosion by uranyl sulfate solutions, 1(2), 52

Z

Zeus reactor, stability, 3(4), 36
Zircaloy, fuel-element cladding, 1(4), 30
Zircaloy-2, corrosion by carbon dioxide, 2(2), 39–40
corrosion by carbon dioxide–helium systems, 2(2), 39–40
corrosion by steam, 2(2), 39
corrosion by uranyl sulfate solutions, 1(2), 53
corrosion by water, 2(2), 38–9
decontamination with hydrofluoric acid–nitric acid–water systems, 3(3), 24–5
high-temperature properties, 1(2), 35–8
neutron absorption, 3(3), 34
nondestructive testing of tubing, 1(2), 45
properties, 1(4), 23, 25, 26, 29
radiation effects, 1(1), 26–7; 1(2), 34; 1(3), 25–7, 29–33
reactions with uranium, 1(4), 29
reactions with uranium dioxide, 1(4), 25
reactions with water, 3(1), 30–3
welding, 2(2), 33
Zircaloy-2–boron systems, radiation effects, 1(1), 30
Zircaloy-2–nickel–uranium compacts, density, 1(2), 31
Zircaloy-2–uranium carbide compacts, density, 1(2), 31
Zircaloy-3, corrosion by steam, 2(2), 39
high-temperature properties, 1(2), 38
Zircaloy-3A, high-temperature properties, 1(2), 37
Zircaloy-B, reactions with water, 1(1), 18
Zirconium, corrosion by carbon dioxide, 2(2), 39–40
corrosion by carbon dioxide–helium systems, 2(2), 39–40
corrosion by steam, 2(2), 39
corrosion by uranyl sulfate, 1(2), 52
corrosion by water, 1(2), 32; 2(2), 38–9
high-temperature properties, 1(2), 35–6
nuclear properties, 1(2), 39
pressure tubes in gas-cooled heavy-water-moderated reactors, 2(3), 56, 58
properties, 1(4), 23
radiation effects, 1(3), 25, 34; 1(4), 40
thermal properties, 1(2), 39
Zirconium alloys
See also Zircaloys
corrosion by steam, 2(2), 39
high-temperature properties, 1(2), 35–8
Zirconium-aluminum alloys, corrosion by uranyl sulfate, 1(2), 52
Zirconium-boron systems
See Boron-zirconium systems
Zirconium-cerium alloys, corrosion by uranyl sulfate solutions, 1(2), 52
Zirconium-chromium alloys, corrosion by uranyl sulfate solutions, 1(2), 52
Zirconium diboride, radiation effects, 1(1), 30
Zirconium hydride, thermal properties, 1(2), 38; 1(3), 37
Zirconium hydride–carbon dioxide systems, coolant-moderator efficiency, 2(3), 59
Zirconium-magnesium couples, diffusion, 1(2), 30
Zirconium-niobium alloys, corrosion by uranyl sulfate solutions, 1(2), 52
Zirconium-niobium-uranium alloys
See Uranium-niobium-zirconium alloys
Zirconium oxide–thorium oxide systems, properties, 1(2), 31
Zirconium oxide–uranium dioxide systems, properties, 1(2), 31

Zirconium-silver alloys, corrosion by uranyl sulfate solutions, I(2), 52
Zirconium–thorium oxide systems, properties, I(2), 31
Zirconium-uranium alloys
See Uranium-zirconium alloys
Zirconium–uranium dioxide systems, properties, I(2), 31
Zirconium-water systems, chemical reactions during irradiation, I(1), 18–19
Zirconium-yttrium alloys, corrosion by uranyl sulfate solutions, I(2), 52

NUCLEAR SCIENCE ABSTRACTS

The U. S. Atomic Energy Commission, Office of Technical Information, publishes *Nuclear Science Abstracts (NSA)*, a semimonthly journal containing abstracts of the literature of nuclear science and engineering.

NSA covers (1) research reports of the U. S. Atomic Energy Commission and its contractors; (2) research reports of government agencies, universities, and industrial research organizations on a world-wide basis; and (3) translations, patents, books, and articles appearing in technical and scientific journals.

Complete indexes covering subject, author, source, and report number are included in each issue. These are cumulated quarterly, semiannually, and annually providing a detailed and convenient key to the literature.

Availability of *NSA*

SALE *NSA* is available on subscription from the Superintendent of Documents, U. S. Government Printing Office, Washington 25, D. C., at $18.00 per year for the semimonthly abstract issues and $15.00 per year for the four cumulated-index issues. Subscriptions are postpaid within the United States, Canada, Mexico, and all Central and South American countries, except Argentina, Brazil, British and French Guiana, Surinam, and British Honduras. Subscribers in these Central and South American countries, and in all other countries throughout the world, should remit $22.50 per year for subscriptions to semimonthly abstract issues and $17.50 per year for the four cumulated-index issues.

EXCHANGE *NSA* is also available on an exchange basis to universities, research institutions, industrial firms, and publishers of scientific information. Inquiries should be directed to the Office of Technical Information Extension, U. S. Atomic Energy Commission, P. O. Box 62, Oak Ridge, Tennessee.

TECHNICAL PROGRESS REVIEWS may be purchased from Superintendent of Documents, U. S. Government Printing Office, Washington 25, D. C. for $2.00 per year for each subscription or for $0.55 per issue. The use of the coupon below will facilitate the handling of your order.

POSTAGE AND REMITTANCE: Postpaid within the United States, Canada, Mexico, and all Central and South American countries except as hereinafter noted. Add $0.50 per year, or $0.15 per single issue, for postage to all other countries, including Argentina, Brazil, British and French Guiana, Surinam, and British Honduras. Payment should be by check, money order, or document coupons, and MUST accompany order. Remittances from foreign countries should be made by international money order, or draft on an American bank, payable to the Superintendent of Documents, or by UNESCO book coupons.

order form

SUPERINTENDENT OF DOCUMENTS
U. S. GOVERNMENT PRINTING OFFICE
WASHINGTON 25, D. C.

Enclosed:
document coupons ☐ check ☐ money order ☐

Charge to Superintendent of Documents No._____

Please send a one-year subscription to

☐ REACTOR CORE MATERIALS
☐ POWER REACTOR TECHNOLOGY
☐ NUCLEAR SAFETY
☐ REACTOR FUEL PROCESSING

(Each subscription $2.00 a year; $0.55 per issue.)

SUPERINTENDENT OF DOCUMENTS
U. S. GOVERNMENT PRINTING OFFICE
WASHINGTON 25, D. C.

(Print clearly)

Name_____

Street_____

City_____ Zone____ State_____